UNIVERSITY OF CALIFORNIA SAN DIEGO

Folding of a beta-barrel membrane protein into nanodiscs

A dissertation submitted in partial satisfaction of the
requirements for the degree Doctor of Philosophy

in

Chemistry

by

DeeAnn Kiyoko Asamoto

Committee in Charge:

Professor Judy E. Kim, Chair
Professor Andrew Kummel
Professor Andrew McCammon
Professor Douglas Smith
Professor Brian Zid

2021

This dissertation of DeeAnn Kiyoko Asamoto is approved, and it is acceptable in quality and form for publication on microfilm and electronically.

University of California San Diego

2021

DEDICATION

To my parents Steven Asamoto
and
Lloyd & Terry Aotaki

TABLE OF CONTENTS

LIST OF FIGURES

LIST OF TABLES

ACKNOWLEDGEMENTS

I feel incredibly grateful to have met such inspiring, intelligent, and supportive mentors and friends throughout my academic career. Without each one of you, I would not be who I am, or where I am, today. I am so thankful.

To my graduate research advisor, Professor Judy E. Kim, I cannot imagine a better mentor, role model, and teacher. From the very beginning you welcomed me into your research lab and believed in me and trusted me enough to be a part of your research team. You have a unique way of making very stressful situations light-hearted and I have always felt a sense of calm and relief after consulting with you about anything chaotic and stressful. I can't thank you enough for guiding me, inspiring me, and being patient and laughing with me as I made mistakes. Thank you for teaching me how to approach and think about research in creative ways. I've learned so much from being your student. I am eternally grateful for the time you've spent teaching me and the countless hours that you've spent working with me, whether it be working together on the laser, trouble shooting instruments, or writing manuscripts together, so that I can learn from you and become a successful scientist. It has always amazed me how incredibly hard-working and involved you are within the department, as a Professor, and with your research lab. I hope that one day I can give presentations and research talks as great as you can.

To my undergraduate research advisor, Professor Stephen P. Mezyk, one of the most hard-working and influential people I have ever met. I am so grateful that I was fortunate enough to be a student in your general chemistry course at CSULB. You invited me to join your research lab, which opened up so many doors and opportunities for me as an undergrad, and I know that I would not be where I am today, without your guidance. Anyone who knows you, knows that you

do everything in your power to help get your students where they want to be. Thank you for providing me the tools so that I could be successful in graduate school.

To my amazing Kim Lab and Tauber Lab family, both former and present members, it has been a pleasure working with each and every one of you. Professor Brian Leigh, Professor Mike Tauber, Dr. Guipuen Kang, Dr. Ignacio López-Peña, Jen Daluz, Joel Rivera, Satavisha Jana, Justine Liang, Christina Trinh, Vanessa Tian, Ivan Kozachenko, Derek Dang, Megan Stone, Dr. Samantha Doyle, and Dr. Maria Hatfield thank you for teaching me, laughing with me, crying with me, and being the most supportive colleagues and friends I could ever imagine. I looked forward to going to work because of you, and you have made my graduate school experience one that I will never forget. I am so lucky to have met and worked with you all.

Thank you to my committee, Professor Andrew Kummel, Professor Andrew McCammon, Professor Brian Zid, and Professor Douglas Smith, who have provided me with excellent research advice and continued support for my projects.

Thank you to the Molecular Biophysics Training Grant (MBTG) for providing me with financial support at UCSD. Thank you for giving me with the opportunity to present my research at multiple conferences so that I could gain valuable feedback on my projects. Thank you to the Inamori Graduate Fellowship at UCSD for your generous scholarship and financial assistance towards my research projects.

To my loving family and friends, you all mean so much to me. I am so lucky to have the love and support of my parents, Steven Asamoto, and Lloyd and Terry Aotaki. Thank you for trusting my decisions and supporting me every step of the way. My brothers, Nathan and Brandan, I am so blessed to have you both and you both continue to inspire me. To my incredible friends that I have met in graduate school, thank you for making these past years such an

unforgettable experience. I can't imagine being in graduate school without you. To my amazing friend, Richard Choi, thank you for being my support system and for your continuous words of encouragement since high school.

Chapter 3, in full, is a reprint of the material as it appears in Methods in Molecular Biology-Lipid Protein Interactions. Methods and Protocols, 2019. Asamoto, DeeAnn K. and Kim, Judy E., Springer Science and Business Media. The dissertation author was the primary investigator and author of this paper.

Chapter 4, in full, is a reprint of the material as it appears in Biophysical Journal, 2019. Asamoto, DeeAnn K.; Kang, Guipeun; and Kim, Judy E., Cell Press. The dissertation author was the primary investigator and author of this paper.

Chapter 5 is currently in preparation for submission. Asamoto, DeeAnn K. and Kim, Judy E. The dissertation author was the primary investigator and author of this paper.

VITA

2014	Bachelor of Science, California State University Long Beach
2014-2015	Teaching Assistant, University of California San Diego
2016	Master of Science, University of California San Diego
2016-2020	Teaching Assistant, University of California San Diego
2021	Doctor of Philosophy, University of California San Diego

PUBLICATIONS

"Bimolecular quenching of tryptophan fluorescence in a membrane protein: Evolution of local solvation and environment during folding into a bilayer"

Asamoto, D.K., Kozachenko, I.A., López-Peña, I., and Kim, J.E. *Spectrochimica Acta Part A: Molecular and Biomolecular Spectroscopy*, **2021**, 260

"The structural basis for monoclonal antibody 5D2 binding to the tryptophan-rich loop of lipoprotein lipase"

Luz, J.G., Beigneux, A.P., **Asamoto, D.K.**, He, C., Song, W., Allan C.M., Morales, J., Tu, Y., Kwok, A., Cottle, T., Meiyappan, M., Fong, L.G., Kim, J.E., Ploug, M., Young, and S.G., Birrane, G. *Journal of Lipid Research*, **2020**, 61(10):1347-1359

"Folding of the β-barrel membrane protein OmpA into nanodiscs"

Asamoto, D.K., Kang, G., and Kim, J.E. *Biophysical Journal*, **2020**, 118,1-12

"UV resonance Raman spectroscopy as a tool to probe membrane protein structure and dynamics. Methods in Molecular Biology- Lipid Protein Interactions. Methods and Protocols"

Asamoto, D.K., and Kim, J.E. Springer Science and Business Media, **2019**, 327-349

PRESENTATIONS

Biophysical Society Meeting, February 2020, *"β-barrel membrane protein folding into nanodiscs"*, poster presentation

Pacific Conference on Spectroscopy and Dynamics, January 2020, *"Spectroscopic tools for a complex problem: membrane protein folding"*, oral presentation

The National American Chemical Society Meeting, August 2019, *"Spectroscopic studies of membrane protein folding into nanodiscs",* poster presentation

American Society for Biochemistry and Molecular Biology, April 2018, *"Folding of a membrane protein into nanodiscs"*, oral presentation

Gordon Research Conference on Membrane Protein Folding, June 2017, *"Investigation of OmpA folding in small unilamellar vesicles and nanodiscs"*, poster presentation

The National American Chemical Society Meeting, March 2016, *"Investigation of membrane protein folding in small unilamellar vesicles and nanodiscs"*, poster presentation

ABSTRACT OF THE DISSERTATION

Folding of a beta-barrel membrane protein into nanodiscs

by

DeeAnn Kiyoko Asamoto

Doctor of Philosophy in Chemistry

University of California San Diego, 2021

Professor Judy E. Kim, Chair

Membrane proteins constitute a significant fraction of cellular proteins due to their vast diversity in function. However, studies of their native structures, folding mechanisms, and dynamics remain a challenge, in part because of their inherent insolubility. One goal of this project is to enhance the tools to study membrane proteins. Small unilamellar vesicles (SUVs) have been used as a bilayer mimetic to investigate membrane protein structures, dynamics, and folding mechanisms. UV resonance Raman spectroscopy (UVRR) has emerged as a powerful technique for probing structures and dynamics of biomolecules. UVRR is particularly valuable

for membrane proteins because of the selective enhancement of signal from key aromatic residues and the ability to probe interactions between membrane protein and the lipid. We present practical considerations and guidelines for UVRR data acquisition, including a detailed description of a typical laser setup as well as the process to analyze the tryptophan vibrational modes of a model β-barrel membrane protein, OmpA, unfolded and folded in SUVs.

An additional need in studies of membrane protein folding is alternate membrane mimics. Nanodiscs (NDs) are an excellent bilayer alternative to SUVs because of their experimental benefits including homogeneity, optical clarity, low light scattering, and enhanced stability. We combine SDS-PAGE mobility studies with fluorescence, circular dichroism, and UVRR spectroscopy to confirm and characterize the folding of OmpA into NDs. Our studies show similar secondary and tertiary structures in both SUVs and NDs as well as efficient folding yields greater than 88% in both bilayers. The folding of OmpA into NDs was slower compared to in SUVs, and this difference can be attributed to the different bilayer characteristics.

Insights into the folding mechanism of OmpA were gained via bimolecular fluorescence quenching with acrylamide quencher. Stern-Volmer analysis utilizing the sphere-of-action model probed changes in local environment and protein solvation during folding into NDs. An initial fast step after initiation of the folding reaction, associated with a large change in polarity to a hydrophobic environment was attributed to a fast adsorption and interaction with the lipid bilayer. Desolvation kinetics were slower than the formation of tertiary structure, indicating that desolvation may occur in the final steps of folding.

Chapter 1
Introduction

1.1 The launch of the protein-folding field

The protein-folding problem was first introduced nearly 60 years ago, after the 1962 Nobel Prize in chemistry was awarded to John Kendrew and Max Perutz for determination of the first atomic structures of globular proteins, haemoglobin and myoglobin, by X-ray crystallography. John Kendrew was a biochemist and X-ray crystallographer who, with the help of his colleagues determined the first 6 Å structure of myoglobin in 1958 [1] and Max Perutz was a molecular biologist who helped determine the first 5.5 Å structure of haemoglobin in 1960 [2]. After studying his 1958 structure of myoglobin, John Kendrew was intrigued by the lack of symmetry and complexity displayed by his structure, which contributed to the launch of the protein-folding problem [3].

The structure determination of myoglobin and haemoglobin sparked the interest in the correlation between globular structure of biomolecules and their biological functions. Three very general and broad questions that encompass the protein-folding problem were presented [3]: 1) The physical folding code: How does a protein's amino acid sequence dictate or encode its native structure? 2) Protein folding mechanisms: How does a protein fold so quickly to the correct native state? 3) Computer algorithms: How can we use technology to accurately predict structures and function based on their sequences? Though there has been much advancement in the field of protein folding over the past decade, many challenges and open questions still remain.

1.2 The significance of studying membrane protein folding

Cellular membrane proteins (MPs) constitute approximately 30% of the human genome and account for about 60% of drug targets [4]. Peripheral MPs are typically associated with the

head group region of a membrane, while integral membrane proteins are incorporated into and traverse the lipid bilayer. Integral MPs serve a variety of cellular roles including but not limited to, the transportation of molecules into and out of a cell, the anchoring of molecules to a membrane surface, as receptors to cell signaling, as enzymes for catalyzed reactions, and as structural support giving shape to the membrane surface [5-8] (Figure 1.1). The structure and dynamics of a MP dictates its specific function within a cell and therefore it is critical to continue developing techniques to study MP structures and dynamics within native-like lipid environments.

Despite their importance to cellular function, relatively little information is known about integral MPs in terms of their native structures, dynamics, and folding mechanisms within lipid bilayers, compared to soluble proteins. MPs in general are challenging to study for a number of reasons, and methods used to study soluble proteins are not always sufficient in the study of MPs. For example, detergents are required to solubilize most MPs, which can alter their native function and stability. Another challenge is that MPs are difficult to work with and most tend to denature or aggregate outside of their native membranes. Lastly, the expression, isolation, and purification of many MPs is not an easy task and may require multiple protein expression protocols to acquire adequate yields of MPs in order to carry out experiments. This disadvantage can result in a significant amount of time to produce sufficient yields of MPs before any experiments can be performed in the lab.

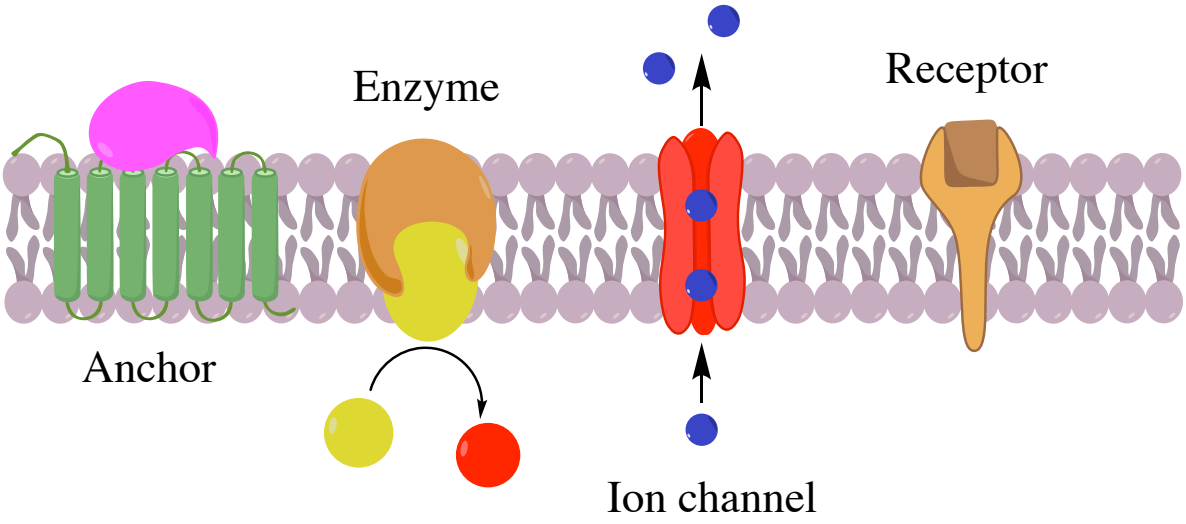

Figure 1.1 Cellular roles of integral membrane proteins; image adapted from reference [9]. Integral membrane proteins can act as anchors to the membrane, enzymes for catalyzed reactions, ion channels for transport into and out of the cell, and receptors for cellular signals.

There has been great progress made in the understanding of the dynamics, structures, and folding mechanisms of MPs within the past few decades. Spectroscopic methods of studying protein folding include the following: circular dichroism (CD) spectroscopy, fluorescence spectroscopy, bimolecular fluorescence quenching, nuclear magnetic resonance (NMR) spectroscopy, Förster resonance energy transfer (FRET), and UV resonance Raman (UVRR) spectroscopy. CD spectroscopy reports on a protein's secondary structure and can elucidate the formation of a MP's α-helical and/or β-sheet content [10]. Fluorescence spectroscopy has been used extensively to report on local changes in the polarity of protein fluorophore environment [10-12].For example, global conformational changes in proteins have been studied using tryptophan fluorescence and can probe whether proteins are in a folded or unfolded state based on the emission maximum [12, 13]. Bimolecular fluorescence quenching has been used to investigate protein dynamics and probe changes in protein solvation [14, 15]. FRET is a spectroscopic technique involving energy transfer via long-range dipole-dipole interactions between an excited state donor and ground state acceptor [10]. Strategic placement of a donor and an acceptor within a protein domain allows for distance determination and can probe changes in tertiary structure and protein dynamics [11, 16]. NMR spectroscopy has been used for studying protein folding mechanisms as well as providing structural information [10]. NMR has the capability to reveal unfolded, folded, and intrinsically disordered protein states [17-19]. UVRR spectroscopy is a vibrational technique used for probing the structures and dynamics of biological macromolecules with experimental advantages, which include enhanced aromatic amino acid signal and selectivity in addition to the absence of the need for extrinsic labeling [20-22]. UVRR reports on MP conformations within bilayers as well as providing information on their molecular dynamics [23-25].

Non-optical structural methods include gel differential mobility assays (SDS-PAGE) and mass spectrometry. Changes in a protein's tertiary conformation can be monitored by observing shifts in their apparent molecular weight gel bands due to differences in the "compactness" of their folded and unfolded structures [10, 26-28]. The fraction of folded to unfolded protein at time points during a folding reaction provides insights into their folding kinetics and folding yields [10, 26, 27, 29]. Mass spectrometry has been used to elucidate the native structures of MPs within membrane mimics and has also been used to probe MP-lipid interactions [10, 30, 31]. Determination of MP native structures within bilayers is vital in understanding their dynamics and folding mechanisms.

Each of the experimental techniques described above comes with their own advantages as well as disadvantages, and the study of MP folding continues to progress. However, fundamental details involved in MP folding mechanisms, structures, and dynamics that could lead to advances in the fields of medicine, pathology, chemistry, biology, and biophysics, remain in question. Thus, improved tools and techniques that enable more extensive studies are desired.

1.3 Structures of integral membrane proteins

The structures of integral MPs within a lipid bilayer can be described by thermodynamic reasoning. The primary sequence of any protein contains a variety of hydrophilic and hydrophobic amino acid residues. Typically, insertion of an integral MP into a lipid bilayer requires that the hydrophilic, especially ionic, residues are oriented away from the hydrophobic interior of the lipid core [32]. It has been estimated that the electrostatic free energy, ΔG, for the transfer of an ion-pair from water to the interior of a lipid bilayer is greater than +50 kcal/mol, making the exposure of an ion-pair to the hydrophobic lipid environment highly unfavorable [33]. A second consideration in the formation of protein structure within a membrane is the

formation of hydrogen bonds. The hydrogen bonds formed from the carbonyl and amide backbone within a protein structure, and within the bilayer environment, must be more energetically favorable than the hydrogen bonds formed with the solvent water [34].

Two structural motifs, a-helix and b-sheet, are found for integral MPs. In the α-helix structure, typically the N-terminal side of the transmembrane domain is exposed to the extracellular region and the C-terminal side of the chain is located on the cytoplasmic side of the membrane [33]. The majority of amino acid residues that form an α-helix chain are hydrophobic and are in direct contact with the lipid membrane. The α-helix structure forms the maximum number of hydrogen bonds within its polypeptide chain and transmembrane proteins can exist either as single-pass or multipass α-helices [35]. The α-helix structure of integral MPs is most common in the inner membrane of a cell, where they are transported into the membrane via the Sec61αβγ (eukaryotes) and SecYEG (bacteria) translocon complexes [36]. Common functions of α-helical membrane proteins include signal recognition, receptors, transporters, and energy translocation and conservation [37].

Polypeptide chains can also be arranged as a β-sheet structure in the form of a β-barrel, which are abundant in the outer membrane of mitochondria, chloroplasts, and bacteria [35]. In this conformation, the transmembrane segments are composed of 8-22 β-strands, where the hydrogen-bonding network occurs between each antiparallel β-sheet [35]. Proteins that form β-barrel structures function as transporters, porins, receptors, enzymes, and act as structural proteins due to their more rigid structure compared to α-helices. MPs which form transmembrane β-barrel structures are comprised of less hydrophobic residues than those that form α-helical structures [38]. Outer membrane proteins are synthesized in the cytoplasm, and are transported across the inner membrane, through the periplasm and peptidoglycan layer, and directed to the

outer membrane via the SecYEG translocon, SurA and Skp chaperones, and the β-barrel assembly machinery (BAM) complex [39].

1.4 Outer membrane Protein A (OmpA) as a model for folding studies

The inherent complications of MPs in their complex lipid environments are an impediment towards comprehensive biophysical studies and as a result, only a limited number of MPs are suitable for *in vitro* folding studies. Outer membrane protein A (OmpA) is an ideal model system for the study of β-barrel MPs because it is completely soluble in 8 M urea and spontaneously folds and inserts into a variety of lipid environments including small unilamellar vesicles (SUVs) [12, 28, 40, 41] and nanodiscs (NDs) [42] without the use of detergents. OmpA consists of 325 amino acid residues, which make up a transmembrane domain of 8 antiparallel β-strands and a soluble C-terminal periplasmic domain [43]. OmpA is the most abundant outer membrane protein found in *Escherichia coli* and serves as a structural protein, providing linkage between the cell's peripheral domain and peptidoglycan layer [29]. In addition, studies have shown OmpA to serve as a bacteriophage receptor and a non-specific small ion channel [44, 45]. The general family of outer membrane proteins has been found in the outer membrane of Gram-negative bacteria, chloroplasts, and mitochondria [46].

The high-resolution structure of OmpA's transmembrane domain has been well characterized by various methods, which makes this protein an ideal system for studies of protein folding. The X-ray crystal structure of the transmembrane domain (PDB ID 1QJP) and the NMR structure of the soluble domain are shown in Figure 1.2. The transmembrane domain of wild type OmpA contains five native tryptophan residues (highlighted in Figure 1.2), which are excellent spectroscopic probes for protein folding studies and are critical to the work in this dissertation.

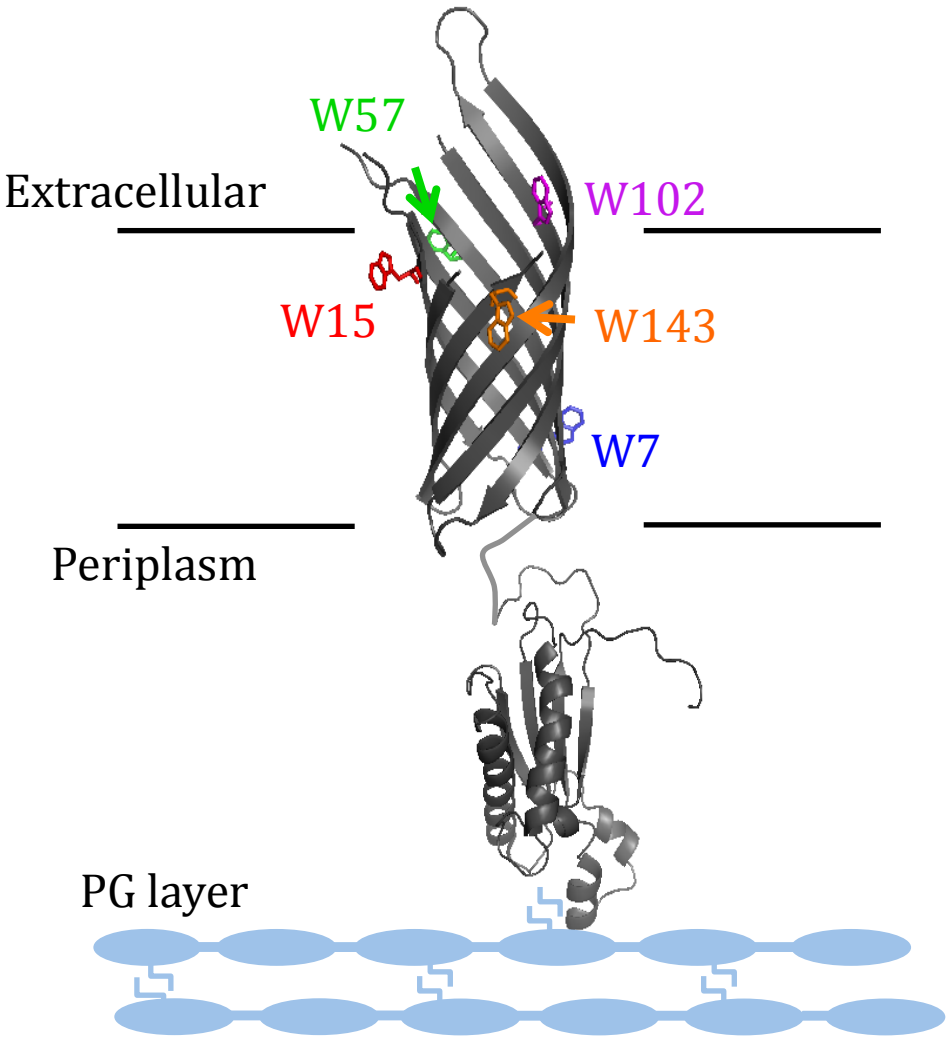

Figure 1.2 The X-ray crystal structure of the transmembrane domain (PDB ID 1QJP) and solution NMR structure (PDB ID 2MQE) of the periplasmic domain of OmpA. Five native tryptophan residues at locations 7, 15, 57, 102, and 143 are shown in blue, red, green, magenta, and orange, respectively. The proposed two-domain structure is adapted from reference [47]. The location and orientation of the soluble domain relative to the lipid bilayer is not known and thus, is arbitrary in this figure. The lipid bilayer is represented as black horizontal lines. The peptidoglycan-layer (PG-layer) is shown as blue ovals, and has been proposed to interact with the soluble tail of OmpA by reference [47].

1.5 Tryptophan is an intrinsic probe for *in vitro* folding studies

Tryptophan is an abundant amino acid in MPs and commonly resides near the membrane-water interface [24, 32, 48]. The prevalence of tryptophan in MPs compared to soluble proteins can be attributed to its amphipathic characteristics, as the structure of its hydrophobic indole moiety contains a nitrogen that is capable of forming hydrogen bonds. In part because of the favorable thermodynamics associated with its presence at the bilayer-water interface, tryptophan plays important roles in stabilizing native protein conformations within a membrane bilayer, anchoring proteins to the membrane, and helping to minimize hydrophobic mismatch [24, 48].

Tryptophan fluorescence is a commonly used tool to study MP folding as it reports on the local tryptophan environment and thus, provides insights into changes in protein conformation [10-12, 40]. This ability to act as a probe originates from the inherent photophysics of indole. The indole moiety of tryptophan has two nearly degenerate excited states, ^1L_a and ^1L_b, which arise from $\pi \rightarrow \pi^*$ transitions, and are oriented perpendicular to one another (Figure 1.3 inset)[49]. The ^1L_a excited state exhibits a large permanent dipole moment, as it is aligned through the nitrogen atom, which gives rise to the high sensitivity of tryptophan to the local environment [11, 49]. The dependence of solvent polarity on tryptophan fluorescence has been well characterized and it is known that when tryptophan is exposed to a nonpolar environment such as a lipid bilayer core, the observed emission maximum will be blue-shifted relative to polar environments like water (Figure 1.3)[40, 49, 50].

In our studies, tryptophan fluorescence is utilized as a marker to distinguish between varying OmpA states in different environments. For example, emission maxima can distinguish between OmpA denatured in urea and OmpA folded in two different bilayer mimetics, small unilamellar vesicles and nanodiscs. Bimolecular tryptophan fluorescence quenching with

acrylamide is used to probe OmpA transmembrane solvation kinetics during folding into vesicles and nanodiscs.

In addition to the use of tryptophan fluorescence for folding studies, we have employed a vibrational technique (UVRR spectroscopy), which, with an appropriate excitation wavelength, can selectively enhance signal from aromatic residues including tryptophan, tyrosine, and phenylalanine. UVRR is an inelastic photon-molecule scattering technique, where the energy of a photon is transferred to or from the molecule and the difference between the scattered and incident photon energies, called the Raman Shift, is a vibrational frequency of the molecule [23]. Membrane proteins contain an abundance of aromatic residues, which readily adsorb light in the UV region. Hence, UVRR with 228 nm excitation allows for the study of MPs with minimal contributions from other residues, amide backbone, and buffer. UVRR studies reveal structures and dynamics of these aromatic residues including but not limited to, hydrogen-bonding, cation-π and π-π interactions, dihedral torsion angles, and environment polarity [21-23].

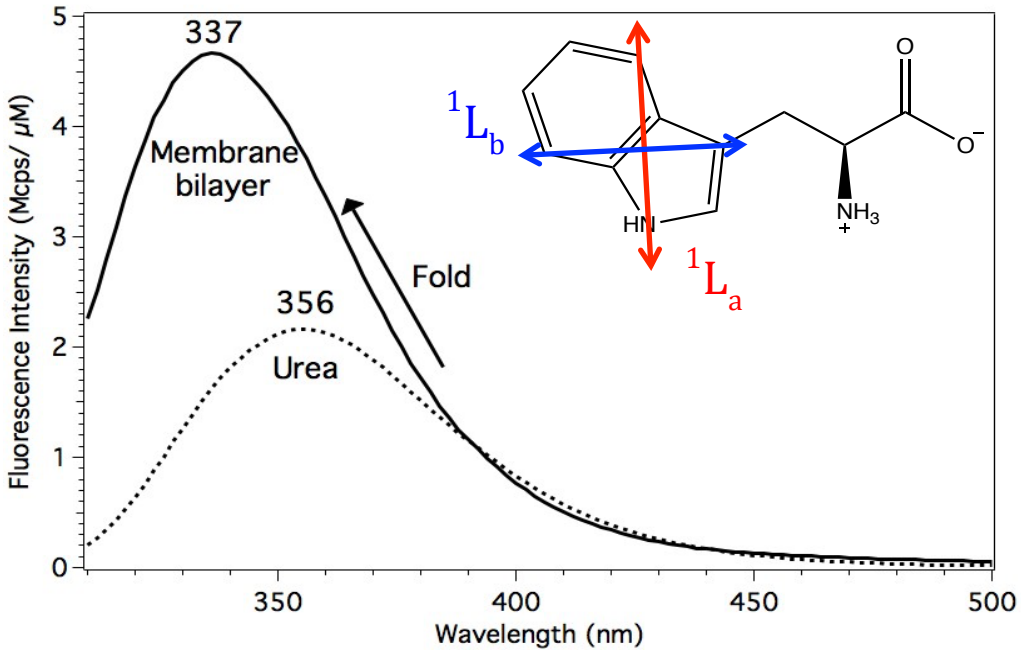

Figure 1.3 Tryptophan fluorescence spectra in folded and unfolded conformations. Tryptophan exhibits a fluorescence maximum of 337 nm when OmpA is folded in small unilameller vesicles (solid). When OmpA is unfolded in aqueous urea, the fluorescence maximum is red-shifted to 356 nm (dashed). The inset shows the indole moiety of tryptophan and the ^1L_a and ^1L_b transition moments are indicated with red and blue arrows, respectively.

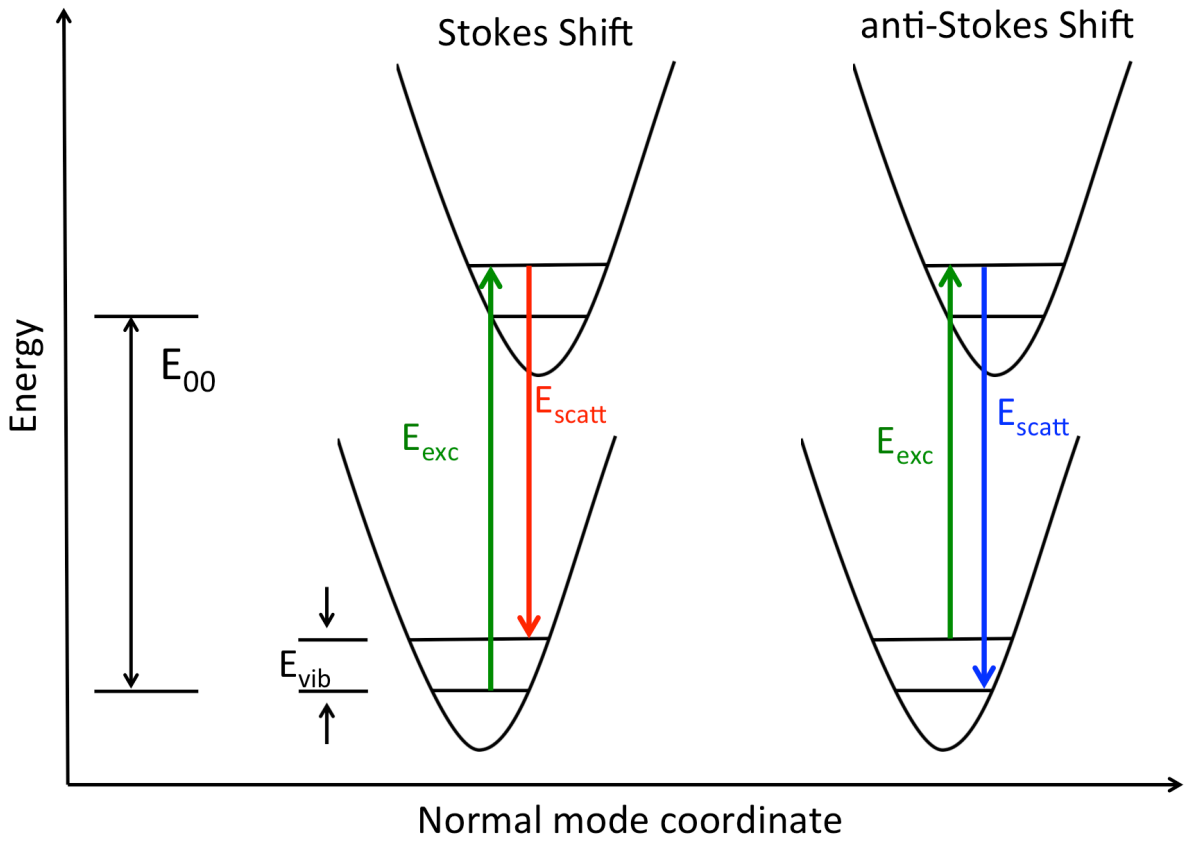

Figure 1.4 Schematic of the resonance Raman scattering process, adapted from reference [21]. The excitation and scattered energies are labeled as E_{exc} (green) and E_{scatt} (red and blue), respectively. The Stokes shift diagram is shown on the left, where $E_{scatt} < E_{exc}$. The anti-Stokes shift diagram is shown on the right, where $E_{scatt} > E_{exc}$. The Raman Shift, denoted as E_{vib}, is the difference in vibrational energy between E_{exc} and E_{scatt}. Also shown is the zero-zero energy of the absorption band, labeled as E_{00}.

1.6 References

[1] J.C. Kendrew, G. Bodo, H.M. Dintzis, R.G. Parrish, H. Wyckoff, D.C. Phillips, A three-dimensional model of the myoglobin molecule obtained by x-ray analysis, *Nature* 181 (1958) 662-6.

[2] H. Muirhead, M.F. Perutz, Structure of haemoglobin. A three-dimensional fourier synthesis of reduced human haemoglobin at 5-5 A resolution., *Nature* 199 (1963) 633-8.

[3] K.A. Dill, J.L. MacCallum, The protein-folding problem, 50 years on, *Science* 338 (2012) 1042-6.

[4] Y. Arinaminpathy, E. Khurana, D.M. Engelman, M.B. Gerstein, Computational analysis of membrane proteins: the largest class of drug targets, *Drug Discovery Today* 14 (2009) 1130-5.

[5] M. Simunovic, E. Evergren, A. Callan-Jones, P. Bassereau, Curving cells inside and out: roles of BAR domain proteins in membrane shaping and its cellular implications, *Ann. Rev. Cell Dev. Biol.* 35 (2019) 111-29.

[6] A.M. Whited, A. Johs, The interactions of peripheral membrane proteins with biological membranes, *Chem. Phys. Lipids* 192 (2015) 51-9.

[7] N. Sukumar, S. Liu, W. Li, F.S. Mathews, B. Mitra, P. Kandavelu, Structure of the monotopic membrane protein (S)-mandelate dehydrogenase at 2.2 Å resolution, *Biochimie* 154 (2018) 45-54.

[8] P.D. Bosshart, D. Fotiadis, Secondary active transporters, *Subcell Biochem.* 92 (2019) 275-99.

[9] B. Alberts, D. Bray, K. Hopkin, A. Johnson, J. Lewis, M. Raff, K. Roberts, P. Walter, Essential Cell Biology, Garland Science, 2010.

[10] J.E. Horne, S.E. Radford, A growing toolbox of techniques for studying β-barrel outer membrane protein folding and biogenesis, *Biochem. Soc. Trans.* 44 (2016) 802-9.

[11] G. Kang, I. Lopez-Pena, S. Bhakta, J.E. Kim. Probing membrane protein structure and dynamics by fluorescence spectroscopy. Encyclopedia of Analytical Chemistry: John Wiley & Sons, Ltd; 2013. p. 1-21.

[12] J.E. Kim, G. Arjara, J.H. Richards, H.B. Gray, J.R. Winkler, Probing folded and unfolded states of outer membrane protein a with steady-state and time-resolved tryptophan fluorescence, *J. Phys. Chem. B* 110 (2006) 17656-62.

[13] M.R. Eftink, The use of fluorescence methods to monitor unfolding transitions in proteins, *Biophys. J.* 66 (1994) 482-501.

[14] M.R. Eftink, C.A. Ghiron, Exposure of tryptophanyl residues in proteins. Quantitative determination by fluorescence quenching studies, *Biochemistry* 15 (1976) 672-80.

[15] M.R. Eftink, C.A. Ghiron, Fluorescence quenching studies with proteins, *Anal. Biochem.* 114 (1981) 199-227.

[16] J. Yoo, J.M. Louis, I.V. Gopich, H.S. Chung, Three-color single-molecule FRET and fluorescence lifetime analysis of fast protein folding, *J. Phys. Chem. B* 122 (2018) 11702-20.

[17] P. Rath, T. Sharpe, B. Kohl, S. Hiller, Two-state folding of the outer membrane protein X into a lipid bilayer membrane, *Angew. Chem. Int. Ed. Engl.* 58 (2019) 2665-9.

[18] V.S. Mandala, J.K. Williams, M. Hong, Structure and dynamics of membrane proteins from solid-state NMR, *Annu. Rev. Biophys.* 47 (2018) 201-22.

[19] B. Liang, L.K. Tamm, NMR as a tool to investigate the structure, dynamics and function of membrane proteins, *Nat. Struct. Mol. Biol.* 23 (2016) 468-74.

[20] S.A. Oladepo, K. Xiong, Z. Hong, S.A. Asher, Elucidating peptide and protein structure and dynamics: UV resonance Raman spectroscopy, *J. Phys. Chem. Lett.* 2 (2011) 334-44.

[21] I. López-Peña, B.S. Leigh, D.E. Schlamadinger, J.E. Kim, Insights into protein structure and dynamics by ultraviolet and visible resonance Raman spectroscopy, *Biochemistry* 54 (2015) 4770-83.

[22] B.S. Leigh, D.E. Schlamadinger, J.E. Kim, Structures and dynamics of proteins probed by UV resonance Raman spectroscopy, Biophysical Methods for Biotherapeutics: Discovery and Development Applications, First Edition (2014) 243-68.

[23] D.K. Asamoto, J.E. Kim, UV resonance Raman spectroscopy as a tool to probe membrane protein structure and dynamics, *Methods Mol. Biol.* 2003 (2019) 327-49.

[24] K.M. Sanchez, G. Kang, B. Wu, J.E. Kim, Tryptophan-lipid interactions in membrane protein folding probed by ultraviolet resonance Raman and fluorescence spectroscopy, *Biophys. J.* 100 (2011) 2121-30.

[25] K.M. Sanchez, T.J. Neary, J.E. Kim, Ultraviolet resonance Raman spectroscopy of folded and unfolded states of an integral membrane protein, *J. Phys. Chem. B* 112 (2008) 9507-11.

[26] J.H. Kleinschmidt, L.K. Tamm, Secondary and tertiary structure formation of the beta-barrel membrane protein OmpA is synchronized and depends on membrane thickness, *J. Mol. Biol.* 324 (2002) 319-30.

[27] G.J. Patel, S. Behrens-Kneip, O. Holst, J.H. Kleinschmidt, The periplasmic chaperone Skp facilitates targeting, insertion, and folding of OmpA into lipid membranes with a negative membrane surface potential, *Biochemistry* 48 (2009) 10235-45.

[28] T. Surrey, F. Jähnig, Kinetics of folding and membrane insertion of a beta-barrel membrane protein, *J. Biol. Chem.* 270 (1995) 28199-203.

[29] J.S. Park, W.C. Lee, K.J. Yeo, K.S. Ryu, M. Kumarasiri, D. Hesek, M. Lee, S. Mobashery, J.H. Song, S.I. Kim, J.C. Lee, C. Cheong, Y.H. Jeon, H.Y. Kim, Mechanism of anchoring of OmpA protein to the cell wall peptidoglycan of the gram-negative bacterial outer membrane, *FASEB J.* 26 (2012) 219-28.

[30] J.R. Bolla, M.T. Agasid, S. Mehmood, C.V. Robinson, Membrane protein-lipid interactions probed using mass spectrometry, *Annu. Rev. Biochem.* 88 (2019) 85-111.

[31] J. Bender, C. Schmidt, Mass spectrometry of membrane protein complexes, *Biol. Chem.* 400 (2019) 813-29.

[32] M.B. Ulmschneider, M.S. Sansom, Amino acid distributions in integral membrane protein structures, *Biochim. Biophy.s Acta* 1512 (2001) 1-14.

[33] S.J. Singer, The structure and insertion of integral proteins in membranes, *Ann. Rev. Cell Biol.* 6 (1990) 247-96.

[34] C.N. Pace, H. Fu, K. Lee Fryar, J. Landua, S.R. Trevino, D. Schell, R.L. Thurlkill, S. Imura, J.M. Scholtz, K. Gajiwala, J. Sevcik, L. Urbanikova, J.K. Myers, K. Takano, E.J. Hebert, B.A. Shirley, G.R. Grimsley, Contribution of hydrogen bonds to protein stability, *Protein Sci* 23 (2014) 652-61.

[35] A. Uzman, Molecular biology of the cell (4th ed.): Alberts, B., Johnson, A., Lewis, J., Raff, M., Roberts, K., and Walter, P, Biochemistry and Molecular Biology Education 31 (2003) 212-4.

[36] M. Heyden, J.A. Freites, M.B. Ulmschneider, S.H. White, D.J. Tobias, Assembly and stability of α-helical membrane proteins, *Soft Matter* 8 (2012) 7742-52.

[37] P.D. Taylor, C.P. Toseland, T.K. Attwood, D.R. Flower, Alpha helical trans-membrane proteins: enhanced prediction using a Bayesian approach, *Bioinformation* 1 (2006) 234-6.

[38] L.K. Tamm, H. Hong, B. Liang, Folding and assembly of beta-barrel membrane proteins, *Biochim. Biophys. Acta* 1666 (2004) 250-63.

[39] J.W. Fairman, N. Noinaj, S.K. Buchanan, The structural biology of β-barrel membrane proteins: a summary of recent reports, *Curr. Opin. Struct. Biol.* 21 (2011) 523-31.

[40] T. Surrey, F. Jähnig, Refolding and oriented insertion of a membrane protein into a lipid bilayer, *Proc. Natl. Acad. Sci. U.S.A.* 89 (1992) 7457-61.

[41] K.M. Sanchez, J.E. Gable, D.E. Schlamadinger, J.E. Kim, Effects of tryptophan microenvironment, soluble domain, and vesicle size on the thermodynamics of membrane

protein folding: lessons from the transmembrane protein OmpA, *Biochemistry* 47 (2008) 12844-52.

[42] D.K. Asamoto, G. Kang, J.E. Kim, Folding of the β-barrel membrane protein OmpA into nanodiscs, *Biophys. J.* 118 (2020) 403-14.

[43] J.H. Kleinschmidt, Membrane protein folding on the example of outer membrane protein A of *Escherichia coli*, *Cell. Mol. Life Sci.* 60 (2003) 1547-58.

[44] R. Morona, C. Krämer, U. Henning, Bacteriophage receptor area of outer membrane protein OmpA of *Escherichia coli* K-12, *J. Bacteriol.* 164 (1985) 539-43.

[45] A. Arora, D. Rinehart, G. Szabo, L.K. Tamm, Refolded outer membrane protein A of *Escherichia coli* forms ion channels with two conductance states in planar lipid bilayers, *J. Biol. Chem.* 275 (2000) 1594-600.

[46] R. Misra, Assembly of the β-barrel outer membrane proteins in gram-negative bacteria, mitochondria, and chloroplasts, *ISRN Mol. Biol.* 2012 (2012) 708203.

[47] H. Ishida, A. Garcia-Herrero, H.J. Vogel, The periplasmic domain of *Escherichia coli* outer membrane protein A can undergo a localized temperature dependent structural transition, *Biochim. Biophys. Acta.* 1838 (2014) 3014-24.

[48] A.J. de Jesus, T.W. Allen, The role of tryptophan side chains in membrane protein anchoring and hydrophobic mismatch, *Biochim. Biophys. Acta* 1828 (2013) 864-76.

[49] J.R. Lakowicz, Principles of Fluorescence Spectroscopy, 3rd Edition, 3 ed, Springer Science + Business Media, LLC, New York, USA, 2006.

[50] D.E. Schlamadinger, J.E. Gable, J.E. Kim, Hydrogen bonding and solvent polarity markers in the uv resonance raman spectrum of tryptophan: application to membrane proteins, *J. Phys. Chem. B* 113 (2009) 14769-78.

Chapter 2
Methods

2.1 Expression, isolation, and purification of OmpA and mutants

The protocol for the expression, isolation, and purification of wild-type OmpA and single tryptophan OmpA mutants was followed according to a previously established procedure [1-3]. Wild-type OmpA contains five native tryptophan residues that span its transmembrane domain at positions 7, 15, 57, 102, and 143. Single tryptophan OmpA mutants were generated by mutation of four of the five native tryptophan residues to phenylalanine residues, leaving single tryptophan residues at positions 7, 15, 57, 102, or 143; these single-tryptophan mutants are referred to as W7, W15, W57, W102, and W143, respectively. OmpA W129 is a mutant with a single non-native tryptophan residue at position 129 and phenylalanine residues at positions 7, 15, 57, 102, and 143 (W7F/W15F/W57F/W102F/W143F/Y129W). The W129 OmpA mutant is particularly interesting because the position of this non-native tryptophan residue is located on the periplasmic side of the barrel, opposite to the native tryptophan residue at position 7. This particular mutant has been previously shown in folding studies to reveal site-specific spectroscopic signatures, unique to the tryptophan at this position [4].

OmpA was overexpressed using the *E. coli* JF733 strain (Genetic Stock Center, Yale University). An *E.coli* cell starter growth was made by inoculating frozen cell stocks into lysogeny broth (LB) media. The starter growth was allowed to incubate at 37 °C and shaken at 180 rpm for at least 10 hours. After 10 hours, the absorbance at 600 nm of the overnight cloudy bacteria solution was obtained. Under sterilized conditions, the cloudy overnight cell growth was transferred to two centrifuge tubes and spun down at 6000 rpm for 10 minutes at 4 °C using a floor centrifuge and JA-14 rotor. The cell pellet was re-suspended and washed twice with fresh

LB media that contains 50 mg/mL ampicillin. The re-suspended cells were evenly distributed to large, 6 L flasks containing 2 L sterilized LB media and ampicillin in each flask. The flasks containing the cells were allowed to incubate at 37 °C and shaken at 180 rpm until the absorbance of the cells at 600 nm reached ~ 1 OD, typically ~ 8 hours. Isopropyl β-D-thiogalactoside (IPTG) was added to each flask (1 mL/L of 1 M IPTG) to allow for the overexpression of OmpA. After reaching an OD_{600} of ~ 1 (~8 hours), the cells were spun down at 6000 rpm into pellets using a centrifuge for 10 minutes at 4 °C. Under sterilized conditions, the pellets were combined and washed twice, using 10 mM Tris buffer. The washed cell pellet was stored at -80 °C until cell lysis. Typically, a 12 L growth produced a pellet that ranged between 10 to 25 grams, depending on the OmpA mutant.

The frozen cell pellet was allowed to defrost for ~ 1 hour in an ice bath. While stirring on ice, 55 mL of cold 0.75 M sucrose in 10 mM Tris-HCl buffer at pH 7.8 was added to the defrosted cells. Additionally, 55 mL of cold 20 mM EDTA and 0.5 mg/mL lysozyme was added slowly to the mixture. Finally, 1-1.5 mL of 100 mM phenylmethylsulfonyl fluoride (PMSF) dissolved in isopropanol was added and the cells were allowed to stir for ~ 1 hour on ice. The cells were lysed fully by sonication using a 1/2" horn sonicator tip at 50% duty cycle for 5 minutes with 70% maximum amplitude until the solution's appearance was a cloudy yellow/brown with no visible clumps. The sonicated solution was centrifuged using a JA-17 rotor for 15 minutes at 5,000 rpm and at 4 °C. The supernatant was transferred to clean centrifuge tubes and spun down for 1.5 hours at 17,000 rpm and at 4 °C. The brownish-red pellets contained OmpA (and other membrane proteins) and were stored at -80 °C until extraction.

When ready for extraction, the pellets were allowed to defrost in an ice bath for ~ 1 hour and 70 mL of pre-extraction buffer which contained 3.5 M urea, 20 mM Tris-HCl, and 0.05% (v/v) 2-ME at pH 9.0 was added to the defrosted pellets. The solution was kept on ice and continuously stirred for 1 hour or until no clumps were visible and the solution was a yellowish/brown color. The dissolved solution was placed in the centrifuge using a JA-17 rotor for 2 hours and spun at 17,000 rpm at 4 °C. The reddish/brown pellets contained the integral membrane proteins, including OmpA.

The pellets were combined and dissolved using a mixture of 1:1 mixture of extraction buffer (8.0 M urea, 20 mM Tris-HCl, and 0.1% (v/v) 2-ME at pH 8.5) and isopropanol. The solution was continuously stirred on ice for ~ 1 hour (or until no visible clumps). The dissolved solution was centrifuged for 1.5 hours at 17,000 rpm at 4 °C. The supernatant contained crude OmpA and the concentration of the crude protein was obtained by taking a UV-Vis absorption spectrum. The molar extinction coefficients used to calculate the crude OmpA concentrations is shown in Table 2.1.

Purification of crude OmpA utilized anion exchange chromatography using a HiTrap Q Sepharose Fast Flow (GE Healthcare) column. Prior to protein injection, the column was equilibrated with a buffer containing 8.0 M urea, 15 mM Tris-HCl, and 0.05% (v/v) 2-ME at pH 8.5. The protein was eluded with increasing concentrations of NaCl ranging from 0 to 200 mM in a buffer containing 8.0 M urea, 15 mM Tris-HCl, and 0.05% (v/v) 2-ME at pH 8.5. Fractions of purified OmpA were collected and their absorbance spectra were obtained using an Agilent 8453 UV-Visible spectrometer. The fractions were concentrated and desalted using an Amicon ultrafiltration stirred cell with YM-3 membrane. The concentration buffer contained 8.0 M urea

in 20 mM potassium phosphate (KP_i) buffer at pH 7.3. The final concentrations of OmpA ranged from 150 – 400 μM and the concentrated samples were stored at -80 °C.

Table 2.1 Molar extinction coefficients used to calculate OmpA concentrations

OmpA	**ε_{280} (M^{-1} cm^{-1})**
Wild-type	54,394
1 W mutant (7,15,57,102,143)	32,326
1 W mutant (129)	30,749
0 W mutant	26,809
1 W mutant truncated transmembrane domain (contains only residues 1-177)	26,018

2.2 Preparation of small and large unilamellar vesicles

Small unilamellar vesicles (SUVs) were prepared according to a published procedure [1]. Briefly, 25 mg of 1,2-dimyristoyl-*sn*-glycero-3-phosphocholine (DMPC, T_m = 23 °C, Avanti Polar Lipids) was continuously dried under nitrogen gas for at least 5 hours. The dried lipids were re-suspended in 5 mL of 20 mM potassium KP_i buffer at pH 8.0 to achieve a final lipid concentration of 5 mg/mL. The lipid solution was sonicated using a probe ultrasonic microtip at 50% duty cycle with 30% maximum amplitude for 30 minutes. The final 50 nm diameter SUVs were passed through a 0.22 μm filter to remove any remaining particles. The SUV solution was allowed to equilibrate overnight at 41 °C prior to experiments. The identical procedure was followed for 1,2-dipalmitoyl-*sn*-glycero-3-phosphocholine (DPPC, T_m = 41 °C, Avanti Polar Lipids).

Large unilamellar vesicles (LUVs) were generated by re-suspending 25 mg of DMPC lipid in 5 mL of 20 mM KP_i buffer at pH 8.0 to create a 5 mg/mL lipid solution. The lipid solution was bath sonicated for 5 minutes and then extruded through a 0.1 or 0.2 μm pore size polycarbonate membrane filter 22 times to produce 100 and 200 nm diameter LUVs [5]. The final LUV solutions were allowed to equilibrate at 41 °C for at least 2 hours prior to use for experiments.

2.3 Preparation of nanodiscs

Nanodiscs (NDs) were prepared according to a published procedure [6]. The 14- residue ND belt peptide, termed 14A, consists of sequence Ac-DYLKAFYDKLKEAF-NH_2 and was purchased from NeoScientific with >98% purity. Lyophilized 14A belt peptide was dissolved in appropriate volumes of 20 mM KP_i buffer at pH 8.0 to make a 10 mg/mL solution. Separately, 25 mg of DMPC lipid was dried by nitrogen gas for at least 5 hours. The dried lipid was re-

suspended in 3.9 mL of 20 mM KP_i buffer at pH 8.0 to make a 6.4 mg/mL lipid solution. A 0.5 mL aliquot of the 10 mg/mL belt peptide solution was added to 0.5 mL of the 6.4 mg/mL re-suspended lipid solution to make a 1 mL total solution of 10 nm diameter NDs [6]. The final lipid:peptide ratio of 1.67 has been shown to produce 10 nm diameter NDs [7]. The final ND solution was allowed to equilibrate at room temperature overnight prior to use for experiments.

2.4 Experimental techniques

2.4.1 UV-Vis absorption spectroscopy

Proteins absorb UV light because of their amide backbone $\pi \rightarrow \pi^*$ transitions (~180-230 nm) [8]. In addition to this absorption by the amide backbone, proteins may also contain electron rich aromatic residues such as tryptophan, tyrosine, and phenylalanine, which contribute to the absorption of UV light around 230-300 nm [8]. Tryptophan possesses four absorption bands which result from $\pi \rightarrow \pi^*$ transitions within its indole moiety: L_a, L_b, B_a, and B_b that correspond to wavelengths: ~ 280, ~ 290, ~ 190, and ~220 nm, respectively. The absorption spectrum with labeled electronic transitions of tryptophan is shown in Figure 2.1. Protein absorption spectra were acquired using an Agilent 8453 UV-Visible spectrometer and protein concentrations were determined by using the tryptophan L_a absorption cross section of 5,500 M^{-1} cm^{-1} at 280 nm [9]. In the data analysis, protein- only absorption spectra were isolated by subtracting absorption and scattering contributions from the solvent, SUV, and ND background.

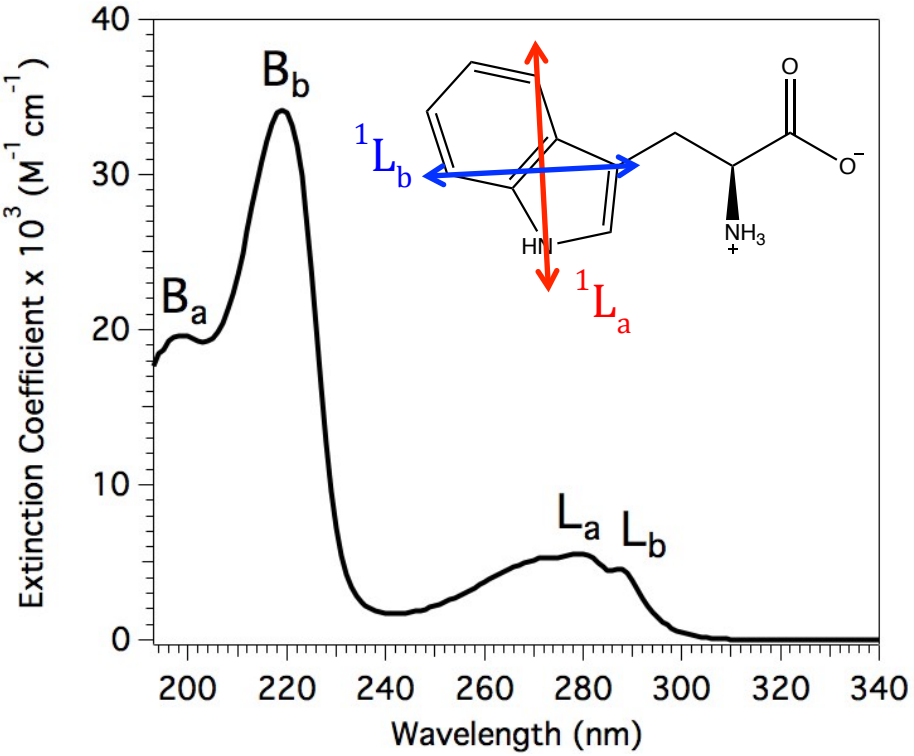

Figure 2.1 The absorption spectrum of L-tryptophan in 20 mM KP_i buffer at pH 7.3. The L_a, L_b, B_a, and B_b transition bands are labeled. The inset shows the structure of L-tryptophan with the labeled transition dipole moments of the excited singlet states ^1L_a and ^1L_b.

2.4.2 Fluorescence spectroscopy

Tryptophan fluorescence is used as an intrinsic probe to report on conformational changes of proteins in different environments. The ^1L_a state possesses a large permanent dipole moment in the excited state, and as a result, this transition gives rise to high sensitivity of the polarity of the local environment surrounding the tryptophan residue [10]. It is well known that when tryptophan is exposed to a polar environment like water, the fluorescence maximum exhibits a relatively red-shifted value of ~ 356 nm. In contrast, when tryptophan is in a more hydrophobic environment, such as buried in a hydrophobic lipid membrane, the fluorescence maximum blue-shifts to ~ 330 nm [10]. The dependence of tryptophan fluorescence maximum with solvent polarity has been well documented [11].

All steady-state fluorescence spectra were acquired using a Jobin-Yvon SPEX Fluorolog FL3-11 spectrofluorometer. A schematic diagram of the model used for all fluorescence experiments is shown in Figure 2.2. Typical protein concentrations for fluorescence experiments ranged from ~5-10 μM. For measurements on folded protein samples, the sample chamber was held at either 33 or 37 °C, which is above the phase transition of the lipid (T_m = 23 °C, Avanti Polar Lipids) to ensure that the lipid bilayer was in the fluid state. Protein measurements on the adsorbed state were obtained at temperatures below the phase transition temperature of the lipid to ensure that the lipid bilayer was in the gel phase. Fluorescence experiments probing the unfolded or aggregated protein states in buffer were carried out at room temperature, without the presence of a lipid bilayer. Various fluorescence cuvettes were used, including 10 × 10 mm (~1.7 mL) or 2 × 10 mm (~200 μL) cells; the specific cuvette is indicated for each experiment. The excitation wavelength for experiments using SUVs or NDs were 290 and 295 nm, respectively. The excitation wavelength of 295 nm for the ND studies was chosen to minimize contribution of

tyrosine residues, particularly from the ND belt peptide. The 14A belt peptide of the NDs used in these experiments contain two tyrosine residues per belt peptide. Typical bandpass and integration time used for experiments were 3 nm and 0.8 seconds, respectively. Protein- only fluorescence spectra were isolated by subtracting fluorescence and scattering signal from the solvent, SUV, and ND background.

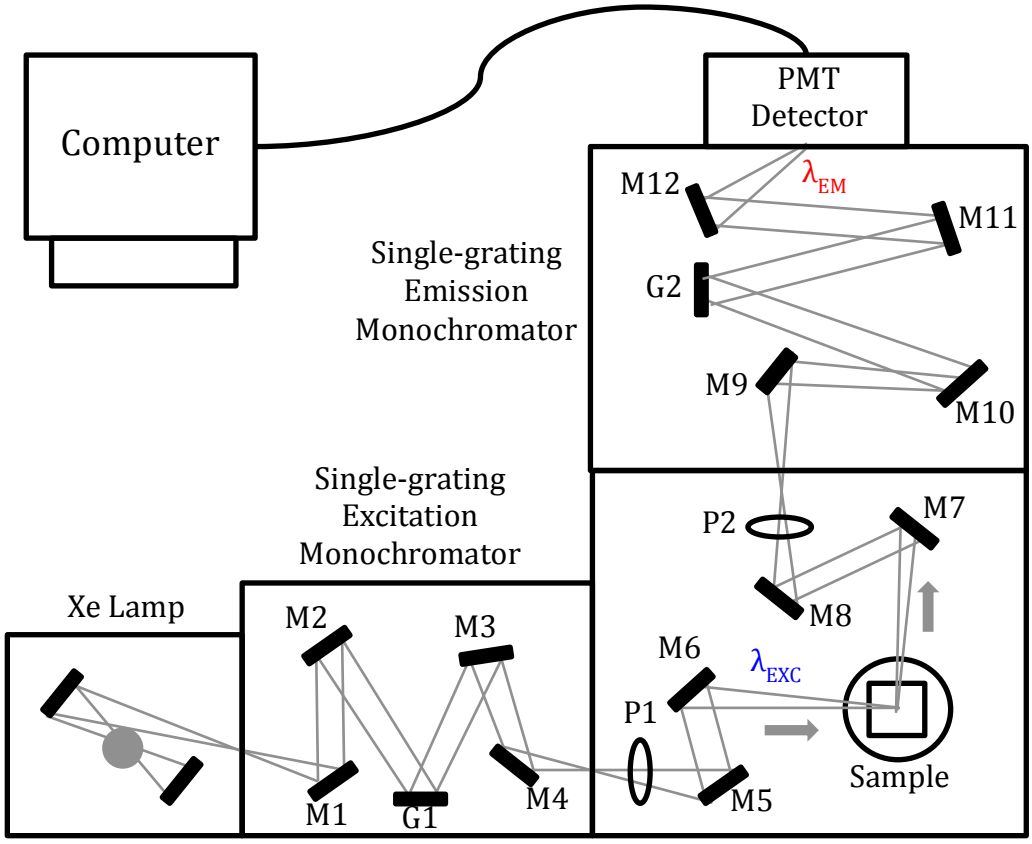

Figure 2.2 Schematic diagram of the Jobin-Yvon FL-11 spectrofluorometer; image adapted from the manual and reference [10]. A high-pressure xenon-arc lamp is used as a white light source (250-750 nm) and light is directed into a single-grating excitation monochromator. The excitation wavelength (λ_{EXC}) is selected and the fluorescence from the sample is collected at right angle geometry to reduce stray-light. The fluorescence photons are directed into a single-grating emission monochromator and the emission wavelength (λ_{EM}) is focused onto a photo multiplier tube (PMT) detector, where the light is transmitted into electronic signal displayed by a computer. Optional polarizers (P1 and P2) are located at the entrance and exit of the sample chamber, respectively, and may be used for anisoptropy measurements. Gratings (G1 and G2) and mirrors (M1-M12) are labeled.

2.4.3 Circular dichroism spectroscopy

Protein secondary structure was probed by circular dichroism spectroscopy using a Jasco J-815 spectrometer. Protein and buffer samples were excited along a 1 mm pathlength sealed quartz cuvette. Typical concentrations of protein for CD experiments ranged from 3-6 μM. The sample chamber was continuously purged with nitrogen gas throughout the duration of the experiment. For protein folding experiments containing SUVs or NDs, the sample chamber was held constant at 37 °C, which is above the lipid phase transition temperature, to ensure the bilayer was present in the fluid phase. All measurements for unfolded or aggregated protein samples in buffer were carried out at room temperature. Measurements on adsorbed protein samples were carried out at temperatures below the phase transition of the lipid, to ensure the presence of the gel phase bilayer. CD spectra were acquired from ~204 – 260 nm, with 1 second digital integration time, 1 nm bandwidth, and 50 nm/min scan speed. An average of 6 scans was obtained for each measurement and background buffer samples were subtracted from protein spectra to isolate signal from protein.

2.4.4 UV Resonance Raman spectroscopy

UV Resonance Raman (UVRR) spectroscopy is a vibrational technique that is sensitive to molecular vibrations of molecules and can report on structural information as well as dynamics of biological macromolecules [12]. UVRR is an excellent spectroscopic tool to study protein dynamics because resonance within UV electronic absorption bands allow for the selective enhancement of signal from aromatic residues including tryptophan, tyrosine, and phenylalanine, as well as the protein amide backbone.

The UVRR Ti:Sapphire laser apparatus has been described elsewhere [12, 13]. A diagram of the UVRR laser used in these studies is shown in Figure 2.3. Briefly, a frequency- doubled

Nd:YLF laser is used to pump a tunable Ti:Sapphire laser, which produces fundamental wavelengths ranging from 826 to 920 nm. The output of the fundamental beam is optimized to produce ~ 1 W of power at a repetition rate of 1 kHz. Second and fourth harmonic wavelengths are generated by use of lithium triborate (LBO) and β-barium borate crystals (BBO), respectively. A Pellin-Broca prism isolates the UV beam and the UV beam is focused onto a vertically mounted fused silica microcapillary. To minimize photodamage, the samples are continuously flowed through the capillary at a flow rate that allows fresh sample for each laser pulse. Typical powers at the sample ranged from ~0.5 – 2.0 mW. A prism-based prefilter collects the scattered photons and substantially minimizes Rayleigh scattering; the Raman scattered photons are passed into a spectrograph which further disperses the Raman photons using a 3600 groove/mm holographic grating (JY Horiba, Spex 500 M). Raman photons are detected with a charge-coupled device (CCD) detector. UVRR protein and buffer spectra were typically collected for 5-10 minutes. Typical protein concentrations ranged from ~5-20 μM, depending on the mutant. To isolate the UVRR spectra of protein, signal from the buffer, SUV and/or ND were subtracted.

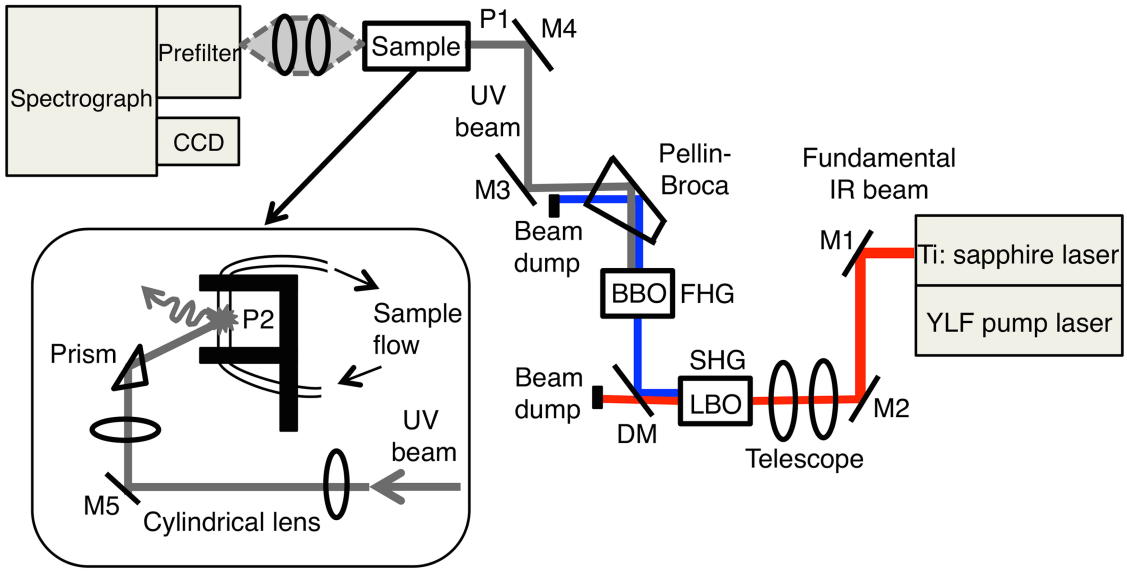

Figure 2.3 Schematic of the UVRR apparatus. The Ti:Sapphire laser is pumped by a YLF laser and produces a fundamental IR beam that is tunable from 700-960 nm. A pair of telescoping lenses collimates the fundamental beam through a lithium triborate (LBO) crystal to produce second harmonic generation (SHG). The second harmonic and fundamental beam is separated by a dichroic mirror (DM). The isolated second harmonic beam enters through a β-barium borate (BBO) crystal to generate a fourth harmonic UV beam (FHG). The UV beam is isolated using a Pellin-Broca prism and the beam is directed to the sample using metal-coated UV enhanced mirrors (M3 and M4). The beam is then directed to the sample using a mirror (M5) and a prism. Two cylindrical lenses focus the beam onto a microcapillary that contains a flowing sample. The Raman scattered photons are collected and focused into a prism-based prefilter and then enters a spectrograph. The Raman spectrum is recorded using a charged-coupled device (CCD) detector. Typically, the beam power is measured at locations P1 and P2. This image is from reference [12].

2.4.5 SDS polyacrylamide gel electrophoresis

Sodium dodecyl sulfate– polyacrylamide gel electrophoresis (SDS-PAGE) is an analytical technique used to separate proteins according to their molecular weight. SDS binds the polypeptide chain and a net negative charge is distributed throughout the molecule. The negatively charged molecule migrates towards an anode (positively charged electrode) in an electric field. Larger molecules migrate at a slower rate relative to smaller molecules within the gel matrix. This differential mobility results in folded and unfolded OmpA having different migration rates and thus, distinct signals on the gel [2].

For SDS-PAGE experiments, approximately 3.5- 6.0 μg of protein was loaded on a 12% polyacrylamide Mini-PROTEAN TGX precast gel. The voltage was set to 150 V and the gels were run at room temperature. The precast gels contained 12% polyacrylamide and the running buffer contained 0.1% SDS. The samples were not boiled prior to loading onto the gels and all gels were stained with Coomassie blue staining buffer.

2.5 References

[1] K.M. Sanchez, J.E. Gable, D.E. Schlamadinger, J.E. Kim, Effects of tryptophan microenvironment, soluble domain, and vesicle size on the thermodynamics of membrane protein folding: lessons from the transmembrane protein OmpA, *Biochemistry* 47 (2008) 12844-52.

[2] T. Surrey, F. Jahnig, Refolding and oriented insertion of a membrane-protein into a lipid bilayer, *Proc. Natl. Acad. Sci. U.S.A.* 89 (1992) 7457-61.

[3] T. Surrey, A. Schmid, F. Jahnig, Folding and membrane insertion of the trimeric beta-barrel protein OmpF, *Biochemistry* 35 (1996) 2283-8.

[4] D.K. Asamoto, G. Kang, J.E. Kim, Folding of the β-barrel membrane protein OmpA into nanodiscs, *Biophys. J.* 118 (2020) 403-14.

[5] R.C. MacDonald, R.I. MacDonald, B.P. Menco, K. Takeshita, N.K. Subbarao, L.R. Hu, Small-volume extrusion apparatus for preparation of large, unilamellar vesicles, *Biochim. Biophys Acta* 1061 (1991) 297-303.

[6] S.H. Park, S. Berkamp, G.A. Cook, M.K. Chan, H. Viadiu, S.J. Opella, Nanodiscs versus macrodiscs for NMR of membrane proteins, *Biochemistry* 50 (2011) 8983-5.

[7] A. Shaw, McLean, M., and Sligar, S., Phospholipid phase transitions in homogenous nanometer scale bilayer discs, *FEBS Lett.* 556 (2003) 260-4.

[8] J.M. Antosiewicz, D. Shugar, UV-Vis spectroscopy of tyrosine side-groups in studies of protein structure. Part 2: selected applications, *Biophys. Rev.* 8 (2016) 163-77.

[9] C.N. Pace, F. Vajdos, G. Grimsley, and T. Gray, How to measure and predict the molar absorption coefficient of a protein., *Protein Sci.* 4 (1995) 2411-33.

[10] G. Kang, Lopez-Pena, I., Bhakta, S., and Kim, J. . Probing membrane protein structure and dynamics by fluorescence spectroscopy. Encyclopedia of Analytical Chemistry: John Wiley & Sons, Ltd; 2013.

[11] D.E. Schlamadinger, J.E. Gable, J.E. Kim, Hydrogen bonding and solvent polarity markers in the UV resonance Raman spectrum of tryptophan: application to membrane proteins, *J. Phys. Chem. B* 113 (2009) 14769-78.

[12] D.K. Asamoto, J.E. Kim, UV resonance Raman spectroscopy as a tool to probe membrane protein structure and dynamics, *Met. Mol. Biol.* 2003 (2019) 327-49.

[13] H.S. Shafaat, K.M. Sanchez, T.J. Neary, J.E. Kim, Ultraviolet resonance Raman spectroscopy of a beta-sheet peptide: a model for membrane protein folding, *J. Raman Spectrosc.* 40 (2009) 1060-4.

Chapter 3

UV Resonance Raman Spectroscopy as a Tool to Probe Membrane Protein Structure and Dynamics

Chapter 3, in full, is a reprint of the material published in Methods in Molecular Biology-Lipid Protein Interactions. Methods and Protocols, Springer Science and Business Media 2019, 327-349.

3.1 Abstract

Ultraviolet Resonance Raman (UVRR) spectroscopy is a vibrational technique that reveals structures and dynamics of biological macromolecules without the use of extrinsic labels. By tuning the Raman excitation wavelength to the deep UV region (e.g. 228 nm), Raman signal from tryptophan and tyrosine residues are selectively enhanced, allowing for the study of these functionally relevant amino acids in lipid and aqueous environments. In this chapter, we present methods on the UVRR data acquisition and analysis of the tryptophan vibrational modes of a model β-barrel membrane protein, OmpA, in folded and unfolded conformations.

3.2 Introduction

Raman spectroscopy has emerged as a powerful tool for probing the structures and dynamics of biomolecules. The Raman effect, first reported in 1928 by physicist C.V. Raman, is an inelastic photon-molecule scattering process in which the energy of the scattered photon is less than or greater than that of the incident photon, called Stokes and anti-Stokes Raman scattering, respectively. In these processes, photon energy has been transferred to or from the molecule, and the difference in photon energy, called the Raman shift, corresponds to a vibrational frequency of the molecule. Hence, a plot of scattered light intensity as a function of Raman shift reveals a vibrational spectrum, which reflects structures, dynamics, and local environment of the molecular scatterer.

The efficiency for the Raman scattering process is proportional to the energies of the photons by $E_{exc}E_{scatt}^3$, where E_{exc} and E_{scatt} are the energies of the excitation and scattered photons, respectively [1, 2]. Because of this strong dependence on photon energy, the Raman effect is inherently weak in the infrared region, with approximately 1 in 10^{10} of incident photons scattered inelastically as Raman photons relative to absorption [1]. Excitation with UV light increases the intensity of Raman scattered photons by orders of magnitude. For example, the efficiency of Raman scattering with 228 nm excitation is approximately 500-fold greater than with 1064 nm excitation. Further enhancement of the Raman effect is achieved under resonance conditions when the energy of the incident photon coincides with an electronic transition of the molecule. Thus in *resonance* Raman spectroscopy, the intensity of scattered light is increased by up to a million-fold, as the case for carotenoids, compared to non-resonant conditions [1, 3, 4].

UV resonance Raman spectroscopy (UVRR) is widely used to selectively enhance Raman signal from chromophores because the vast majority of molecules have an absorption band in the UV region that is easily accessible by modern lasers. Additionally, UVRR offers the benefit of avoiding chemical labels or other modification to the molecule of interest. UVRR with 228 nm excitation is particularly valuable for studies of proteins because this technique selectively reveals vibrational spectra of aromatic residues with minimal contributions of other residues, backbone, or buffer. The fact that membrane proteins are enriched with aromatic residues near the lipid-water interface [5, 6] makes this class of proteins amenable to UVRR. Hence, UVRR is an excellent tool to probe the interactions between membrane proteins and lipid bilayers [5, 7, 8].

Tryptophan is one of the most widely studied chromophores because of its amphipathic nature, ability to participate in hydrogen bonding, and relatively high electrostatic potential to

participate in cation-π and π-π interactions [5, 9, 10]. These non-covalent interactions contribute to the stability of membrane proteins. These important interactions directly impact or are impacted by the orientation of the tryptophan residue in its native conformation. The indole C2-C3-Cα-Cβ dihedral torsion angle, also called $\chi^{2,1}$, can be determined by the Raman frequency of the tryptophan W3 (~1551 cm^{-1}) mode; the correlation between the tryptophan W3 frequency (νW3) and dihedral torsion angle $\chi^{2,1}$ has been reported: $\nu W3 = 1542 + 6.7[\cos 3(\chi^{2,1}) + 1]^{1.2}$ [11, 12].

Another commonly-analyzed vibrational mode of tryptophan is the W7 Fermi doublet. This doublet provides site-specific information about the local environment of a tryptophan residue. The ratio of the intensities of the two peaks that comprise the Fermi doublet (R_{FD}) at ~1362 and ~1340 cm^{-1} is higher for tryptophan exposed to hydrophobic environments relative to hydrophilic environments. For example, excitation of model compound *N*-acetyl tryptophan ethyl ester (NATEE) with 230 nm light results in a relatively high R_{FD} value when NATEE is in hydrophobic environments (up to a value of 1.7 in cyclohexanone), and a lower ratio of 1.1 in the polar environment of water [7]. Hence, UVRR can be used to distinguish tryptophan residues that are buried within the hydrophobic lipid core from those that are in polar environments of bulk water or the water-lipid interface.

Other tryptophan and tyrosine vibrations serve as spectral markers for structure and dynamics [2, 13-15]. The intensities of the W18 indole-breathing mode, W16 benzene-breathing mode, and W1 benzene ring-stretch mode elucidate the local environment polarity. The frequency of the W17 N-H bend mode (~878 cm^{-1}) reveals hydrogen-bonding structure, where lower W17 frequencies correlate to stronger hydrogen bonds [16]. Tyrosine modes also provide valuable molecular information. The intensity ratio of the Fermi doublet (Y1 + 2Y16a) at ~848

and ~827 cm^{-1} is a hydrogen-bond marker. The hydrogen-bond donating or accepting characteristic of tyrosine is revealed in the frequencies of the Y7a and Y8a modes. A tyrosine structural marker is the Y9a mode; the frequency of this mode is sensitive to the extent that the OH group is out of the ring plane. A summary of the vibrational markers is presented in Table 1.

This chapter focuses on the practical considerations for a successful UVRR experiment. The instrumentation as well as considerations of the experimental conditions are discussed first, followed by an analysis of power-dependence data of the model compounds L-tryptophan and L-tyrosine. Representative experiments on mutants of Outer membrane protein A (OmpA) that contain a single tryptophan residue at position 143 (W143) or no tryptophan residues (W0) are presented. The crystal structure of OmpA, showing the residue trp143, is shown in Figure 1. The study of the mutant W143 is particularly insightful because there are vibrational changes associated with folded and unfolded conformations. Three detailed vibrational analyses presented here include the W7 Fermi doublet region, which provides insight into the polarity of tryptophan microenvironment, the tryptophan W3 mode, which provides insight into tryptophan structure via elucidation of the indole C2-C3-Cβ-Cα dihedral torsion angle, and the W17 mode, which reveals the hydrogen-bonding environment of the indole N-H group [5, 11, 12, 16]. Tyrosine modes are not analyzed in this chapter because there are multiple tyrosine residues in OmpA, so site-specific information cannot be easily obtained in this particular protein. Additionally, analysis of absolute tryptophan intensities is not pursued because a proper procedure for instrument-response correction is beyond the scope of this chapter. Overall, the present guidelines should enable a researcher to utilize UVRR to probe any tryptophan- and tyrosine-containing protein, including membrane proteins, in terms of frequency shifts and relative intensities.

Table 3.1 Summary of the prominent L-tryptophan and L-tyrosine vibrational modes in phosphate buffer and their corresponding Raman shifts (cm^{-1}) as shown in Figure 5. The molecular/environmental property that is elucidated by the mode is described as "Marker".

Compound	Mode	Vibrational energy (cm^{-1})	Marker
L-trp	W18	759	environment polarity, π-interactions
	W17	878	H-bonding
	W7	1340, 1362	environment polarity, π-interactions
	W3	1551	structure
L-tyr	Y1+ 2Y16a	827, 848	H-bonding
	Y9a	1178	structure
	Y7a	1207	proton-donating strength
	Y8a	1615	H-bonding, protonation state

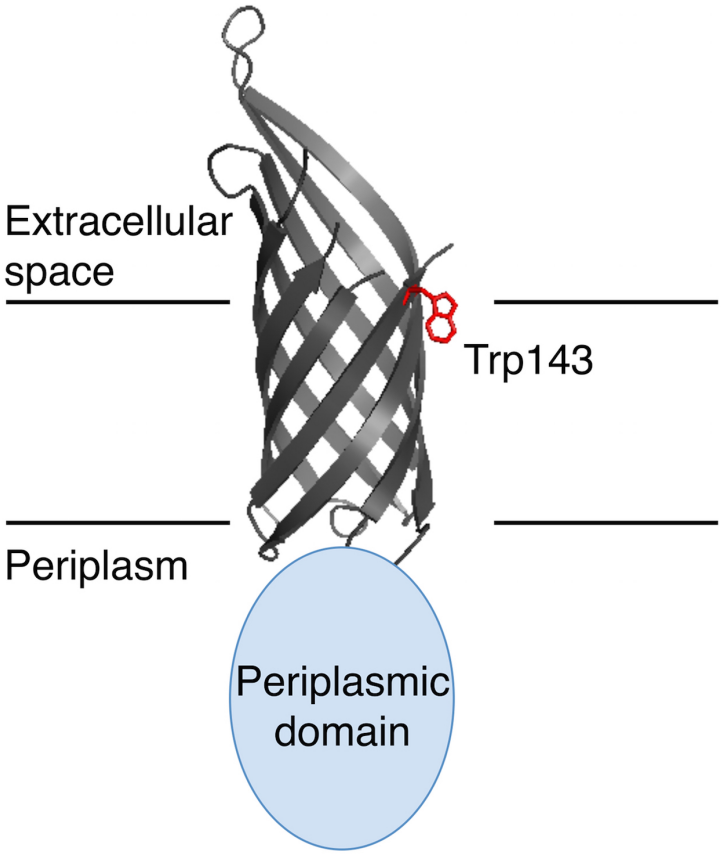

Figure 3.1 Crystal structure of the transmembrane domain of OmpA (PDB 1QJP) with a cartoon representation of the periplasmic domain. The single tryptophan residue located at position 143 (Trp143) is shown in red. An approximate lipid-water boundary is indicated with horizontal lines.

3.3 Materials

Prepare all solutions using ultrapure water with high resistivity of 18.2 MΩ-cm at 25 °C (e.g. Milli-Q Water System). Prepare and store all buffers at room temperature (unless indicated otherwise). Dispose of waste contents appropriately.

1. 500 mL of potassium phosphate buffer: 20 mM phosphate buffer, pH 8.0. Add 0.190 g of monobasic potassium phosphate and 1.500 g of dibasic potassium phosphate to 500 mL of water (both masses refer to anhydrous reagents). Adjust pH to 8.0 with 1.0 M NaOH. Filter final solution through a 0.45 μm pore size membrane filter.
2. 50 mL of denaturant (urea) buffer: 8.0 M urea in 20 mM phosphate buffer, pH 8.0. Add 24.000 g of urea, 0.019 g of monobasic potassium phosphate and 0.150 g of dibasic potassium phosphate to 31.8 mL of water (total volume should be 50 mL) (*see* **Note 1**). Adjust pH to 8.0 with 1.0 M NaOH. Filter final solution through a 0.45 μm pore size membrane filter.
3. OmpA primary stocks: OmpA mutants W143 (single tryptophan at position 143) and W0 (no tryptophan residues). OmpA W143 is a full-length mutant with a single tryptophan residue located at native position 143. The other four native tryptophan residues were mutated to phenylalanine. OmpA W0 mutant is a full-length mutant with all five native tryptophan residues mutated to phenylalanine. Calculations presented here assume primary stock protein solutions that contain ~300 μM OmpA with 8.0 M urea and 20 mM phosphate buffer (pH 7.3).
4. 5 mL 1,2-dimyristoyl-*sn*-glycero-3-phosphocholine (DMPC) small unilamellar vesicles (SUVs): 5 mg/mL lipid solution in 20 mM phosphate buffer, pH 8.0. Dry 25 mg of DMPC dissolved in chloroform under nitrogen gas for at least 5 hours. Prepare a 5

mg/mL lipid concentration by re-suspending the dried lipid in 5 mL of phosphate buffer from Step 1 above. To generate SUVs with approximately 50 nm diameter, sonicate the aqueous lipid solution for 30 minutes with a probe ultrasonic microtip at 50% duty cycle (0.5 second on, 0.5 second off) and 30% maximum amplitude in a warm water bath. Filter the sonicated vesicles through a 0.22 μm filter and equilibrate the final vesicle solution above 30 °C (T_C = 23 °C, Avanti Polar Lipids) overnight before use.

5. 50 mL L-tryptophan aqueous solution: 30 μM L-tryptophan in 20 mM phosphate buffer, pH 8.0. Prepare 20 mL of a 1 mM L-tryptophan primary stock solution by adding 4.0 mg of solid L-tryptophan to 20 mL of phosphate buffer from Step 1 above. Aliquot 1.5 mL of the L-tryptophan primary stock into 48.5 mL of phosphate buffer to make a 30 μM L-tryptophan final solution in a total of 50 mL. Filter the final solution through a 0.22 μm filter.
6. 50 mL L-tyrosine aqueous solution: 100 μM L-tyrosine in 20 mM phosphate buffer, pH 8.0 (the higher concentration of tyrosine relative to tryptophan is because the molar absorptivity of tyrosine is ~2x lower than tryptophan at 228 nm). Prepare 20 mL of a 1 mM L-tyrosine primary stock solution by adding 3.6 mg of solid L-tyrosine to 20 mL of phosphate buffer from Step 1 above. Aliquot 5 mL of the L-tyrosine primary stock solution into 45 mL of phosphate buffer f to make a 100 μM L-tyrosine final solution in a total of 50 mL. Filter the final solution through a 0.22 μm filter.
7. 10 mL acetonitrile (ACN): HPLC grade, submicron filtered
8. 5 mL Luer-Lok tip syringes
9. Luer-Lok tip needles
10. 1.5 mL microcentrifuge tubes

11. Temperature-controlled water bath set to 39 °C
12. Neutral density filters (optical densities of filters depend on output power of laser, see below). A set of filters in the range of OD 2.0 to 0.1 is recommended.
13. Power meters capable of measuring powers over the range of 1 W to 0.01 mW
14. UV resonance Raman (UVRR) laser apparatus (Figure 2): The setup for the UVRR Ti:Sapphire laser system has been previously published [17]. All protein samples, blanks, and model compound solutions should be excited with a 228 nm excitation beam, which is ideal to enhance protein tryptophan signal. Scattered photons are collected and focused through a prism-based prefilter that eliminates elastically-scattered photons (Rayleigh scattering). If a prism prefilter is not available, other filtering optics could be utilized, such as edge or notch filters. The inelastically-scattered, Raman photons are focused into a single spectrograph that further disperses the Raman light via a 3600 groove/mm holographic grating. The spectrum is recorded on a charged-coupled device (CCD) detector. All protein samples and blanks are pumped through a single-pass flow system equipped with a quartz microcapillary with an inner diameter of 100 μm and a flow rate of 0.16 mL/min to ensure fresh sample for each laser pulse.

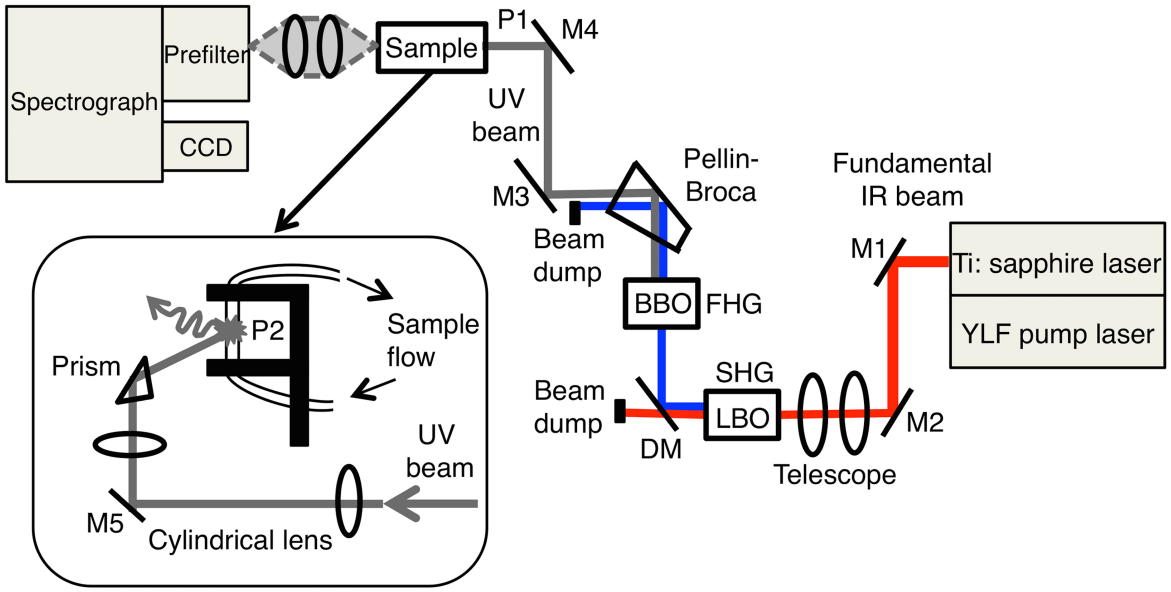

Figure 3.2 Schematic of the UVRR apparatus. The fundamental IR beam (912 nm) from a YLF-pumped Ti:Sapphire laser is directed by two mirrors (M1 and M2) to a pair of telescoping lenses for beam collimation and reduction, and passed through a lithium triborate (LBO) crystal for second harmonic generation (SHG) of 456 nm light. A dichroic mirror (DM) separates the residual fundamental from the second harmonic beam, and this residual IR light impinges on a beam dump. The isolated 456 nm beam is passed through a β-barium borate (BBO) crystal for fourth harmonic generation (FHG) of the UV beam (228 nm). A Pellin-Broca prism isolates the 228 nm beam, and the UV light is directed to the sample via two UV-enhanced mirrors (M3 and M4). A convenient location to measure UV power is after M4, labeled P1. After M4, the beam is directed vertically towards the sample via a mirror (M5) and small right-angle prism. Two cylindrical lenses focus the beam into a cylindrical shape on the vertically-mounted, fused silica microcapillary that contains the sample. The power at the sample is measured at location P2. The Raman-scattered photons are collected by a pair of UV lenses (F/1 and F/4) and focused into a prism-based prefilter before entering a spectrograph that further disperses the Raman-light using a 3600 groove/mm holographic grating. The Raman spectrum is recorded using a charged-coupled device (CCD) detector.

3.4 Methods

Carry out all procedures at room temperature unless otherwise specified. The general procedure for collection of UVRR data involves optimization of the laser and sample setup (3.4.1), determination of appropriate UV incident power via power-dependence measurements (3.4.2), and collection of UVRR spectra of protein (3.4.3). These steps ensure optimal signal-to-noise ratio and resolution of UVRR spectra, with minimal sample use and absence of artifacts from photodamaged protein. Alternate laser setups, including commercial systems, and sample flow systems can be utilized. The guidance below describes the minimum components and steps for a homebuilt UVRR apparatus.

3.4.1 Laser and sample optimization

3.4.1.1 Power and beam characteristics

1. The 1 kHz Ti:Sapphire laser should be tuned such that the wavelength of the fundamental output is 912 nm, approximately 1W.
2. The 912 nm beam is reduced in diameter with a pair of telescoping lenses and passed through a doubling crystal (LBO). The 456 nm second harmonic output is separated from the fundamental light via a dichroic mirror. In our apparatus, the output of the 456 nm beam should be at least 170 mW.
3. The 456 nm beam is passed through another doubling crystal (BBO) to generate a 228 nm beam. This 228 nm fourth harmonic UV beam is separated from the 456 light via a Pellin-Broca prism, and redirected by two mirrors. In our apparatus, the output of the 228 nm beam should be at least 6 mW after the mirrors.
4. At the sample spot, the size of the focused 228 nm beam should be smaller than that of the microcapillary; a typical size is ~75 μm width × 300 μm height.

3.4.1.2 Spectral resolution and spectrograph setting

1. The grating in the spectrograph should be positioned for the appropriate window for Stokes Raman scattering. A rough calculation is needed to determine the central wavelength for a photon that is Raman-shifted approximately 1500 cm^{-1} from the excitation wavelength. For example, if the excitation wavelength is 228.0 nm, the 1500 cm^{-1} Stokes-shifted photon will have a wavelength of 236.1 nm. After the spectrograph is centered at 236.1 nm, minor adjustment in the spectrograph central wavelength may be needed to ensure that the Rayleigh scattering is not incident on the CCD, and that the window displays the desired range of Raman shifts.
2. The resolution of the Raman spectra should be determined for a given spectrograph wavelength setting, and depends on several factors. Some of these factors are inherent to the apparatus and cannot be adjusted easily, such as natural bandwidth of the laser and size of the commercial CCD pixels. One experimental variable that significantly affects spectral resolution and is controllable by the user is the width of the entrance slit of the spectrometer. In our apparatus, the entrance slit is located on the prism prefilter, and can be adjusted from completely closed (0.00 mm) to 6.00 mm opening.
3. The bandwidth of the spectral resolution should be less than ~15 cm^{-1} for reasonable UVRR spectra. The bandwidth can be determined by measuring the dispersion of the spectrograph, and using the dispersion information to determine the appropriate slit opening. The next two steps (#4-5) describe this process.
4. The dispersion can be determined by measuring a spectrum of a solvent with known vibrational peaks. For example, the spectrum of ethanol has peaks at 883.3, 1051.6, 1095.2, 1275.6, and 1453.7 cm^{-1}. The pixel positions of these peaks should be noted,

and this information should be combined with the pixel size to determine dispersion. In the case of ethanol, if the 883.3 and 1453.7 cm^{-1} peaks show up at pixels 34 and 258, respectively, and the size of each CCD pixel is 20 μm square, the dispersion becomes $\frac{1453.7-883.3\ cm^{-1}}{258-34\ pixels} \times \frac{1\ pixel}{20.\ \mu m} = 0.12_7\ \frac{cm^{-1}}{\mu m}$.

5. With knowledge of the dispersion, the slit width that gives rise to the targeted bandwidth can be calculated. In the example above, in order to maintain the bandwidth smaller than 15 cm^{-1}, the slit should be open to no more than $\frac{15\ cm^{-1}}{0.127\ \frac{cm^{-1}}{\mu m}} =$ 118 μm (approximately 0.12 mm).
6. The actual experimental bandwidth should be confirmed by measuring the width of an inherently narrow peak as a function of slit width. One of the numerous UV emission lines from a mercury vapor lamp can serve as the inherently narrow peak. Select one emission line for observation. The full-width-at-half-maximum (FWHM) for the selected peak should be recorded at 10 or 20 μm intervals of the slit width, from 20 μm to at least double the targeted slit width, e.g. 20, 40, 60… μm up to 240 μm opening. With knowledge of the dispersion, the bandwidth can be determined. For example, if a mercury emission line is 6.0 pixels FWHM with a slit opening of 120 μm, the bandwidth from the example above is $\frac{1453.7-883.3\ cm^{-1}}{258-34\ pixels} \times 6.0\ pixels =$ 15 cm^{-1}. Hence, 120 μm is an appropriate spectrometer slit opening.

3.4.1.3 Sample setup

1. Ultraviolet light can easily damage biological samples in an irreversible manner, so it is essential that UV-photolyzed protein be discarded after a single-pass through the laser.

Thus, a single-pass sample system is essential to eliminate buildup of unwanted photoproduct. The next three steps (#2-4) describe this system.

2. To minimize the amount of sample required for a UVRR spectrum, the single pass system should utilize a narrow fused silica microcapillary, with sample pumped through the capillary at the minimal flow rate to ensure fresh sample for each laser pulse. In our lab, we use a polyimide-coated microcapillary with inner diameter 100 μm (outer diameter of 160 μm). The polyimide coating is burned off using a Bunsen burner in the region exposed to UV light, approximately 1" height. This capillary is mounted vertically in a home-built, aluminum holder, and is coupled to flexible 250 μm inner-diameter PEEK tubing (1.59 mm outer-diameter).
3. One end of the PEEK tubing is attached to a Luer-Lok tip syringe, and the syringe is mounted on a syringe pump. This is the front of the flow system. The other end of the PEEK tubing is inserted into a waste container to collect and discard photolyzed sample.
4. The flow rate of the syringe pump is set such that the sample linear velocity at the focused laser spot is at least 10% greater than the minimum flow rate necessary for fresh sample. For a 1 kHz laser system (1 ms per pulse) and focused spot size of 300. μm height, the minimum flow rate should be 300. μm per ms, or volume of $0.00236\ \text{mm}^3$ per ms (from $\pi\times(0.100\ \text{mm diameter}/2)^2\times 0.300\ \text{mm height}$). This volumetric flow rate is equivalent to 0.00236 mL per second, or 0.141 mL per minute. Hence, the syringe pump should deliver at least 0.155 mL per minute (10% higher than the minimum flow rate). Typical UVRR spectra are collected over 10 minutes, so a total of 1.55 mL is needed for one spectrum.

3.4.2 Power-dependence experiment

3.4.2.1 Power-dependence data acquisition

1. Set the laser current to obtain 1 W output of the fundamental IR beam. Optimize the doubling crystals to obtain the highest possible UV output power measured before the first cylindrical lens (Figure 2, P1).
2. Record the UV power at P1 and at the sample (Figure 2, P2). These recordings at P1 and P2 are the powers before and after the sample optics, respectively. The attenuation in power from P1 and P2 is attributed to losses from reflection and/or absorption of the UV beam by the mirrors and lenses.
3. Use appropriate neutral density filters to obtain a range of UV powers, ideally a range of at least 20-fold from ~0.3 mW to 6 mW at P1 (*see* **Note 2**). Record the power at both P1 and P2.
4. A plot of power at P2 vs. power at P1 should be linear, indicating that the attenuation factor is constant over the range of powers. All subsequent UV powers should be measured at position P1, and the graph of P2 vs P1 can be used to determine the power at the sample position P2.
5. A spectrum of ACN is used to calibrate the x-axis by converting from pixel number to Raman shift (cm^{-1}), and to check for slight misalignments upon changing ND filters. At the highest UV power, collect the appropriate number of spectra such that the total acquisition time is 2-3 minutes. For example, we typically collect 10 spectra, each with acquisition time of 15 seconds, and add the spectra to generate a single, 2.5-minute spectrum of ACN. The specific number of spectra and exposure time

depend on the sensitivity of the CCD and efficiency of the collection options. A spectrum of ACN should be collected for each power (*see* **Note 3**).

6. Collect spectra of L-tryptophan and L-tyrosine at each power (*see* **Notes 4 and 5**). Collection times may need to be longer for lower powers. The flow rate for a 100 μm i.d. quartz capillary should be set appropriately to ensure fresh sample for each laser pulse (see above, 3.1.3). The photodegradation of L-tryptophan is obvious in the UV-Vis absorption as well as fluorescence spectra of the sample before, during, and after UVRR experiments; typical sample degradation during a UVRR power-dependence experiment for L-tryptophan is shown in Figure 3 (top).
7. After UVRR spectra of L-tryptophan and L-tyrosine have been collected over the desired range of powers, collect spectra of phosphate buffer with the same UV powers that were used for L-tryptophan and L-tyrosine. These buffer spectra will be used for background subtraction during data analysis.

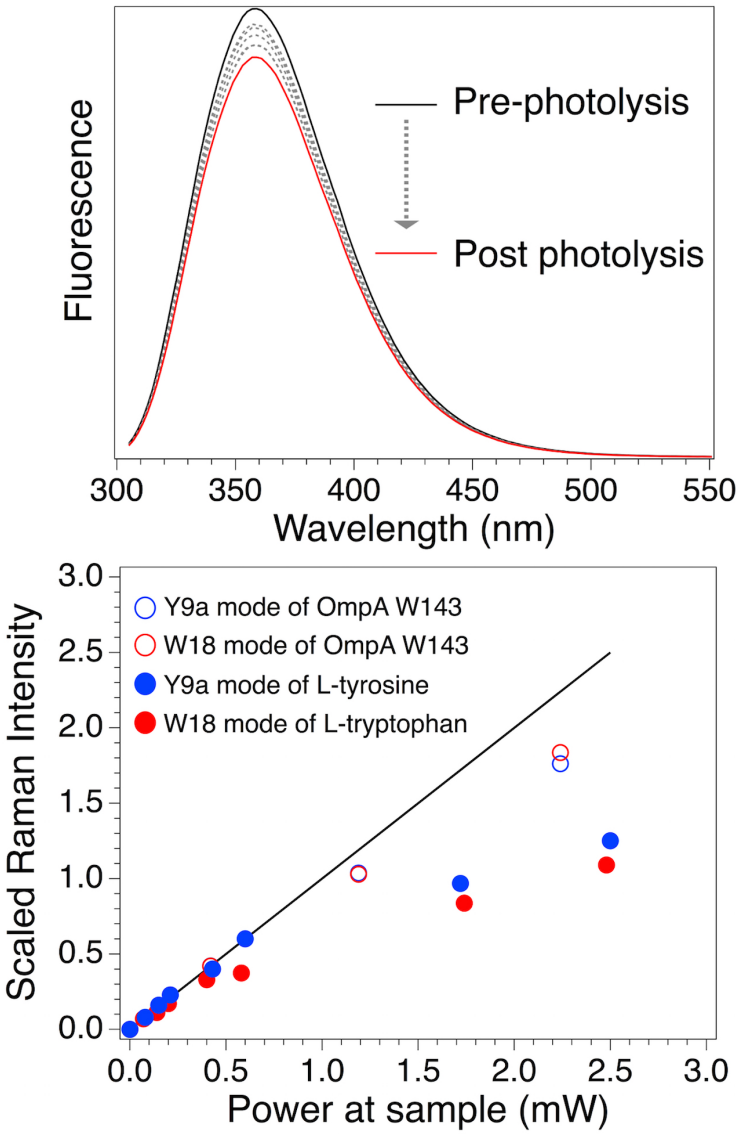

Figure 3.3 Top: Fluorescence spectra of L-tryptophan during power-dependence experiments. The solid black spectrum is of sample prior to the experiment, and the red spectrum is after the highest power. Dashed spectra are samples after intermediate powers listed in the text. Bottom: Graph of scaled Raman intensity of L-tryptophan and L-tyrosine and single tryptophan OmpA mutant W143 as a function of power at P2. The line has slope of 1 and is the expected trend if Raman signal scales linearly and proportionally with laser power (see text).

3.4.2.2 Power-dependence data analysis

All data analysis for UVRR spectra was performed using Igor Pro (Wavemetrics) software.

1. Convert pixel number to Raman shift (cm^{-1}) with the following steps. Plot the Raman spectrum of ACN (or other solvent with well-resolved peaks) as a function of pixel number, and determine the pixel numbers that correspond to known ACN vibrational energies. For example, an ACN spectrum may have the following correspondence of (energy (cm^{-1}), pixel number): (379.5, 78); (918.9, 325); (1374.4, 539); (2942.3, 1324). A minimum of four known peaks should be used. A graph of Raman shift as a function of pixel number is created, and the data are fit to a 3rd-order polynomial. The coefficients of this polynomial fit are then used to generate an x-axis of Raman shift (cm^{-1}).
2. Plot raw UVRR data with any x-axis (pixel number or Raman shift). Remove all peaks that can unequivocally be attributed to cosmic rays from all sample and buffer spectra. Signal from cosmic rays are very narrow (FWHM of 2-3 pixels) and spurious. The cosmic ray peaks can be removed manually, where a user replaces a high-intensity cosmic ray peak with a value that is the average of nearby baseline values. Alternatively, numerous software filters can be used to eliminate cosmic peaks, such as derivative filter or window-to-window comparison (*see* **Note 6**).
3. At this stage, all spectra should be plotted with Raman shift as the x-axis. Sum all accumulations of the spectra to generate a single UVRR spectrum of L-tryptophan, L-tyrosine, and buffer (Figure 4 top, spectra A, B, and C). Subtract the buffer spectrum from L-tryptophan and L-tyrosine at each power to isolate signal from the amino acids (Figure 4 middle and bottom, spectra D and H, respectively).

4. There is a residual, broad background on the isolated amino acid spectra that can be attributed to fluorescence and scattering. This residual background is removed by generating an interpolated curve that reproduces the residual background (dashed lines F and J in Figure 4). These interpolated curves are subtracted from the isolated amino acid spectra to yield the final, background-free spectra of L-tryptophan and L-tyrosine (Figure 4, spectra G and K, respectively).
5. Normalize the final UVRR spectra for total acquisition time and misalignments if needed (*see* **Note 7**).
6. Plot Raman intensity (counts) vs. UV power at sample; the Raman counts can be standardized to an arbitrary value that generates a graph with slope 1 at low power (Figure 3 bottom). Focus on dominant Raman peaks, such as the 759 cm^{-1} W18 mode of L-tryptophan and the 1178 cm^{-1} Y9a mode of L-tyrosine.
7. Identical power-dependence experiments should be performed on the protein sample (see below for instructions on protein preparation). Power-dependence data for both model compounds and protein, with Raman intensity values scaled to generate a slope of 1 at lowest powers, are shown in Figure 3.
8. The graph of Raman counts vs. power should be linear and proportional at low power, where doubling the power results in doubling the Raman signal; at high powers, the Raman signal becomes non-linear as a function of excitation power (typically there are fewer Raman counts than is expected if the slope were 1) because of two-photon and other non-linear events. The power used in all UVRR experiments should be in the linear regime of low powers. In the example in Figure 3, Raman signal from L-tryptophan and L-tyrosine deviate from linearity at ~0.5 mW whereas the protein is

more robust, and exhibits linearity up to ~1 mW. Hence, the power incident on protein should be less than 1 mW.

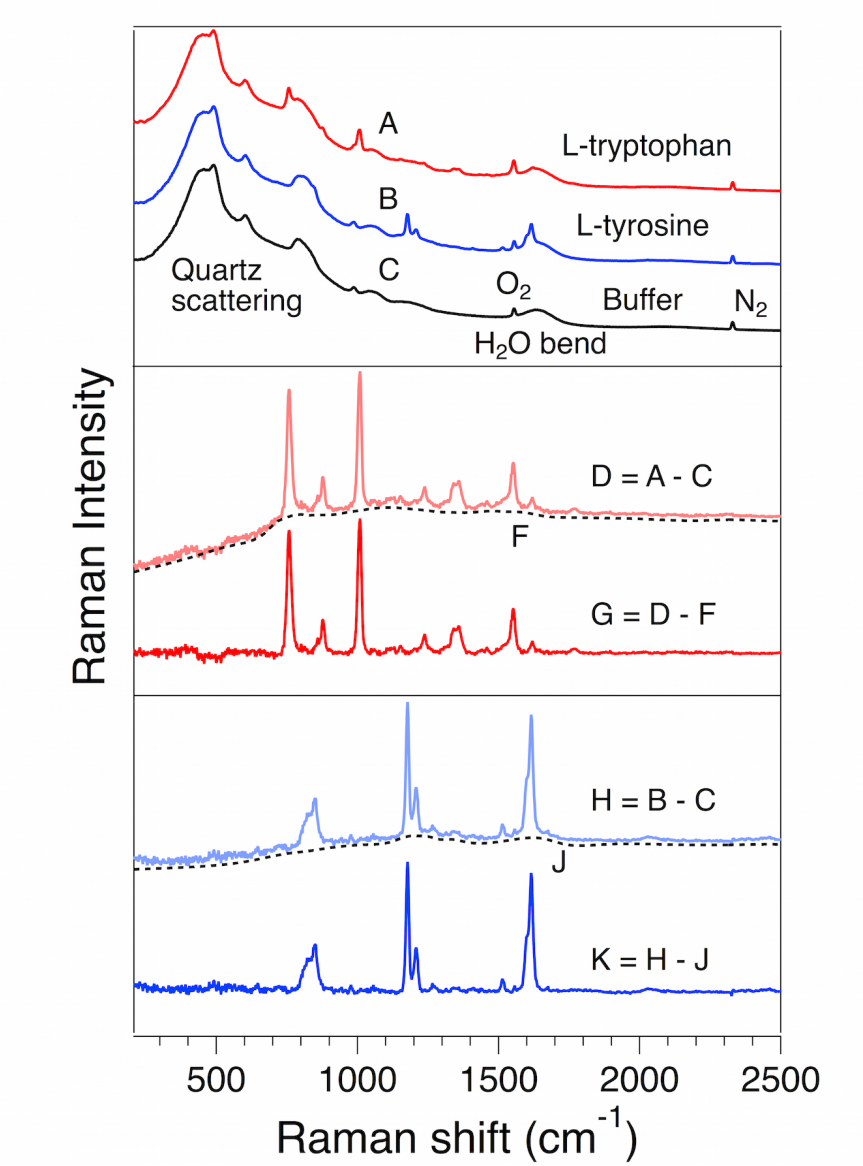

Figure 3.4 Typical UVRR data analysis of model compounds L-tryptophan and L-tyrosine. The top panel shows the raw UVRR spectra of L-tryptophan (A), L-tyrosine (B), and phosphate buffer (C) after removal of peaks from cosmic rays. Signal from the quartz capillary, H_2O bend, and sharp peaks from dissolved O_2 and N_2 are indicated. The middle and bottom panels are difference spectra that show isolated peaks of L-tryptophan (D) and L-tyrosine (H) followed by baseline-corrected isolated spectra (G and K) of L-tryptophan and L-tyrosine, respectively. The interpolated baselines are shown as dashed curves F and J.

3.4.3 UVRR of a membrane protein: Outer membrane protein A (single-tryptophan mutant W143)

The following instructions are for OmpA, a membrane protein that is stored in the unfolded conformation. The final concentrations of protein, urea, and lipids in a total volume of 1.1 mL should be 20 μM, 0.5 M, and 300:1 lipid:protein (6 mM lipid if protein is 20 μM), respectively, unless otherwise specified. The presence of urea is unavoidable because the protein primary stock is stored in 8.0 M urea. This residual urea from the stock protein solution must be taken into account, and additional volumes of urea may need to be added to achieve a final urea concentration of 0.5 M.

3.4.3.1 Preparation of folded protein samples and blanks

1. The following volumes are based on an OmpA W143 primary stock concentration of 300 μM. Aliquot 895.0 μL of the 5.0 mg/mL stock DMPC SUV solution and 132.0 μL of phosphate buffer into a 1.5 mL microcentrifuge tube. Label this tube as “Folded W143” and place the tube in a 39.0°C water bath and let it equilibrate for 15 minutes to ensure that the vesicles are in the fluid phase prior to adding the W143 protein.
2. The following volumes are based on an OmpA W0 primary stock concentration of 300 μM. Aliquot 895.0 μL of the 5.0 mg/mL stock DMPC SUV solution and 132.0 μL of phosphate buffer to a second 1.5 mL microcentrifuge tube. Label this tube as “Folded W0” and place the tube in the 39.0°C water bath and let it equilibrate for 15 minutes to ensure that the vesicles are in the fluid phase prior to adding the W0 protein.
3. Prepare a third microcentrifuge tube that contains the blank, which is a solution with urea, vesicles, and buffer, but without protein. This blank will be used in

subtractions to isolate OmpA peaks from non-protein peaks, e.g. urea, vesicles, and buffer, in the UVRR spectra (*see* **Note 8**). The blank should contain 895.0 μL of DMPC SUV solution, 73.0 μL of urea buffer, and 132.0 μL of phosphate buffer (assuming the protein primary stock is 300 μM with 8.0 M urea, leading to a final urea concentration in the microcentrifuge tube of 0.5 M). Label this tube as "DMPC/urea blank" and incubate the tube in the 39.0°C water bath until ready to collect spectra.

4. When ready to add protein to the "Folded W143" and "Folded W0" tubes, add 73.0 μL of primary stock OmpA W143 (300 μM with 8.0 M urea) to the tube labeled "Folded W143" and 73.0 μL of primary stock OmpA W0 (300 μM with 8.0 M urea) to the tube labeled "Folded W0". Place these tubes back into the water bath and let them incubate for at least 5 hours (no more than 8 hours) to allow the protein to fold into the vesicles. These samples will have 0.5 M urea because of the presence of 8.0 M urea in the primary stock protein solution.

3.4.3.2 Preparation of unfolded protein samples and blanks

Prepare the unfolded protein samples in phosphate buffer at room temperature ~30 minutes prior to UVRR acquisition to avoid protein aggregation.

1. Add 73.0 μL of primary stock OmpA W143 (300 μM) and 1027.0 μL of phosphate buffer to a 1.5 mL microcentrifuge tube and label this tube as "Unfolded W143". This sample will have 0.5 M urea because of the presence of 8.0 M urea in the primary stock protein solution.
2. Add 73.0 μL of primary stock OmpA W0 (300 μM) and 1027.0 μL of phosphate buffer to another 1.5 mL microcentrifuge tube and label this tube as "Unfolded

W0". This sample will have 0.5 M urea because of the presence of 8.0 M urea in the primary stock protein solution.

3. The corresponding blank for the unfolded protein samples is 0.5 M urea in 20 mM phosphate buffer. Add 73.0 μL of urea buffer and 1027.0 μL of phosphate buffer to a 1.5 mL microcentrifuge tube and keep at room temperature until ready to collect the UVRR spectrum.

3.4.3.3 OmpA W143 and W0 UVRR data acquisition

1. Make sure the entrance slit is opened to the appropriate width for optimal throughput and resolution (Step 3.1.2). In the present laser apparatus, the entrance slit in the prefilter was set to 0.11 mm, which corresponds to a bandwidth of 11 cm^{-1}.
2. Set the laser for an output of ~1.0 W of IR.
3. Use appropriate neutral density filters to adjust the UV power at sample to a value within the linear regime; in the present experiment, the power at the sample should be no more than ~1.0 mW.
4. Flow ACN through the capillary at the appropriate flow rate for fresh sample at each laser shot (Step 3.1.3). While collecting UVRR spectra of ACN (1-second acquisitions), optimize the optics near the sample to maximize the counts of the 918.9 cm^{-1} ACN peak per second per mW of UV power. The optics should be adjusted in a systematic manner.
5. Once optimized, collect a 2.5-minute spectrum (15 seconds, 10 acquisitions) of ACN that should be used for calibration of the Raman shift axis.

6. Wash the capillary flow system with water (or buffer) between each new sample collection. Collect 5-minute spectra (60 seconds, 5 acquisitions) of each protein sample and blank under flow (*see* **Note 9**).

3.4.3.4 OmpA W143 and W0 UVRR data analysis

Data analysis was performed on Igor Pro (Wavemetrics) software, but any advanced data analysis software is acceptable (e.g. Origin, Matlab). The procedure is similar to that of the power-dependence experiments (Figure 3), with the additional steps of subtracting contributions from non-protein peaks.

1. Convert the x-axis from pixel number to Raman shift (cm^{-1}) using ACN; this conversion is identical to that used in the power-dependence experiments for L-tryptophan and L-tyrosine (Step 3.2.2).
2. Remove all peaks from cosmic rays from each individual 1-minute raw spectrum of protein and blank samples.
3. Add the resulting1-minute spectra for each protein and blank sample to generate summed 5-minute spectra that are devoid of cosmic peaks.
4. At this stage, all spectra should be plotted with Raman shift as the x-axis. Generate a spectrum that displays signal only from protein by subtracting contributions from vesicle, urea, and buffer via:

   Summed protein sample – [c × summed (SUVs + urea + buffer) blank]

   where ‘summed (SUVs + urea + buffer) blank’ is a spectrum of SUVs and urea in phosphate buffer (*see* **Note 10**). The coefficient ‘c’ is a scalar that results in optimal subtraction of SUVs + buffer + urea from the protein spectrum such that signal from these species is eliminated from the protein spectra

5. Generate and then subtract an interpolated baseline from each spectrum of isolated protein.
6. Normalize the resulting UVRR spectra such that the peak height of the largest Raman peak is identical in both W143 and W0 spectra. The final, normalized, UVRR spectra of folded W143 and W0 in DMPC SUVs and unfolded W143 and W0 in phosphate buffer are shown in Figure 5 and summarized in Table 2.

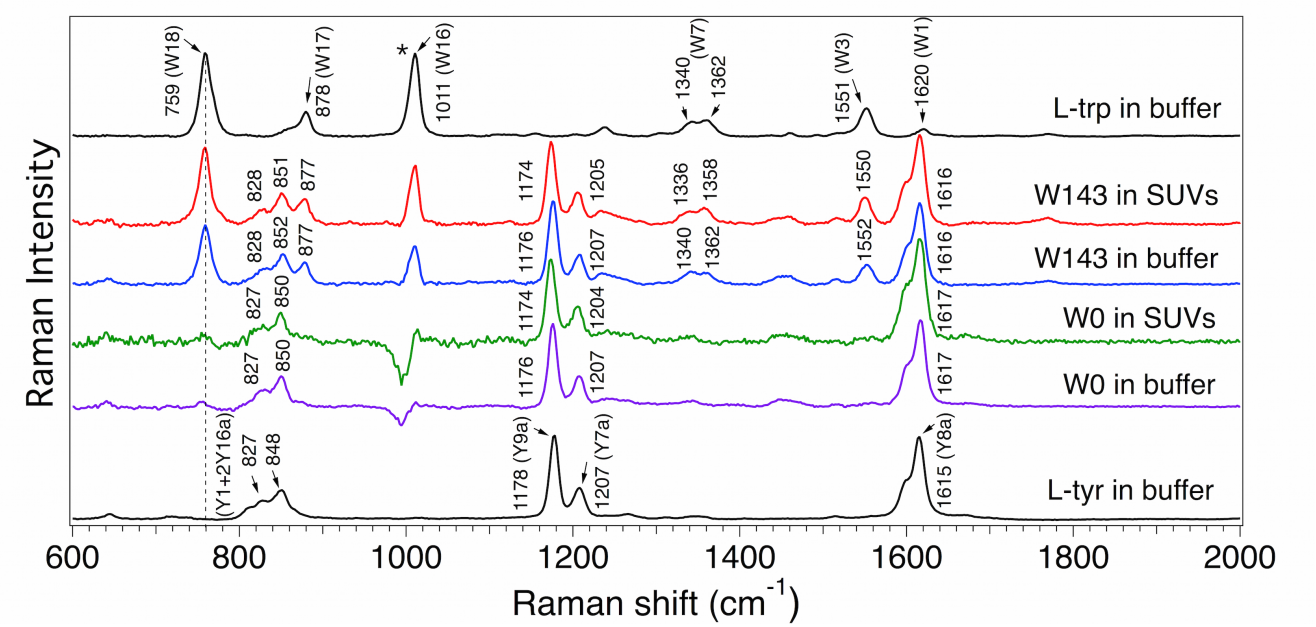

Figure 3.5 UVRR difference spectra of OmpA W143 and W0 folded in DMPC SUVs and unfolded in phosphate buffer. The UVRR spectra of W143 and W0 are normalized such that the tyrosine Y9a peak has equal intensity. There is a strong urea peak at 1003 cm^{-1} (indicated with *) that may result in subtraction artifacts near this region. UVRR spectra of model compounds L-tryptophan and L-tyrosine are also shown for comparison. Prominent tryptophan (W18, W17, W16, W7, W3, and W1) and tyrosine (Y1+2Y16a, Y9a, Y7a, and Y8a) are labeled.

Table 3.2 Summary of key tryptophan and tyrosine modes in OmpA W143 and W0 as shown in Figure 5. The W143 spectrum displays signal from the single tryptophan residue and 17 tyrosine residues. W0 exhibits only tyrosine peaks because this mutant has no tryptophan residues.

	Mode	Vibrational energy (cm^{-1})
W143	W18	Folded (759) Unfolded (759)
	W17	Folded (877) Unfolded (877)
	W7	Folded (1336, 1358) Unfolded (1340, 1362)
	W3	Folded (1550) Unfolded (1552)
	Y1+2Y16a	Folded (828, 851) Unfolded (828, 852)
	Y9a	Folded (1174) Unfolded (1176)
	Y7a	Folded (1205) Unfolded (1207)
	Y8a	Folded (1616) Unfolded (1616)
W0	Y1+2Y16a	Folded (827, 850) Unfolded (827, 850)
	Y9a	Folded (1174) Unfolded (1176)
	Y7a	Folded (1204) Unfolded (1207)
	Y8a	Folded (1617) Unfolded (1617)

3.4.3.5 Interpretation of the tryptophan W7, W3, and W17 Raman modes

1. To analyze the tryptophan W7 Fermi doublet (~1340 and ~1360 cm^{-1}) region of the UVRR spectrum, the contribution from the 17 native tyrosine residues and protein backbone must first be subtracted from the protein spectrum. The OmpA W0 mutant contains all 17 native tyrosine residues with the 5 native tryptophan residues mutated to phenylalanine. Therefore, the W0 mutant will be used to subtract contribution of tyrosine and protein backbone in the W7 Fermi doublet region of tryptophan. Generate a spectrum that displays signal only from the tryptophan side chain by subtracting contributions from tyrosine and protein backbone via:

   Summed W143 protein spectrum – [c × summed W0 protein spectrum] (*see* **Note 11**)
2. If needed, subtract an interpolated baseline from each isolated tryptophan spectrum.
3. Decompose the W7 Fermi doublet region in the W143 protein UVRR spectrum into two Gaussian peaks. The intensity ratio of the Fermi doublet peaks (R_{FD}) at ~1360 and ~1340 cm^{-1} reveals the environment polarity of the tryptophan residue independent of hydrogen-bonding environment. Figure 6 shows the isolated Fermi doublet region for the Fermi doublet region for folded and unfolded W143 along with L-tryptophan in buffer for comparison. The R_{FD} values for trp143 in the folded and unfolded conformation are 2.4 and 1.3, respectively. The high value of 2.4 indicates that trp143 is in a highly non-polar environment when folded. In the

unfolded conformation, the value of 1.3 is comparable to the value for L-tryptophan in buffer.

4. To calculate the tryptophan dihedral torsion angle C2-C3-Cβ-Cα when OmpA is folded in DMPC SUVs, determine the frequency of the W3 mode (~1552 cm^{-1}) from the isolated spectrum of trp143 in OmpA (the contribution of tyrosine in the W3 region is negligible, so it is not necessary to subtract tyrosine peaks in the form of W0 from the W143 spectrum in the W3 analysis). The frequency may be determined directly from the spectrum or through a Gaussian fit to the W3 mode.
5. The correlation of the W3 mode as a function of dihedral angle is published [11] and quantified: $\nu W3 = 1542 + 6.7[\cos 3(\chi^{2,1}) + 1]^{1.2}$ [12]. For trp143 in OmpA folded in SUVs, the frequency of the W3 mode is 1550 cm^{-1}, which corresponds to a dihedral torsion angle of 93°. A comparison of the structure from UVRR to that of the crystal structure is shown in Figure 7.
6. To determine changes in hydrogen-bonding of the indole N-H group, determine the frequency of the W17 mode (~877 cm^{-1}) for folded and unfolded OmpA. The frequency may be determined directly from the spectrum or through a Gaussian fit to the W17 mode. The W17 peak may overlap with the nearby Y1+2Y16a doublet; in this situation, a Gaussian decomposition of the multiple peaks may be needed to more reliably determine the W17 frequency. Alternatively, the W0 spectrum may be subtracted from W143 spectrum to isolate the W17 peak. In the case of trp143 in OmpA, the W17 frequency is identical for folded and unfolded proteins, with a frequency of 877 cm^{-1}. The frequency of L-tryptophan in aqueous solution is 878 cm^{-1}. This finding suggests that trp143 remains hydrogen-bonded

in folded and unfolded conformations, and is similar (or perhaps more strongly hydrogen-bonded) than L-tryptophan in solution.

7. Collectively, the data for trp143 supports a model where trp143 remains hydrogen bonded (based on the W17 mode) in the hydrophobic environment of the lipid (based on the W7 doublet), with a dihedral angle that deviates about 9° from the crystal structure (based on the W3 mode).

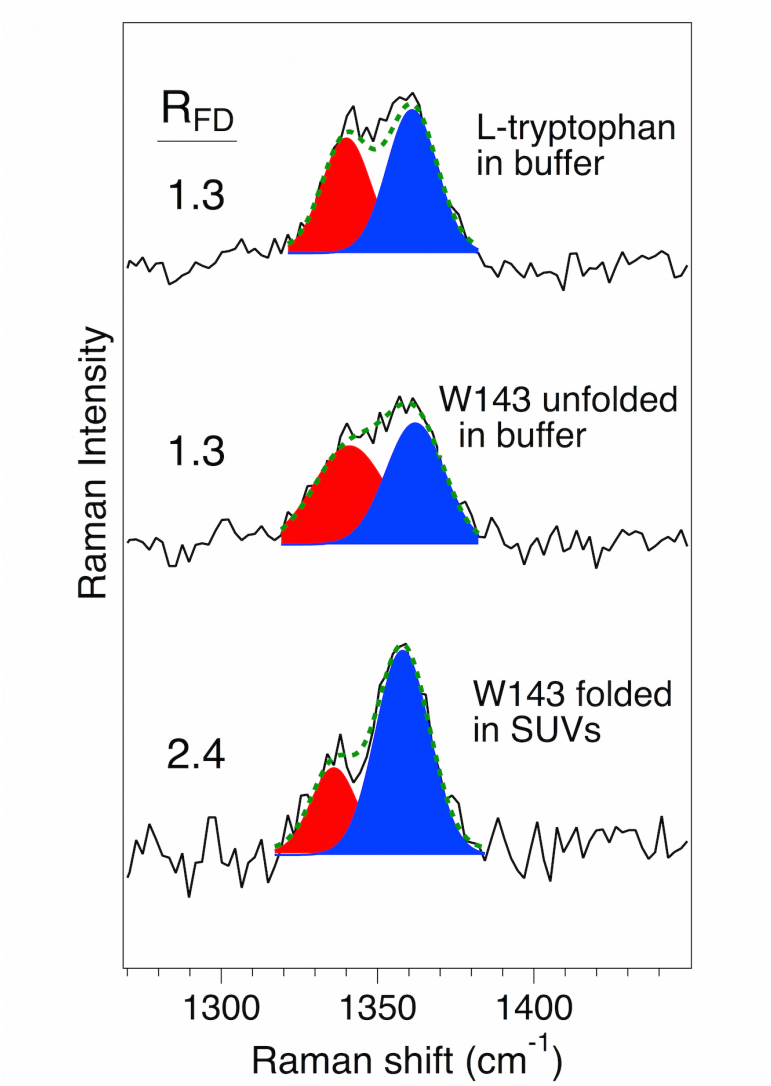

Figure 3.6 Double difference UVRR spectra of the W7 Fermi doublet region of OmpA W143 unfolded in phosphate buffer and folded in DMPC SUVs. Signal from tyrosine has been subtracted via (W143 spectrum minus W0 spectrum). The UVRR W7 Fermi doublet region of L-tryptophan in phosphate buffer is shown for comparison. Gaussian decompositions of the W7 Fermi doublet are shown in red and blue. The sum of the two Gaussian peaks of the W7 Fermi doublet is shown as green dashed curves. The Fermi doublet ratio based on the intensities of the decomposed Gaussian peaks (R_{FD}) is indicated.

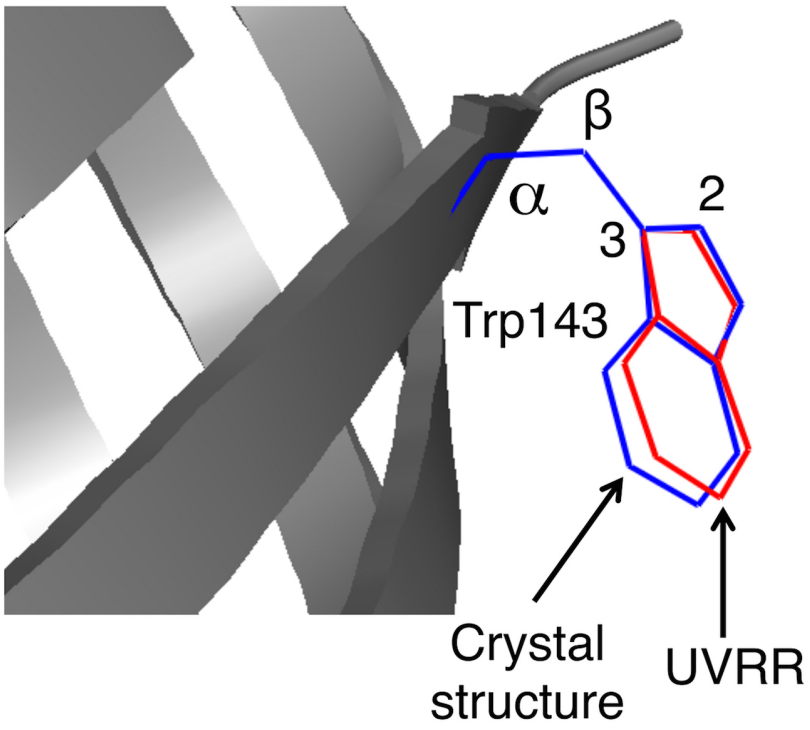

Figure 3.7 Comparison of the structure of trp143 based on UVRR (red) and X-ray diffraction (PDB 1QJP, blue). The dihedral angles are 93° and 102° for the UVRR and X-ray structures, respectively. The C2, C3, Cβ, and Cα carbons are labeled.

3.5 Notes

1. The mixture is endothermic and can be placed in a warm water bath to expedite dissolution. Stir continuously in the water bath for ~30 minutes, until all solids are dissolved.
2. Use a single neutral density filter for each power so the beam position and profile are reproducible at each power.
3. The acquisition time for any single UVRR spectrum should be less than 1-minute in order to minimize the number of cosmic rays that appear in the spectra. For our experiments, all ACN spectra were collected for a total of 2.5 minutes (10 spectra of 15-second acquisitions each).
4. For the present experiments, the powers for the power-dependence experiments were 0.07, 0.15, 0.21, 0.43, 0.60, 1.74, and 2.50 mW at the sample. The total collection times were 5 minutes for 1.74 and 2.50 mW and 20 minutes for 0.07, 0.15, 0.21, 0.43, and 0.60 mW at the sample.
5. It is critical to filter all solutions (using a 0.45 or 0.22 μm membrane) that will flow through the sample microcapillary to avoid obstructions and decreased flow rate while collecting spectra. If the capillary becomes obstructed such that there is no flow of the sample, pump water or ethanol from both ends of the capillary to flush out the obstruction. If the capillary remains plugged despite the water/ethanol flow, this obstructed capillary should be discarded and a new capillary must be attached.
6. Signal from cosmic rays may appear on top of Raman peaks, and care must be taken to preserve the shape of Raman peaks during post-processing. Additionally, when two or more cosmic ray peaks overlap on adjacent pixels, the FWHM will be broader (4-5

pixels), and may be undetected by software. Regardless of the method used to eliminate cosmic ray peaks from the Raman spectra, it is important to confirm that the removal of these peaks did not alter the desired Raman signal.

7. The ACN counts should scale linearly and proportionally with power (e.g. if the power is doubled, the ACN count for any given peak should double). If the ACN counts do not scale linearly and proportionally with power, and the shape of the ACN spectra are not perturbed (e.g. the FWHM is constant with different powers) there was likely a misalignment of the laser beam upon changing ND filters, causing the loss or gain in signal that is unrelated to the actual incident photon flux. The factor of lost (or gained) signal outside the expected linear/proportional range should be determined, and this factor should be applied to the L-tryptophan and L-tyrosine counts to take into account misalignment that may arise from the switching of ND filters.
8. Urea is hygroscopic and therefore, it is difficult to make urea solutions with high accuracy. To take into account slight differences in urea concentration for protein samples and blanks, it may be necessary to perform isolated subtractions, where signal from phosphate buffer and SUVs is subtracted in one step, followed by subtraction of urea in a subsequent step. Thus, an additional blank solution that contains SUVs in phosphate buffer (without urea) is useful. An additional blank of phosphate buffer (without urea or SUVs, item 1 under Section 2) may be needed because an isolated spectrum of urea-only is generated via subtraction of a buffer spectrum from the urea + buffer solution (item 2 under Section 2).
9. Fluorescence spectroscopy is used as a complementary method to UVRR and should be acquired for each protein sample and blank before and after UVRR acquisition to confirm

the folded and unfolded conformations (data not shown) and confirm minimal photodamage. In addition, for OmpA, gel electrophoresis differential mobility studies were also carried out to confirm the folded and unfolded conformations (data not shown). The absorption spectrum of each protein and blank sample should also be obtained before and after UVRR acquisition (data not shown) to confirm minimal photodamage.

10. Residual urea concentrations in the protein samples and blanks may be slightly different, making it difficult to fully subtract contribution from urea in the protein spectrum. An alternative subtraction scheme allows independent variation of urea relative to vesicle + buffer:

    Summed protein spectrum – [c × summed (SUVs + buffer) blank] ± [d × summed (urea) blank]

    where 'summed (SUVs + buffer) blank' is a spectrum of SUVs in phosphate buffer and 'summed (urea) blank' is the difference spectrum of (urea + buffer) minus buffer-only. The coefficients 'c' and 'd' are scalars that result in optimal subtraction of SUVs + buffer and urea, respectively.

11. Residual urea concentrations in the W143 and W0 protein samples may be slightly different, making it difficult to fully subtract contribution from urea in the protein spectrum. An alternative subtraction scheme allows independent variation of urea relative to W0:

    Summed W143 spectrum – [c × summed (W0)] ± [d × summed (urea) blank]

    where 'summed (W0)' is the summed spectrum of W0 in the corresponding environment (e.g. SUVs or urea) and 'summed (urea) blank' is the difference spectrum of (urea + buffer) minus buffer-only.

3.6 Acknowledgement

D.K.A acknowledges the UCSD Molecular Biophysics Training NIH Grant T32 GM008326 for funding support of this work.

Chapter 3 in full, is a reprint of the material with permission from D.K. Asamoto and J. E. Kim, UV resonance Raman Raman spectroscopy as a tool to probe membrane protein structure and dynamics. Methods in Molecular Biology-Lipid Protein Interactions. Methods and Protocols, Springer Science and Business Media, 2019, 327-349. The dissertation author was the primary investigator and author of this paper.

3.7 References

[1] I. Lopez-Pena, B.S. Leigh, D.E. Schlamadinger, J.E. Kim, Insights into protein structure and dynamics by ultraviolet and visible resonance Raman spectroscopy, *Biochemistry* 54 (2015) 4770-83.

[2] B.S. Leigh, D.E. Schlamadinger, J.E. Kim, Structures and dynamics of proteins probed by UV resonance Raman spectroscopy, *Biophysical Methods for Biotherapeutics: Discovery and Development Applications* (2014) 243-68.

[3] J.C. Merlin, Resonance Raman-spectroscopy of carotenoids and carotenoid-containing systems, *Pure. Appl. Chem.* 57 (1985) 785-92.

[4] B.B. Johnson, W.L. Peticolas, Resonant Raman effect, *Annu. Rev. Phys. Chem.* 27 (1976) 465-91.

[5] K.M. Sanchez, G.P. Kang, B.J. Wu, J.E. Kim, Tryptophan-lipid interactions in membrane protein folding probed by ultraviolet resonance Raman and fluorescence spectroscopy, *Biophys. J.* 100 (2011) 2121-30.

[6] A.J. de Jesus, T.W. Allen, The role of tryptophan side chains in membrane protein anchoring and hydrophobic mismatch, *Biochim. Biophys. Acta* 1828 (2013) 864-76.

[7] D.E. Schlamadinger, J.E. Gable, J.E. Kim, Hydrogen bonding and solvent polarity markers in the UV resonance Raman spectrum of tryptophan: application to membrane proteins, *J. Phys. Chem. B* 113 (2009) 14769-78.

[8] K.M. Sanchez, T.J. Neary, J.E. Kim, Ultraviolet resonance Raman Spectroscopy of folded and unfolded states of an integral membrane protein, *J. Phys. Chem. B* 112 (2008) 9507-11.

[9] J.P. Gallivan, D.A. Dougherty, Cation-pi interactions in structural biology, *Proc. Natl. Acad. Sci. U.S.A* 96 (1999) 9459-64.

[10] S. Millefiori, A. Alparone, A. Milleflori, A. Vanella, Electronic and vibrational polarizabilities of the twenty naturally occurring amino acids, *Biophys. Chem.* 132 (2008) 139-47.

[11] T. Miura, H. Takeuchi, I. Harada, Tryptophan Raman bands sensitive to hydrogen-bonding and side-chain conformation, *J. Raman Spectrosc.* 20 (1989) 667-71.

[12] L.J. Juszczak, R.Z. Desamero, Extension of the tryptophan chi2,1 dihedral angle-W3 band frequency relationship to a full rotation: correlations and caveats, *Biochemistry* 48 (2009) 2777-87.

[13] S.A. Asher, UV resonance Raman studies of molecular structure and dynamics: applications in physical and biophysical chemistry, *Annu. Rev. Phys. Chem.* 39 (1988) 537-88.

[14] I. Harada, Takeuchi, H, Raman and ultraviolet resonance Raman spectra of proteins and related compounds, *Spectrosc. Biol. Systems* (1986) 113-75.

[15] J.C.J. Austin, T, Spiro, T, G, Ultraviolet resonance Raman studies of proteins and related model compounds, *Adv. Spectrosc.* 1993.

[16] T. Miura, Takeuchi, H, Harada, I, Characterization of individual tryptophan side chains in proteins using Raman spectroscopy and hydrogen-deuterium exchange kinetics, J. *Am. Chem. Soc.* 27 (1987) 88-94.

[17] H.S. Shafaat, K.M. Sanchez, T.J. Neary, J.E. Kim, Ultraviolet resonance Raman spectroscopy of a beta-sheet peptide: a model for membrane protein folding, *J. Raman Spectrosc.* 40 (2009) 1060-4.

Chapter 4
Folding of the β-barrel membrane protein OmpA into nanodiscs

Chapter 4, in full, is a reprint of the material published in Biophysical Journal, 2019, 118, 1-12.

4.1 Abstract

Nanodiscs (NDs) are an excellent alternative to small unilamellar vesicles (SUVs) for studies of membrane protein structure, but it has not yet been shown that membrane proteins are able to spontaneously fold and insert into a solution of freely-diffusing NDs. In this report, we present SDS-PAGE differential mobility studies combined with fluorescence, circular dichroism (CD), and UV resonance Raman (UVRR) spectroscopy to confirm the spontaneous folding of Outer Membrane Protein A (OmpA) into preformed NDs. Folded OmpA in NDs was incubated with Arg-C protease, resulting in the digestion of OmpA to membrane-protected fragments with an apparent molecular mass of ~26 kDa (major component) and ~24 kDa (minor component). The OmpA folding yields were greater than 88% in both NDs and SUVs. An OmpA adsorbed intermediate on NDs could be isolated at low temperature and induced to fold via an increase in temperature, analogous to the temperature-jump experiments on SUVs. The CD spectra of OmpA in NDs and SUVs were similar, and indicated β-barrel secondary structure. Further evidence of OmpA folding into NDs was provided by UVRR, which revealed the intense 785 cm^{-1} structural marker for folded OmpA in NDs. The primary difference between folding in NDs and SUVs was the kinetics; the rate of folding was 2- to 3-fold slower in NDs compared to in SUVs, and this decreased rate can be attributed to the properties of NDs. These data indicate that NDs may be an excellent alternative to SUVs for folding experiments, and offer benefits of optical clarity, sample homogeneity, control of ND-to-protein ratios, and greater stability.

4.2 Statement of significance

Integral membrane proteins constitute a significant fraction of cellular proteins, yet their folding mechanisms in cellular bilayers remain largely unknown. The spontaneous *in vitro* insertion and folding of a model β-barrel membrane protein, OmpA, into lipid bilayers in the absence of molecular chaperones can provide insight into the intrinsic protein-lipid interactions that may help guide the *in vivo* folding mechanisms. The folding of OmpA into nanodiscs, an improved bilayer mimetic compared to traditional vesicles, opens doors for more extensive studies of membrane protein folding. Insights into lipid-protein interactions as well as inter- and intra- protein interactions during folding and insertion events into membrane bilayers would greatly benefit numerous areas of research, such as pathology, medicine, chemistry, biology, and biophysics.

4.3 Introduction

Membrane proteins are integral to key processes of life. They act as regulators of communication between the cell and its environment. Membrane proteins also serve as targets for the majority of pharmaceuticals [1]. The biological activity and chemical reactivity of membrane proteins depend on their structure, dynamics, and stability. Improper folding of integral membrane proteins can lead to the development of diseases, such as cystic fibrosis, retinitis pigmentosa, and Charcot-Marie-Tooth disease [2, 3].

The characterization of membrane proteins in their native environment is important to better understand their functions and assembly mechanisms. Soluble proteins have been successfully characterized with a variety of experimental methods, such as X-ray crystallography, NMR, and mass spectrometry. However, the insolubility of membrane proteins combined with the complexity of the lipid bilayer makes it difficult to study the dynamics and structures of these biomolecules, including the folding and insertion of membrane proteins in the amphipathic environment of lipid membranes. Another complication is that membrane proteins are not thermodynamically stable in aqueous solution, and easily denature or aggregate outside of the lipid bilayer. These issues are an impediment to comprehensive biophysical studies on membrane proteins, thus improved methods for study are needed.

Outer membrane protein A (OmpA) is a model protein for studies of membrane protein folding. It is one of the most abundant proteins found in the outer membrane of *Escherichia coli*. OmpA consists of 325 amino acid residues: a transmembrane domain of 8 antiparallel β-strands in a barrel and a soluble C-terminal periplasmic domain [4]. OmpA is an ideal β-barrel system to study protein folding because it has been previously shown to spontaneously and reversibly fold into synthetic bilayers [5, 6] and has been characterized by various biophysical methods.

Additionally, wild-type OmpA contains five native tryptophan residues that span the transmembrane domain, and these residues are excellent spectroscopic probes for studies of protein folding.

OmpA spontaneously inserts and folds into small unilamellar lipid vesicles (SUVs), spherical synthetic membrane mimics commonly used to study the *in vitro* insertion and folding mechanisms of membrane proteins [5-8]. It has been proposed that high-curvature membranes are needed for spontaneous folding because of their propensity for defects [5, 6, 9, 10]. Preformed SUVs are straightforward to generate in the lab but there are limitations in terms of experimental conditions. They are small (<50 nm diameter) and have high surface curvature, and the turbidity of SUV solutions results in strong Rayleigh scattering that complicates spectral analysis. Additionally, SUVs are thermodynamically unstable, fusing to form larger vesicles, including in the presence of membrane-associated proteins [11, 12]. OmpA is also able to fold into some large unilamellar vesicles (LUVs) that have a diameter of greater than 100 nm, but the ability to fold into LUVs as well as the kinetics of folding and insertion depend on the hydrocarbon chain [9, 10, 13]. Despite the prevalence of published reports with vesicles, an improved bilayer model could enhance studies of membrane protein folding.

Nanodiscs (NDs) are water-soluble nanoscale discoidal phospholipid bilayers encircled by membrane scaffold proteins or styrene-maleic-acid lipid particles (SMALPS) in a belt conformation, first assembled by the Sligar lab in 2002 [14]. Unlike vesicles, NDs are planar and therefore excellent biological membrane mimics that are well suited for controlled *in vitro* experiments because of their homogeneity, optical clarity, low light scattering, faster diffusion rates, and greater stability [15, 16]. NDs have emerged as a valuable membrane mimic, and numerous reports used NDs to incorporate membrane proteins for structural and functional

studies. We are aware of a single folding study, published in 2016, that utilized cell free expression and surface enhanced IR absorption spectroscopy to monitor the insertion and folding of bacteriorhodopsin into immobilized NDs on a gold film [17].

In this report, we present SDS-PAGE differential mobility studies combined with fluorescence, circular dichroism (CD), and UV resonance Raman (UVRR) spectroscopy to confirm and characterize the folding reaction of OmpA into NDs. The concerted insertion and folding mechanisms that describe β-barrel membrane protein systems like OmpA have only been discussed using a small set of proteins because of experimental challenges. The study of OmpA in NDs is important because ND technology offers important experimental advantages that enable more extensive studies of membrane protein folding.

4.4 Materials and methods

4.4.1 Expression, isolation, and purification of OmpA and mutants

The expression, isolation, and purification of wild-type and mutant OmpA were performed according to an established procedure [18]. The five native tryptophan residues in wild-type OmpA are located at positions 7, 15, 57, 102, and 143. OmpA W129 is a mutant with a single tryptophan residue at a nonnative position (Y129W) and phenylalanine residues at positions 7, 15, 57, 102, and 143 (W7F/W15F/W57F/W102F/W143F). Stock protein solution that contained 130-335 μM protein, 8.0 M urea, and 20 mM potassium phosphate buffer (KP_i, pH 7.3) were diluted to appropriate concentrations for the present experiments. All reagents were purchased from Thermo Fisher Scientific (Waltham, MA), Genesee Scientific Corporation (El Cajon, CA), MP Biomedicals (Santa Ana, CA), and GoldBio (St. Louis, MO) unless otherwise indicated, and used without further purification.

4.4.2 Preparation of vesicles and nanodiscs

The procedure for the preparation of SUVs is described elsewhere [18]. Briefly, 25 mg of 1,2-dimyristoyl-*sn*-glycero-3-phosphocholine (DMPC, T_C = 23 °C, Avanti Polar Lipids, Alabaster, AL) was dried under nitrogen gas for several hours. A lipid concentration of 5 mg/mL was achieved by re-suspending the dried lipid in 5 mL of 20 mM KP_i buffer at pH 8.0. SUVs with approximately 50 nm diameter were made by sonicating the aqueous lipid solution for 30 minutes with a probe ultrasonic microtip at 50% duty cycle with 30% maximum amplitude. The vesicles were passed through a 0.22 μm filter and equilibrated at 39 °C overnight before use. The identical procedure was followed for 1,2-dipalmitoyl-*sn*-glycero-3-phosphocholine (DPPC, T_C = 41 °C, Avanti Polar Lipids).

Large unilamellar vesicles (LUVs) were prepared by re-suspending 25 mg of dried DMPC lipid in 20 mM KP_i buffer, pH 8.0, to obtain a 5 mg/mL lipid concentration. The resuspended lipids were bath-sonicated for 5 minutes and extruded through a 0.1 or 0.2 μm pore-size polycarbonate membrane filter (SPI Supplies) [19]. The lipid solutions were passed through the appropriate membrane filter 22 times using two 5 mL extruder syringes to produce 100 and 200 nm diameter LUVs. The LUV solutions were equilibrated at 39 °C for at least 2 hours prior to use.

Preparation of NDs was based on a published procedure [20]. The belt peptide 14A, which is a 14-mer belt peptide with sequence Ac-DYLKAFYDKLKEAF-NH_2 (truncated analog of 18A peptide), was purchased from NeoScientific (>98% purity, Cambridge, MA). The appropriate mass of the 14A belt peptide (molecular weight 1792.06 g/mol) was dissolved in 0.7–1.1 mL of 20 mM KP_i at pH 8.0 to create a 10 mg/mL solution. Separately, 25 mg of DMPC (molecular weight 677.95 g/mol) in chloroform was dried under nitrogen gas for several hours to

evaporate the solvent. A final DMPC concentration of 6.4 mg/mL was achieved by re-suspending the dried lipid in 3.9 mL of 20 mM KP_i buffer at pH 8.0. An appropriate volume of the 10 mg/mL peptide solution (0.5 mL) was added to 0.5 mL of the 6.4 mg/mL aqueous lipid solution to achieve a final lipid-to-peptide molar ratio of 1.67 in 1.0 mL of buffer; this lipid-to-peptide ratio was reported to generate 10 nm diameter NDs (T_C = 29 °C [21]). The NDs were equilibrated at room temperature overnight prior to use.

4.4.3 Lipid:protein ratios

An important experimental variable in studies of membrane protein folding is the lipid:protein ratio. For these studies, appropriate volumes of stock NDs (4.7 mM lipid) or SUVs (7.4 mM lipid) were added to a buffer solution, followed by addition of protein in order to achieve a target lipid:protein ratio. For the majority of the experiments (gel electrophoresis and fluorescence), the target lipid:protein ratio was 300:1 or 400:1; for two experiments, the target ratios were 200:1 (CD), 190:1 (UVRR), or 70:1 (UVRR) because the amount of belt peptide had to be reduced on account of strong CD and UVRR signal from the belt peptide. The actual lipid:protein ratio was determined from calculated amount of lipid in sample and measured concentration of protein based on UV-vis absorption spectroscopy (a one-to-one subtraction of the ND/SUV signal from protein sample isolated the absorbance from OmpA). The 280-nm molar attenuation coefficient for wild-type OmpA is 54,390 cm^{-1} M^{-1} [22]. The lipid:protein ratios were within 15% of the target ratios, and two isolated experiments had larger deviations of 30% of the target ratios. For some experiments, e.g. digestion studies, the lipid:protein ratios could not be experimentally determined. In this report, the stated lipid:protein ratios are the target ratios. Separate experiments of OmpA folding as a function of lipid:protein ratios were

performed to ensure that the 30% variability of actual lipid:protein ratio did not impact the results, as described below.

It is also valuable to consider protein-to-SUV and protein-to-ND ratios, which can be determined with assumed input values (see Supplemental Information for calculations). In all experiments described here, there was less than one OmpA per ND; if a single OmpA were to fold into a ND, the percent coverage of the ND would be 4% for an OmpA pore diameter of 2 nm (based on distance between Cβ atoms across the pore). Depending on the experiment, there was a range of 37-200 OmpA per SUV, with a maximum coverage of 8% of the outer leaflet of the SUV if all 200 OmpA units were to fold into the SUV. The max value of 200 OmpA per SUV was for UVRR experiments that required higher concentration of protein.

4.4.4 Digestion of folded OmpA in SUVs and NDs

Digestion experiments with Arg-C endoproteinase (clostripain) purchased from Protea Biosciences (Morgantown, WV) were performed to confirm that OmpA inserted and folded into NDs. Parallel digestion experiments of OmpA folded into SUVs were performed for comparison. Arg-C was selected as a protease for digestion experiments because it is predicted to specifically cleave at the C-terminal side of arginine residues [23]; arginine exists in OmpA but not the ND belt peptide (Figure 1). Arg-C is described as exhibiting minor activity towards lysine residues [24]. Wild-type OmpA was added to preformed ND or SUV solutions in 50 mM ammonium bicarbonate buffer, pH 8.0. For both samples, the lipid:protein ratio and residual urea concentration were 300:1 and 0.3 M, respectively, and the final OmpA concentration was 14 μM. The samples were incubated at 37 °C for 6 hours, allowing OmpA to fold. The folded state was confirmed with fluorescence and/or SDS-PAGE analysis (see below). After the 6-hour folding period, appropriate amounts of these folded stocks were incubated at 37 °C with Arg-C

to achieve a final OmpA concentration of 9.0 μM (in the presence of NDs) and 8.0 μM (in the presence of SUVs). The final Arg-C concentration was 0.6 μM in the ND sample and 0.5 μM in the SUV sample, which gave OmpA:Arg-C ratios of 15:1 and 16:1, respectively. These OmpA:Arg-C ratios were within the manufacturer-suggested OmpA:Arg-C ratio range of 10:1 to 20:1. Digestion of the folded samples in NDs or SUVs with Arg-C was carried out for 3 hours and 24 hours. Dithiothreitol (3.5 μL of 1.0 M stock solution) and calcium acetate (4-5 μL of 20 mM stock solution) were added to the samples (final concentrations of 50 mM and 1.0 mM, respectively) to aid in digestion. A sample of unfolded 5.0 μM OmpA in 3.6 M urea was incubated at room temperature for at least 30 minutes, and digested with Arg-C (OmpA:Arg-C ratio 20:1) at 37 °C for 4 hours. Approximately 6 μg of the folded protein samples with and without Arg-C was loaded on 12% polyacrylamide Mini-PROTEAN TGX precast gels. For the unfolded samples with and without Arg-C, approximately 3.5 μg of protein was loaded on the gel. The samples were not boiled prior to loading on the gel.

4.4.5 Digestion of adsorbed OmpA on NDs and SUVs

OmpA may be stabilized as an adsorbed intermediate that interacts with, but does not insert into, a lipid bilayer in the gel phase. Digestion experiments of wild-type OmpA adsorbed onto NDs or SUVs were performed to determine the extent of accessibility of the adsorbed state to Arg-C protease in solution. An aliquot of OmpA from a stock solution was added to equilibrated solutions of NDs or SUVs in ammonium bicarbonate buffer, pH 8.0, at 16 °C in a 10 mm x 4 mm quartz cuvette, and sealed with a rubber septum. At 16 °C, both DMPC ND and DMPC SUV bilayers are in gel phase, preventing the insertion and folding of OmpA into the bilayer [25]. The temperatures of the ND and SUV protein samples were monitored with a thermocouple immersed at the top of the sample (sensor type T with Omega HH201A). Prior to

addition of the protease, the lipid:protein ratio was 300:1, the residual urea concentration was 0.2 M in both ND and SUV samples, and the concentration of OmpA was 8.0 μM. The samples were continuously stirred using a micro stir bar and incubated at 16 °C for 4 hours prior to digestion.

Fluorescence spectra of the adsorbed samples were measured after 4 hours of incubation, prior to digestion, at 16 °C using a Jobin Yvon-SPEX Fluorolog FL3-11 spectrofluorometer to confirm the presence of the slightly blue-shifted (relative to unfolded protein) adsorbed intermediate. The samples were excited with a wavelength of 295 nm along the 4 mm path and emission was collected along the 10 mm path. The excitation and emission bandpass were set to 3 nm. SDS-PAGE confirmed the absence of folded OmpA via the apparent molecular weight of the adsorbed intermediate, ~33 kDa [5, 25], prior to the addition of Arg-C.

Aliquots of adsorbed OmpA were added to equilibrated solutions of Arg-C protease (OmpA:Arg-C ratio of 10:1) that also contained 50 mM dithiothreitol and 1.5 mM calcium acetate in ammonium bicarbonate buffer, pH 8.0, at 16 °C. The final concentrations of OmpA and urea during digestion were 5 μM and 0.1 M, respectively. The samples were incubated at 16 °C, and the digested products were analyzed via SDS-PAGE using 12% polyacrylamide Mini-PROTEAN TGX precast gels after 4 and 24 hours of digestion. A control sample was analyzed in parallel with the digestion experiment. This control solution was comprised of 5 μM OmpA adsorbed onto NDs or SUVs and 0.1 M urea, but did not contain Arg-C protease, dithiothreitol, or calcium acetate. Approximately 5 μg of digested and control OmpA was added to the wells. The samples were not boiled prior to loading onto the gel.

4.4.6 Circular dichroism spectroscopy

OmpA secondary structure was probed by CD spectroscopy. CD spectra of wild-type and the single tryptophan mutant, W129, folded in NDs or SUVs and unfolded in 4.0 M urea were

obtained with a Jasco J-815 spectrometer. The sample chamber was continuously purged with nitrogen gas and held at a temperature of 37 °C for measurements of folded OmpA. Samples of folded OmpA in NDs or SUVs contained 3-6 μM protein, 0.3 M urea, and 200:1 lipid:protein ratio in 20 mM KP_i buffer (pH 8.0). Samples of unfolded OmpA contained 4-6 μM protein and 4.0 M urea in 20 mM KP_i buffer (pH 8.0). Folded samples were allowed to incubate in the presence of NDs or SUVs at 37 °C for 5 hours prior to the collection of CD spectra. Unfolded samples were incubated in their buffered urea solutions for at least 30 minutes at room temperature prior to the collection of spectra. CD spectra were acquired from 204-260 nm (208-260 nm for unfolded samples) in a 1 mm pathlength quartz cuvette with 1 sec digital integration time, 1 nm bandwidth, and 50 nm/min scan speed. A total of 6 accumulations for each protein sample were collected and averaged. Background samples, which contained the appropriate buffer (including NDs or SUVs for folded samples and urea for unfolded samples) without protein were also acquired and subtracted from each protein spectrum to isolate the signal from protein only. Fluorescence spectra of folded and unfolded protein were also collected to confirm the conformation of each state.

4.4.7 SDS-PAGE differential protein mobility assay during folding

Aliquots of unfolded OmpA from the stock solution were added to buffered (KP_i, pH 8.0), preformed solutions of NDs or SUVs equilibrated at 33 °C to achieve an OmpA concentration of 7-15 μM. The lipid:protein ratio in SUVs and NDs was 400:1. This mixing initiated the folding reaction because the urea concentration was diluted to 0.2 M. Samples were maintained at 33 °C during the experiment. The folding reaction was quenched at 9 time points (t = 4, 8, 16, 30, 46, 60, 120, 180, 240 min after initiation of the folding reaction) by addition of Laemmli loading dye [26] and kept at room temperature until they were loaded onto the gel. The

samples were analyzed via SDS-PAGE using 12% polyacrylamide Mini-PROTEAN TGX precast gels at a constant voltage of 150 V with 0.1% SDS in the running buffer. Approximately 3 μg of protein were added to each well of the gel. The gels were stained with Coomassie blue. The samples were not boiled prior to loading onto the gel.

4.4.8 Fluorescence spectroscopy

The folding reactions of wild-type OmpA in NDs and SUVs were monitored using fluorescence spectroscopy. The folding reactions were initiated by addition of stock unfolded OmpA into equilibrated ND or SUV solutions. The final samples contained 4 μM OmpA, 0.2 M residual urea, and a lipid:protein ratio of 400:1 in pH 8.0 KP_i buffer. Fluorescence spectra from a Jobin Yvon-SPEX Fluorolog FL3-11 spectrofluorometer were acquired at 10 time points: 1, 4, 8, 16, 30, 46, 60, 120, 180, and 240 min after initiation of the folding reaction. Samples were maintained at 33 °C during the 4-hour period in a 10 mm x 2 mm quartz cuvette sealed with a Teflon cap. The samples were excited with 295 nm wavelength light along the 2 mm path, and emission was collected along the 10 mm path. The excitation and emission bandpass were set to 3 nm. Samples were gently shaken before and after fluorescence spectra were acquired to ensure thorough mixing throughout the duration of the experiment. Spectra of NDs and SUVs without OmpA were acquired at the beginning and end of each experiment; these spectra of ND-only and SUV-only were subtracted from OmpA spectra to isolate fluorescence signal from protein. The fluorescence spectrum of folded OmpA in SUVs (98% folding yield based on gel) and unfolded OmpA in 8.0 M urea served as basis spectra for Gaussian decompositions, and all fluorescence data were analyzed by the intensity-corrected decomposition method described elsewhere [27] using Igor Pro software.

Folding reactions of wild-type OmpA in 100-nm and 200-nm diameter LUVs were investigated using fluorescence spectroscopy. Appropriate volumes of 5 mg/mL 100-nm and 200-nm diameter LUV aqueous solution were added to OmpA stock solutions to yield final OmpA concentrations of 2.0 and 0.5 μM, respectively. The lipid:protein ratios were 1,250:1 (100-nm LUV) and 5,000:1 (200-nm LUV); these ratios were selected to maintain the same vesicle:OmpA ratio of 1:49 for all three vesicles, including SUVs. A sample of 5 μM OmpA with SUVs (lipid:protein ratio of 300:1) was also prepared for comparison. The residual urea concentration in all samples was 0.2 M. The OmpA-LUV and OmpA-SUV samples were incubated overnight for 12 hours at 33 °C in a temperature-controlled water bath. After the 12-hour folding period, fluorescence spectra were measured for each sample. All samples were excited with 290 nm light along the 2 mm pathlength and emission was collected from 305 to 500 nm along the 10 mm pathlength. The excitation and emission bandpass were set to 3.5 nm. Spectra of vesicles-only in 0.2 M urea and 20 mM KP_i, pH 8.0, were also acquired, and these spectra were used to remove background scattering and isolate signal from protein only.

Fluorescence spectra of wild-type OmpA were acquired above and below the transition temperature for the lipid bilayers. The temperature of the samples was monitored with a thermocouple inserted at the top of the sample. Stock unfolded wild-type OmpA was added to an equilibrated solution of NDs or SUVs (pH 8.0) at 15 °C in a 10 mm x 4 mm quartz cuvette and sealed with a rubber septum. After mixing, the samples contained 4 μM OmpA and 0.2 M urea. The lipid:protein ratio in both ND and SUV samples was 300:1. The samples were excited with 295 nm light along the 4 mm path, and emission was collected along the 10 mm path. The excitation and emission bandpass were set to 3 nm. Fluorescence spectra were acquired at 15 °C at times 2-, 3-, and 4-hours after addition of protein. The temperature was then raised to 36 °C

and fluorescence spectra were acquired after 2- and 4-hours at this elevated temperature. Samples were gently shaken before and after spectra were acquired to ensure thorough mixing throughout the experiment. Spectra of ND-only and SUV-only in 0.2 M urea were also acquired at the same time points and temperatures as protein solutions. The ND-only and SUV-only spectra were used for background subtraction.

4.4.9 UV resonance Raman spectroscopy

UVRR spectroscopy was employed to further confirm the folding of OmpA into NDs. The UVRR Ti:Sapphire laser system has been previously described [28]. A 228-nm excitation beam was used to measure the UVRR spectra of OmpA mutant W129. This mutant was selected for UVRR experiments because it exhibits an intense and unique peak at 785 cm^{-1} that is indicative of folded protein [7]. Protein samples of 20 μM W129 OmpA were prepared in four aqueous solutions that contained 10 mg/mL N-octyl-β-D-glucoside (OG) detergent micelles with 0.8 M urea, 1 mg/mL DMPC SUVs (lipid:protein ratio of 70:1) with 0.8 M urea, 1 mg/mL DPPC SUVs (lipid:protein ratio of 70:1) with 0.8 M urea, and 0.8 M urea. Experiments with DPPC probed the adsorbed state of OmpA on SUVs. The 1.3 mg/mL DMPC ND samples contained 10 μM OmpA with 0.6-0.8 M urea, and a lipid:protein ratio of 190:1. All UVRR spectra were collected for 10 minutes, with the exception of the OmpA in ND samples, which were collected for 5 minutes.

4.5 Results

4.5.1 Digestion of folded OmpA

The extent of protection of the OmpA transmembrane domain in NDs and SUVs was investigated with digestion experiments. Arg-C protease selectively cleaves at arginine sites and is reported to also cleave at lysine sites at slower rates [29]. Figure 4.1 shows that there are 13

arginine residues in OmpA, with 5 arginine residues predicted to be in the transmembrane domain and thus, protected from digestion in the folded state. SDS-PAGE bands that correspond to OmpA folded in NDs, folded in SUVs, folded and digested, unfolded in 3.6 M urea, and unfolded and digested are shown in Figure 4.2. The differential mobility shift of folded (~29 kDa) and unfolded (~33-35 kDa in the presence of 3.6 M urea) OmpA (calculated MW of 35,172 Da) is consistent with previous studies [5, 25, 30], and is attributed to the increase in compactness in the native form relative to the denatured conformation [31]. Analysis of the optical band densities in Figure 2 using UN-SCAN- IT gel analysis software determined the folding yield to be 89% in NDs and 96% in SUVs. Folded OmpA in NDs or SUVs incubated with Arg-C for 3- or 24-hours was digested to a protected major ~26 kDa fragment and a minor ~24 kDa fragment; the native ~29 kDa folded band was eliminated with Arg-C digestion. The first exposed Arg residue outside the membrane-protected region of OmpA is position 242, and the resulting folded fragment has a calculated MW of 26,300 Da. Given that folded OmpA exhibits an apparent MW that is typically lower than the calculated MW on gels, the observed values of ~26 kDa and ~24 kDa bands correspond to membrane-protected fragments. A 24 kDa membrane-protected portion of OmpA has been previously published with trypsin as the cleaving enzyme [5, 25]. The observation of a smaller membrane-protected fragment with trypsin (24 kDa) compared to Arg-C (~26 kDa) is consistent with the presence of several lysine residues (positions 192, 197, 206, 210, 230) that precede the first exposed Arg residue (position 242), resulting in a smaller membrane-protected fragment with trypsin. Unfolded OmpA in the presence of Arg-C was digested to fragments with apparent molecular weights of 10-17 kDa (data not shown).

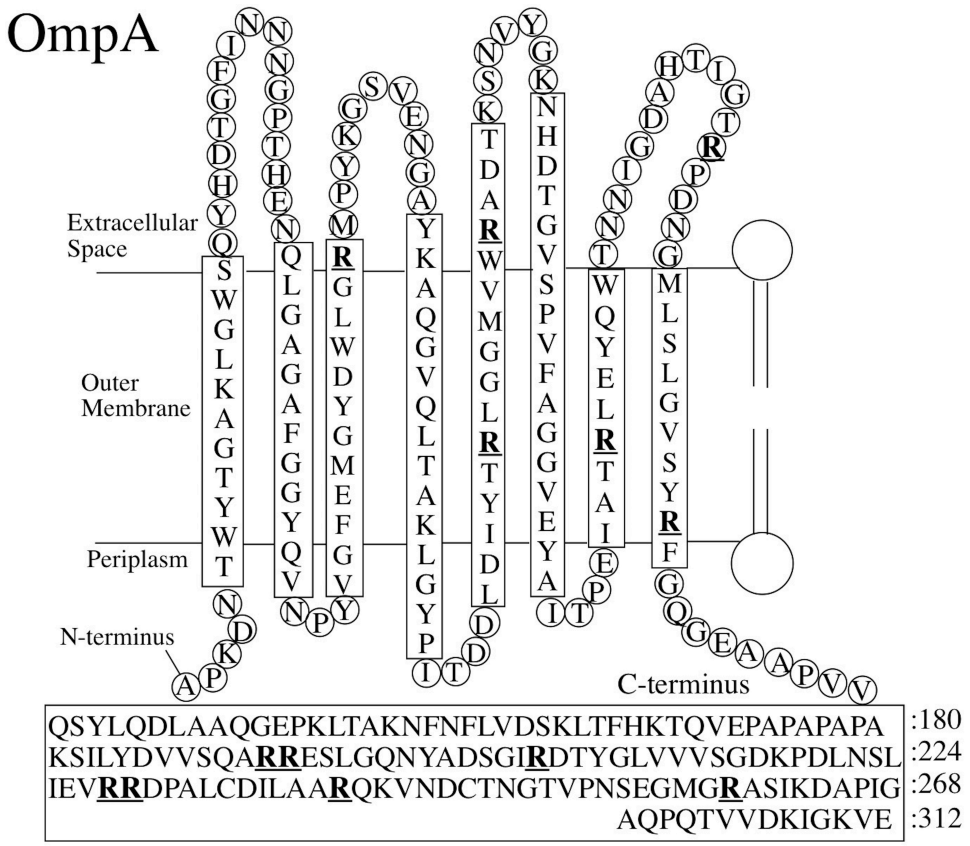

14A

Ac-DYLKAFYDKLKEAF-NH_2

Figure 4.1 The top shows the membrane topology of OmpA. Arginine residues are indicated in bold and are underlined. The bottom shows the primary sequence of 14A, the belt peptide.

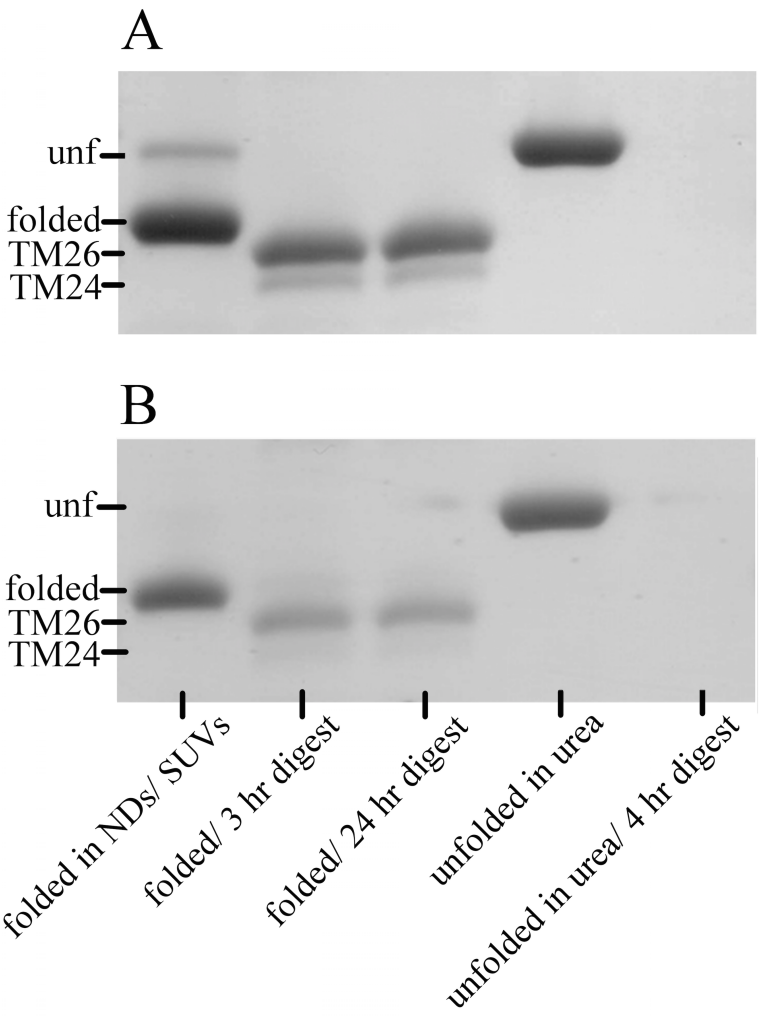

Figure 4.2 SDS-PAGE result of OmpA digestion. Gels show digestion of OmpA in NDs (A) and in SUVs (B). The lipid:protein ratio was 300:1 and the residual urea concentration was 0.3 M before digestion. Samples during folding and digestion were incubated at 37 °C. For both gels: lane 1: folded in NDs (A) or in SUVs (B); lane 2: folded in NDs (A) or SUVs (B) and digested with Arg-C for 3 hrs; lane 3: folded in NDs (A) or SUVs (B) and digested with Arg-C for 24 hrs; lane 4: unfolded (unf) OmpA in 3.6 M urea; and lane 5: unf OmpA in 3.6 M urea and digested with Arg-C for 4 hrs. The bands for folded, unf, and the ~26 kDa transmembrane fragments (TM26 and TM 24) are indicated.

4.5.2 Digestion of OmpA adsorbed intermediate

Digestion experiments were carried out to determine the accessibility of Arg-C protease to adsorbed OmpA. Gels in Figure 4.3 show bands near 35 kDa which correspond to OmpA adsorbed [5] onto DMPC SUVs and NDs. After 4 hours of digestion with Arg-C protease at 16 °C, the intensities of the bands for adsorbed OmpA are significantly decreased. After 24 hours of digestion at 16 °C, the adsorbed band is completely eliminated.

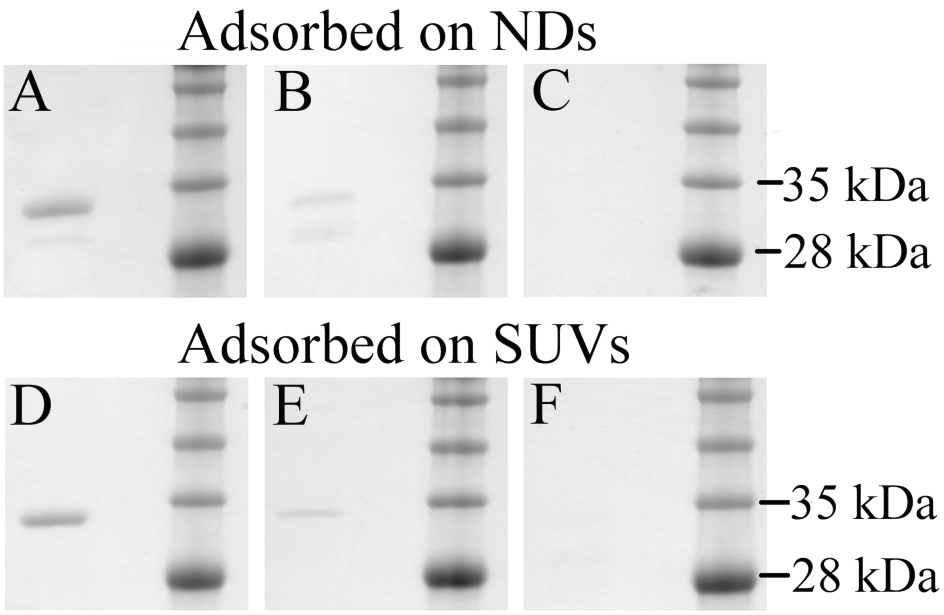

Figure 4.3 Arg-C digestion of wild-type OmpA adsorbed on NDs (top) and SUVs (bottom) at 16 °C. In each image, the left lane contains protein, and the right lane is the molecular weight ladder. Gels are of OmpA adsorbed on (A) NDs, no digestion; (B) NDs, 4 hr digestion; (C) NDs, 24 hr digestion; (D) SUVs, no digestion; (E) SUVs, 4 hr digestion; and (F) SUVs, 24 hr digestion. The residual urea concentration in the samples before digestion was 0.2 M.

4.5.3 Folding of OmpA in NDs and SUVs

The secondary structure of wild-type OmpA in NDs and SUVs was investigated with CD. The CD spectra for folded OmpA exhibited a minimum near 215 nm, characteristic of folded OmpA (Figure 4.4) [22, 32]. The CD spectrum of OmpA unfolded in the presence of urea exhibited a large negative feature that extends into the far UV region, which has been characterized as denatured OmpA [22, 32].

The insertion and refolding of wild-type OmpA into NDs and SUVs was monitored at 33 °C for 4 hours by SDS-PAGE differential mobility studies. A representative data set is shown in Figure 4.5. The folding reaction was initiated by mixing protein with equilibrated ND or SUV samples; this mixing resulted in a reduction in urea concentration to 0.2 M. The conversion of denatured to native conformation is evident in protein bands at the two distinct apparent molecular weights of ~33 kDa and ~29 kDa, respectively, based on calculated R_f values. The fraction of folded OmpA at different time points during the folding reaction was assessed by density analysis of the bands, and the evolution of population was fit to a single exponential function. The folding time, τ, is the reciprocal rate constant ($1/k$), and was 28 ± 4 min (5 trials); the folding yield was 88 ± 12% (7 trials) for OmpA in NDs. Analogous values for OmpA in SUVs were 10 ± 5 min (3 trials) for the folding rate and 97 ± 2% (4 trials) for folding yield. These results are summarized in Table 4.1.

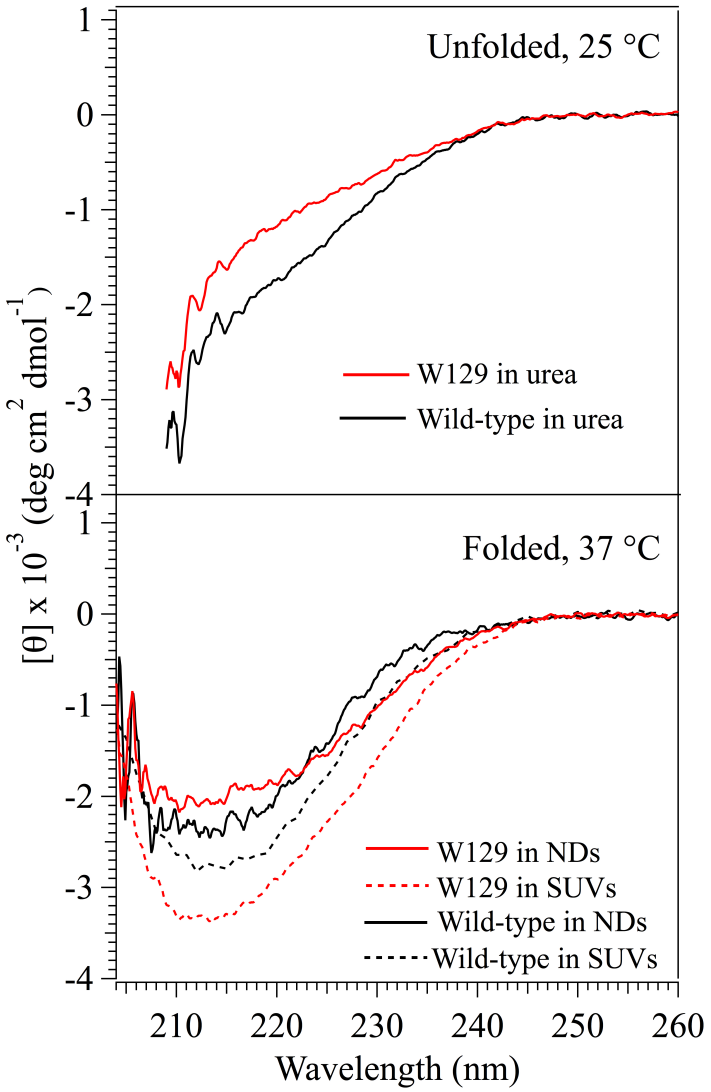

Figure 4.4 Circular dichroism spectra of wild-type and single tryptophan mutant W129 OmpA unfolded in 4.0 M urea (top panel) and folded in NDs or SUVs (bottom panel. OmpA was incubated for 5 hrs in the presence of NDs or SUVs. Solid lines in the bottom panel represent folding into NDs. Dashed lines in the bottom panel represent folding in SUVs. The lipid:protein ratio was 200:1 and the residual urea concentration was 0.3 M.

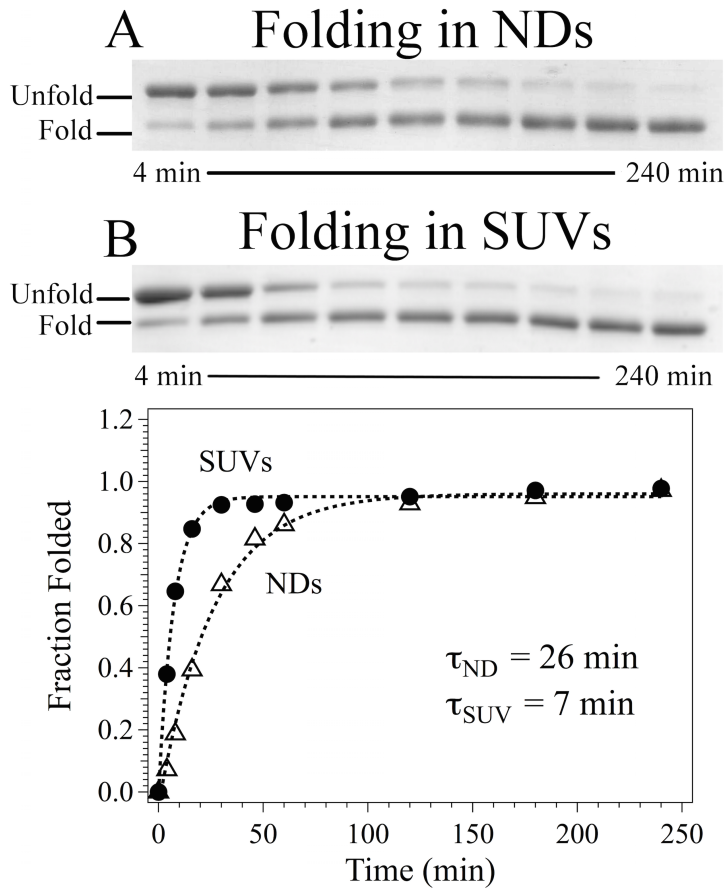

Figure 4.5 Wild-type OmpA folding reaction monitored by SDS-PAGE at 33 °C for 4 hrs. Data were collected at 4, 8, 16, 30, 46, 60, 120, 180, and 240 minutes after initiation of the folding reaction. The top shows SDS-PAGE gels of OmpA folding in the presence of (A) NDs and (B) SUVs. The bottom shows fraction folded based on gel band densities for OmpA in NDs (triangles) and SUVs (solid circles). The lipid:protein ratio in SUVs and NDs was 400:1 and the residual urea concentration was 0.2 M. The curves and resulting folding times are based on single exponential fits to the data, including a value of 0 at time 0 minutes.

Table 4.1 Summary of folding time constants (τ) and yields for wild-type OmpA in DMPC bilayers.

	NDs	**SUVs**
SDS-PAGE		
τ (min)	28 ± 4 (*n* = 5)	10 ± 5 (*n* = 3)
Folding yield (%)	88 ± 12 (*n* = 7)	97 ± 2 (*n* = 4)
Fluorescence		
τ (min)	21 ± 5 (*n* = 4)	9 ± 4 (*n* = 3)
Folding yield (%)	97 ± 2 (*n* = 4)	99 ± 1 (*n* = 3)

The results were determined by SDS-PAGE differential mobility studies and fluorescence spectroscopy. The data from SDS-PAGE gels were quantified using UN-SCAN-IT gel analysis software. The data from fluorescence spectra were quantified via Gaussian decompositions.τis the reciprocal rate constant, 1/*k*, based on the exponential fit and is reported as τ ± standard deviation for the indicated number of *n* trials; a value of 0 was included at time 0 minutes in the fits. The reported folding yields are the average of the fraction folded at 240 minutes for each of the trials.

The folding reaction of OmpA was also investigated with fluorescence spectroscopy. The folding of OmpA into SUVs and LUVs has been previously reported [9, 10, 22, 30, 33, 34], and it is well known that there is a characteristic emission λ_{max} blue-shift and increase in fluorescence quantum yield upon folding [27]. Figure 4.6 shows representative fluorescence spectra of OmpA in the presence of NDs and SUVs, and illustrates the λ_{max} blue-shift from 356 nm (in 8 M urea) to 337 nm (in SUVs and NDs) over 4 hours. These experimental fluorescence spectra were decomposed into two Gaussian, intensity-weighted basis spectra for fully folded (337 nm) and unfolded (357 nm) spectra, where the fully folded spectrum exhibited an increased fluorescence quantum yield by a factor of 3.2 relative to unfolded OmpA. This decomposition method has been used to determine the fraction of folded protein during folding [27]. The folding rate ($\tau = 1/k$) based on single exponential fit was 21 ± 5 min (4 trials), and the folding yield was 97 ± 2% (4 trials) for OmpA in NDs. Analogous values for folding rate and yield for OmpA in SUVs were 9 ± 4 min (3 trials) and 99 ± 1% (3 trials), respectively. Representative decompositions of OmpA in NDs is shown in Figure 4.7. Use of alternate functions, such as the log-normal function as opposed to Gaussian, did not affect the resulting kinetics. The kinetic parameters are summarized in Table 4.1.

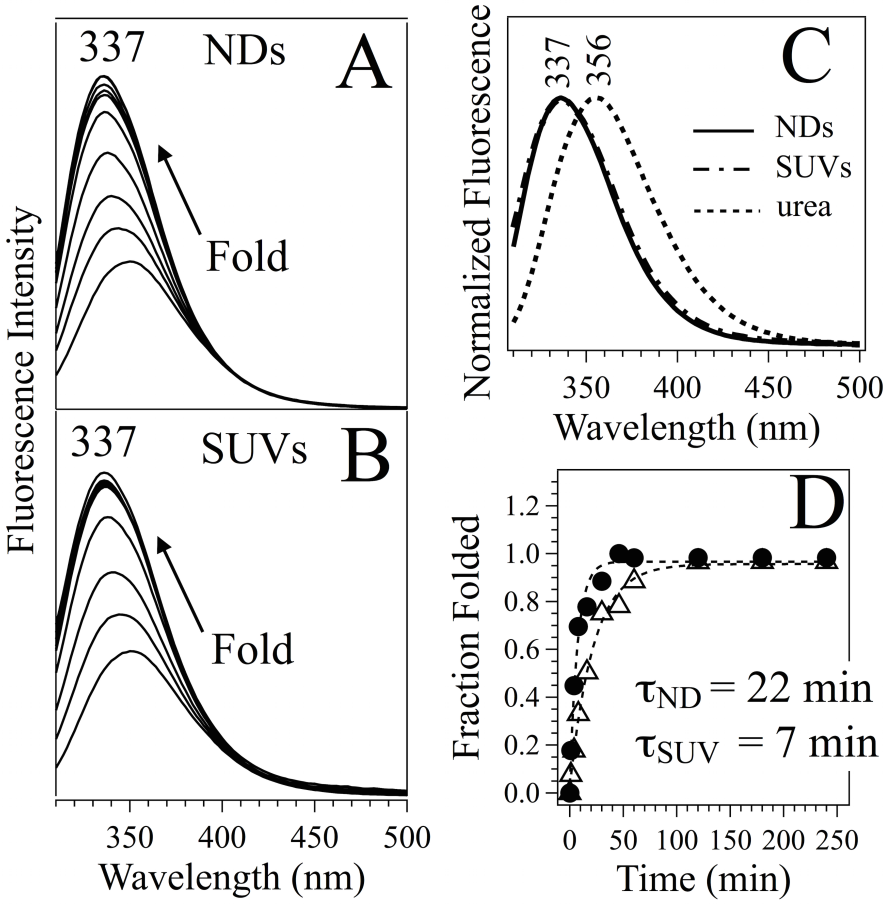

Figure 4.6 Wild-type OmpA folding reaction monitored by fluorescence spectroscopy at 33 °C for 4 hrs. Spectra were acquired 1, 4, 8, 16, 30, 46, 60, 120, 180, and 240 minutes after initiation of the folding reaction in DMPC NDs (A) or SUVs (B). The lipid:protein ratio was 400:1 and the residual urea concentration was 0.2 M for both samples. The steady-state spectra of OmpA folded in NDs and SUVs and unfolded in 8 M urea are shown in (C). The fraction folded during folding reactions in SUVs (solid circles) and NDs (triangles) are shown in (D), with single exponential fits (including a value of 0 at time 0 minute).

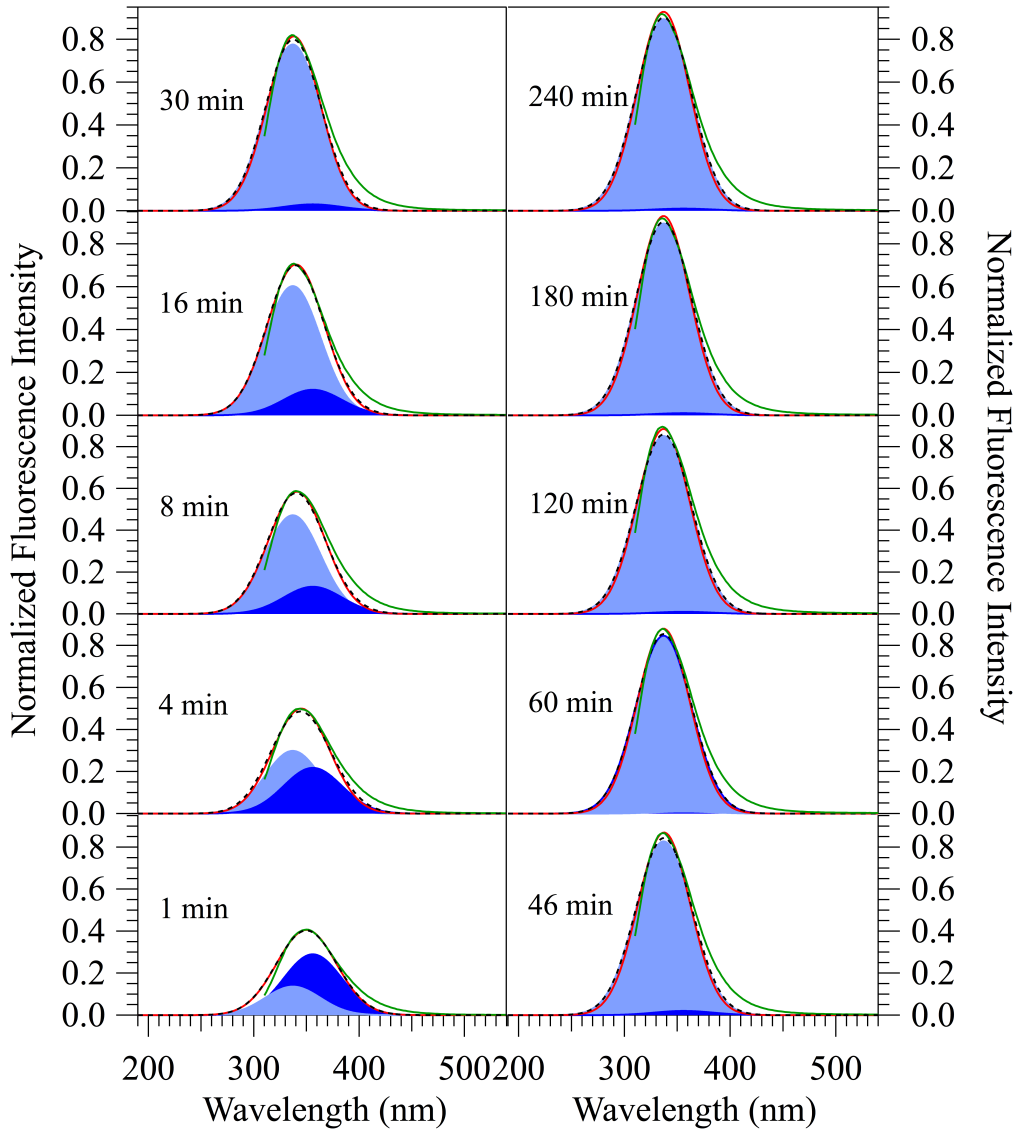

Figure 4.7 The experimental fluorescence spectrum from 310 to 550 nm (green solid) was fit to a Gaussian curve (red solid) for each time point. Each Gaussian fit was decomposed into two basis spectra that corresponded to the folded (light blue filled) and unfolded (dark blue filled) populations. The sum of the two basis spectra is shown (black dashed).

The dependence of folding rates and yields on different lipid:protein ratios were also investigated with SDS-PAGE differential mobility and fluorescence measurements. Actual lipid:protein ratios of 70:1, 170:1, 230:1, and 300:1 were confirmed by absorption spectroscopy, and results of folding experiments are shown in Figure 4.8. The yields of folding after 4-hours of incubation was 94-97% based on gels and 98-100% based on fluorescence; these are high folding yields regardless of lipid:protein ratio. The folding rate assessed by fluorescence did depend on the lipid:protein ratio when the ratio was low; at the lowest ratio of 70:1, the folding rate was 36 minutes whereas for the higher ratios of 170:1, 230:1, and 300:1, the rates were similar at 26, 22, and 20 min, respectively.

The folding of OmpA into lower curvature, 100-nm and 200-nm diameter LUVs, was probed with fluorescence spectroscopy. Figure 4.9 shows that the emission maxima of OmpA in LUVs are 342 and 341 nm, which are red-shifted relative to the λ_{max} value of 337 nm in the presence of SUVs. The folding yields of wild-type OmpA into 100-nm and 200-nm diameter LUVs were 42% and 53%, respectively, as determined by the intensity-weighted Gaussian-decomposition method. The basis spectra in the decomposition analysis for folding into 100- and 200- nm diameter LUVs was the same set of basis spectra used in the decomposition analysis for folding into SUVs.

The ability to initiate folding of adsorbed OmpA by converting the bilayer to the fluid phase was investigated with variable-temperature fluorescence experiments. Previous fluorescence reports demonstrated that the low-temperature intermediate form of OmpA can be converted to native, folded OmpA by increasing the temperature above the phase transition of the bilayer [35]. Figure 4.10 shows fluorescence spectra corresponding to the low temperature adsorbed intermediate on NDs and SUVs. The adsorbed intermediate is characterized by

fluorescence λ_{max} values of 343 (NDs) and 345 (SUVs) nm. The adsorbed species was formed rapidly [35] and over the course of 4 hours at 15 °C, the fluorescence λ_{max} emission and quantum yield did not change significantly. When the ND and SUV sample temperatures were increased above the phase transition of the bilayer, to 36°C, the fluorescence λ_{max} emission values shifted to 337 nm and the quantum yield increased.

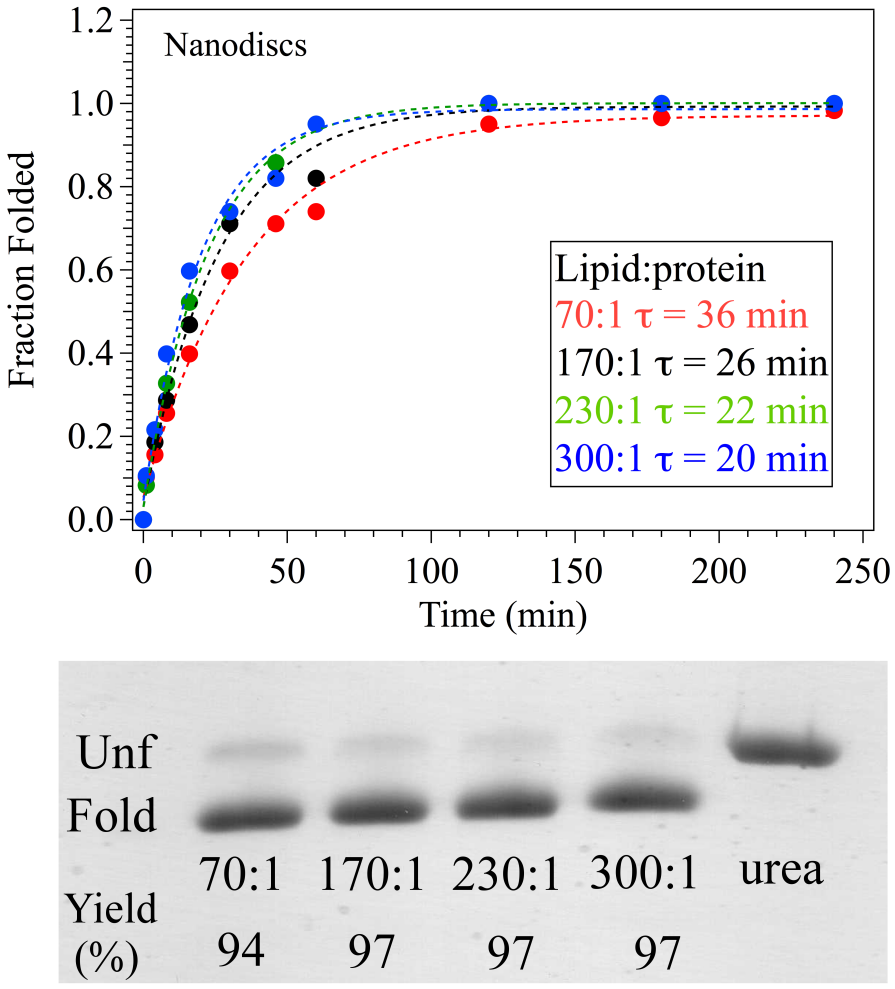

Figure 4.8 Top: Wild-type OmpA refolding reaction monitored by fluorescence at 33 °C for 4 hrs for different lipid:protein ratios. The fraction folded was based on intensity-weighted decomposition analysis for OmpA in NDs at times 1, 4, 8, 16, 30, 46, 60, 120, 180, and 240 minutes after initiation of the folding reaction. The actual lipid:protein ratios as measured by absorption spectroscopy are indicated. The curves and resulting folding times are based on single exponential fits to the data, including a value of 0 at time 0 minutes. Bottom: SDS-PAGE gels of OmpA incubated with NDs after 4 hrs in different lipid:protein ratios as well as unfolded in urea. The actual lipid:protein ratios based on absorption spectroscopy and percent folded yields in NDs based on gel densities are indicated. The residual urea concentration for both sets of experiments was 0.3 M.

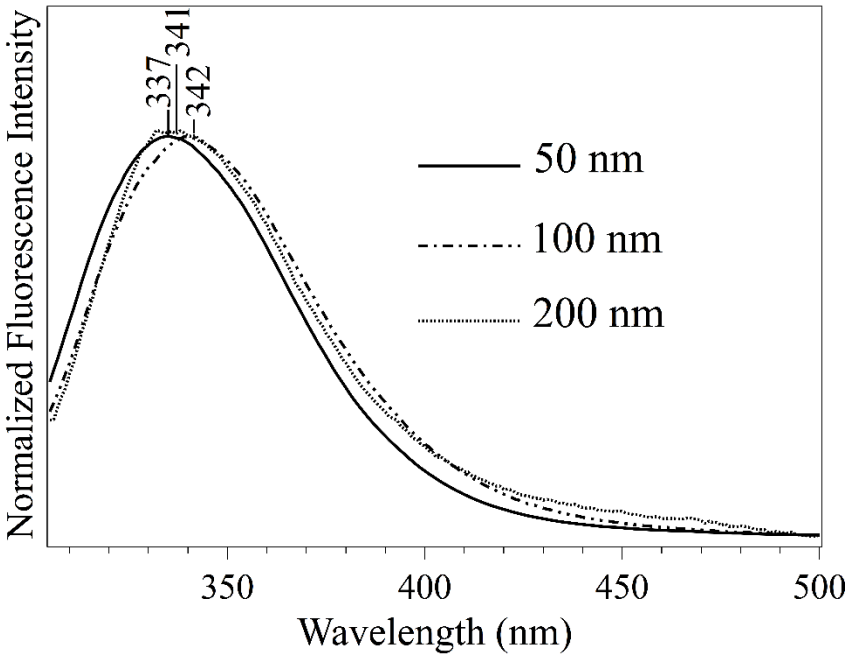

Figure 4.9 Wild-type OmpA (5 μM) folded into 50 nm diameter DMPC SUVs (solid, emission max 337 nm); 2 μM OmpA in the presence of 100 nm LUVs (dash-dotted, emission max 342 nm); and 0.5 μM OmpA in the presence of 200 nm diameter LUVs (dotted, emission max 341 nm) after 12 hrs at 33 °C. The vesicle:OmpA ratio was 1:49 and the residual urea concentration was 0.2 M for all samples.

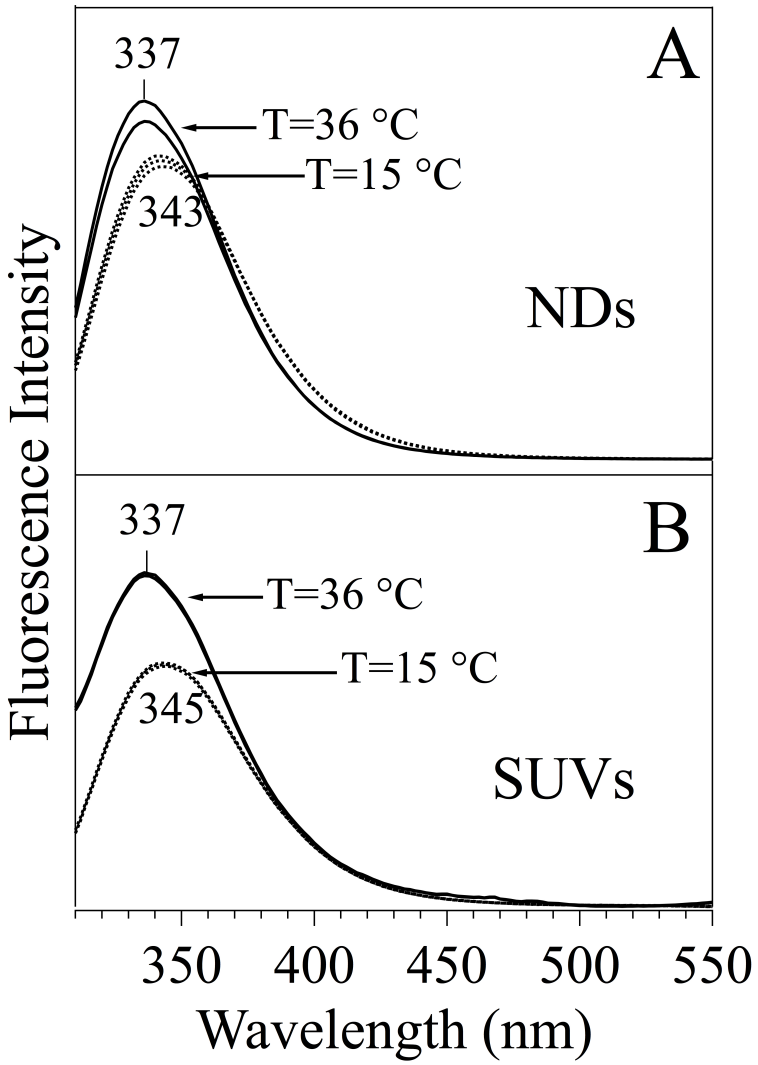

Figure 4.10 Variable-temperature fluorescence experiments. Spectra are of wild-type OmpA at 15 °C (dashed curves) and 36 °C (solid curves) in the presence of (A) NDs and (B) SUVs. Spectra were obtained at 15 °C at time 2-, 3-, and 4-hrs after mixing OmpA with NDs or SUVs. The temperature was increased to 36 °C and spectra were acquired after 2- and 4-hrs at this elevated temperature. The lipid:protein ratio was 300:1 and the residual urea concentration was 0.2 M for both samples.

4.5.4 UVRR spectroscopy of folded OmpA

The folding of OmpA into NDs was further investigated with UVRR spectroscopy. Single tryptophan mutant W129 was selected for this analysis because this mutant exhibits a unique peak at 785 cm^{-1} that is assigned a hydrogen-out-of-plane (HOOP) mode [18, 36] for natively-folded protein. The mutant W129 exhibited similar folding kinetics, yield, and secondary structure as wild-type (Figures 4.4 and 4.11). Figure 4.12 shows UVRR difference spectra of W129 in various conformations of folded, adsorbed, and unfolded. The HOOP mode is observed only under folding conditions in the presence of OG detergent micelles, DMPC SUVs, and DMPC NDs. Additional UVRR spectra for a tryptophan + tyrosine mixture to mimic OmpA mutant W129, 10 mg/mL OG detergent, 1 mg/mL DMPC SUVs, and 20 mM KP_i buffer can be found in Figure 4.13.

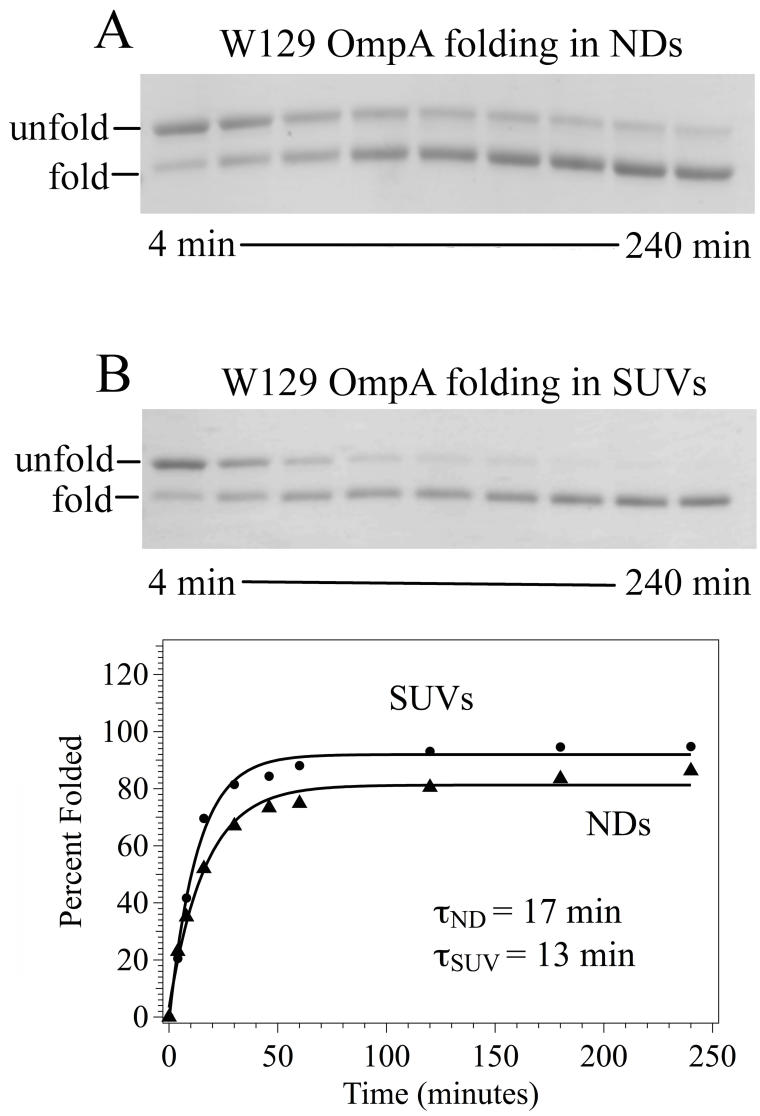

Figure 4.11 W129 OmpA folding reaction monitored by SDS-PAGE at 33 °C for 4 hours. Data were collected at 4, 8, 16, 30, 46, 60, 120, 180, and 240 min after initiation of the folding reaction. Top shows SDS-PAGE gels of OmpA folding in the presence of (A) DMPC NDs and (B) DMPC SUVs. Bottom shows fraction folded based on gel band densities for OmpA in NDs (▲) and SUVs (●). The lipid: protein ratio was 400:1 and the residual urea concentration was 0.4 M. The curves and resulting folding times are based on single exponential fits to the data, a value of 0 at time 0 min. The folding yield at 240 minutes was 86% (NDs) and 95% (SUVs).

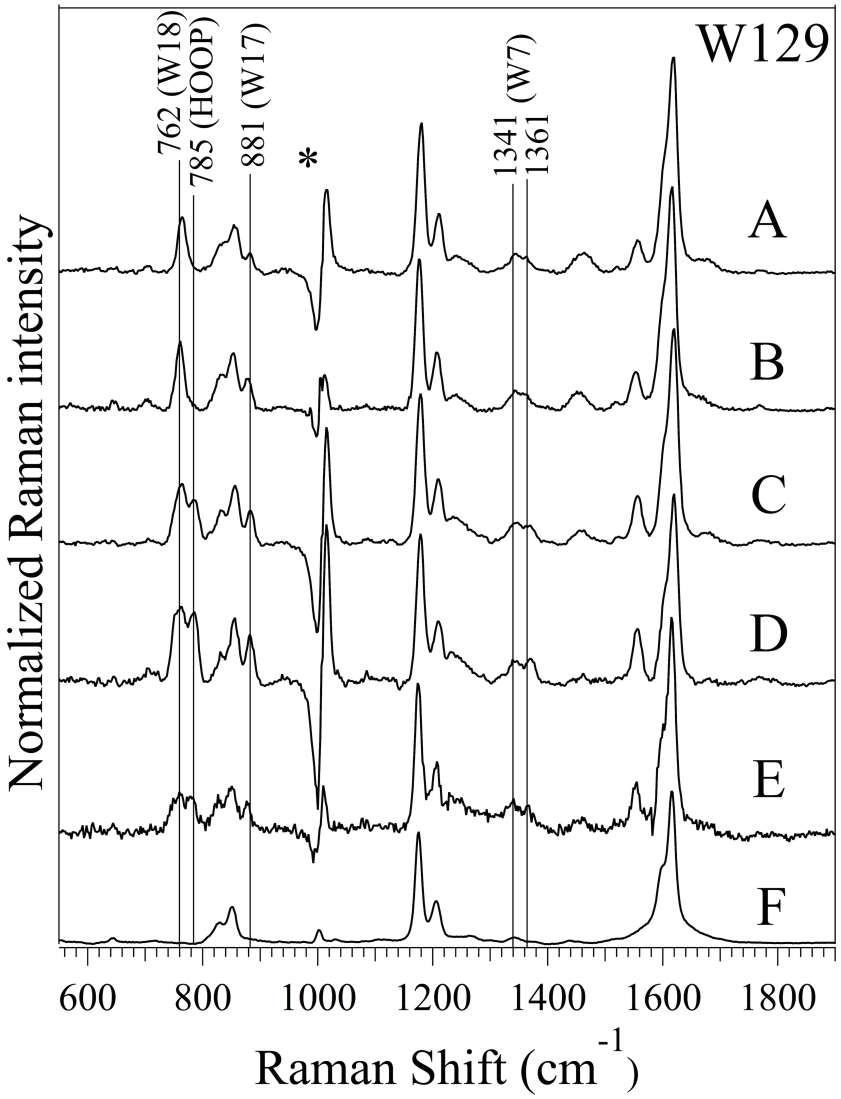

Figure 4.12 UVRR difference spectra. Signal from the buffer, urea, SUVs, and NDs as well as general scattering have been subtracted for OmpA W129 mutant in (A) 0.8 M Urea; (B) adsorbed on DPPC SUVs; (C) folded in detergent (OG); (D) folded in DMPC SUVs; and (E) folded in DMPC NDs. The spectrum of ND-only in which signal from buffer is subtracted is shown as (F). All spectra were collected at room-temperature and for 10 minutes, with the exception of the spectrum of OmpA in NDs (spectrum E), which was collected for 5 minutes. The region near 1000 cm^{-1} (indicated with *) has strong urea signal in each sample except (F), resulting in a subtraction artifact.

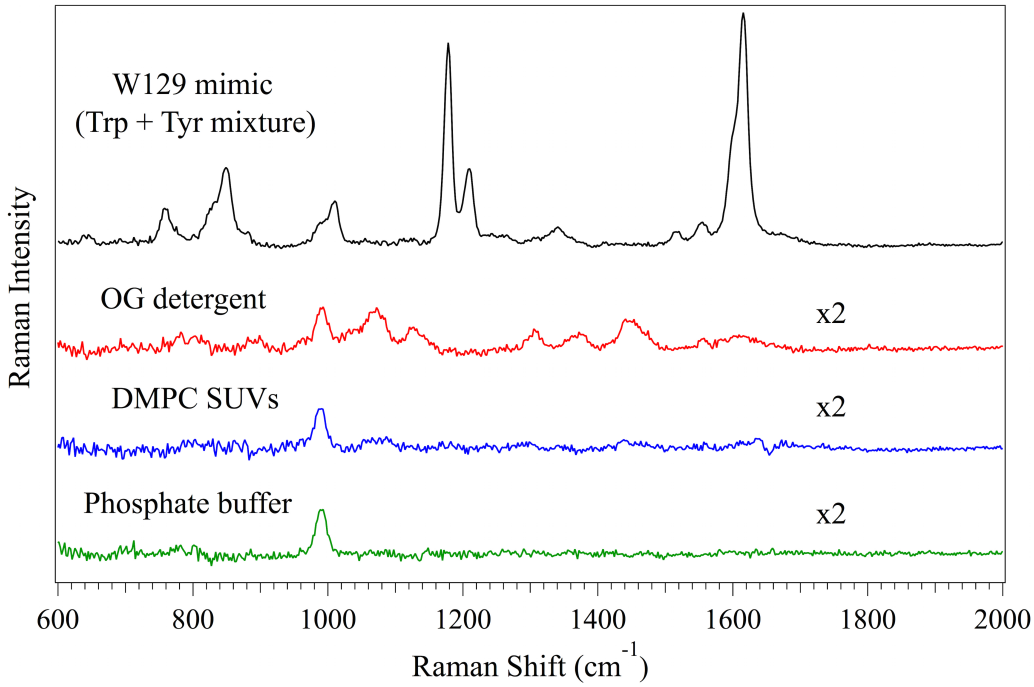

Figure 4.13 UVRR difference spectra of tryptophan (Trp) and tyrosine (Tyr) mixture to mimic W129 OmpA mutant (10 µM Trp and 170 µM Tyr), 10 mg/mL OG detergent, 1 mg/mL DMPC SUVs, and 20 mM KP_i pH 8.0 buffer. All spectra were acquired for 10 minutes. The scalar by which the spectra of detergent, SUVs, and buffer spectra were multiplied is indicated.

4.6 Discussion

The results from this study indicate that OmpA spontaneously inserts and folds into NDs with similar yield and approximately 2 to 3-fold decreased rate as into SUVs. This finding is significant because the majority of research on NDs and membrane proteins typically focuses on structure and function of membrane proteins [37-39], and not on the process of folding. The present data indicate that NDs can also elucidate dynamics of protein folding and are an excellent alternative to vesicles with additional benefits of homogeneity, optical clarity, better control of ND:protein ratio, and greater stability.

4.6.1 OmpA folding into bilayers

Several factors influence the yield and kinetics of the folding of OmpA into lipid bilayers, including pH, temperature, lipid head group, lipid chain length, lipid concentration, and lipid saturation [9, 32, 40]. The impact of membrane thickness and vesicle curvature on the rates of formation of OmpA secondary and tertiary structures has been investigated [9]. Fluorescence, CD, and gel electrophoresis showed that OmpA does not spontaneously insert and fold into low-curvature LUVs that contain lipid chains with more than 12 carbon atoms, such as DMPC. However, when these long-chain lipids of >12 carbons were incorporated into high-curvature SUVs, OmpA successfully folded into these SUVs [9]. Additional studies showed that high curvature is not required for folding; when LUVs were comprised of short-chain lipids of 12 or fewer carbon atoms, OmpA was able to insert and fold into these LUVs [9, 10]. The enhanced folding rates and yields in thin or highly-curved bilayers are attributed to bilayer defects; the transient pores and flexibility that result from the defects facilitate folding [6, 9, 34, 41].

4.6.2 Properties of NDs

Discoidal planar NDs formed from the membrane scaffold protein 18A, which is an α-helical peptide derived from apolipoprotein A-1, has been previously described [42, 43]. It was shown by NMR and single-particle electron microscopy that the 14-residue amphipathic truncated analogue of 18A, referred to as 14A, (Figure 1B) is able to generate stable 10 nm diameter planar NDs when mixed with DMPC lipids at a lipid to peptide molar ratio of 1.67 [20, 44]. Based on the circumference of the 10 nm diameter ND, and using typical properties of an α-helix (e.g. 3.6 amino acids per turn, pitch of 5.4 Å), the scaffold belt may consist of up to 28 α-helical 14A peptides (14 peptides per single belt, and two belts per ND). The ND double belt arrangement of 14A using DMPC lipid was confirmed by solid-state NMR spectroscopy [45]. To the best of our knowledge, extensive biophysical studies of the 14A peptide in NDs have not been published, certainly not to the extent as the 18A peptide. Hence, we rely on findings of 18A to help understand the properties of the 14A peptide.

The properties of NDs comprised of the 18A belt peptide have been compared to those of vesicles. FRET experiments on NDs with the 18A belt peptide and 1-palmitoyl-2-oleoyl-*sn*-glycero-3-phosphocholine (POPC) showed that NDs have a higher lipid-exchange rate by a factor of 20 compared to vesicles; the rate of exchange in NDs is about 20 minutes compared to 440 min for vesicles [44]. The collision-induced, enhanced lipid exchange between NDs was ascribed to the discontinuities between the multiple belt peptides that constitute the overall ND belt [44]. The membrane surface packing state and hydration level of NDs consisting of 18A peptide were probed by fluorescence lifetime experiments, and the results indicated that these NDs were more similar to planar NDs and LUVs as opposed to curved or the “saddle” surface of NDs that are generated with longer belt peptides [44].

The fluidity of NDs differs from liposomes, and this variation has been attributed to the presence of the scaffold peptide belt that can impact the motions of the lipid chains enveloped by the belt. Solid-state NMR experiments have shown that NDs exhibit greater lipid internal ordering than liposomes at 298 K (above the lipid phase transition) [46]. The same study showed that both fluid and gel phase bilayer characteristics exist at temperatures below the phase transition of a ND using the scaffold protein MSP1ΔH5. These results are consistent with the general finding that NDs exhibit broader and higher phase transition temperatures compared to large vesicles on account of the presence of the scaffold belt and loss of cooperativity of the lipids of NDs because of their small size [21, 37, 46].

4.6.3 OmpA folds into NDs and SUVs

The spectroscopic and gel data presented here indicate that OmpA successfully folds into NDs. Fluorescence spectra reveal changes in environment for tryptophan residues in OmpA in the presence of NDs. As tryptophan inserts into a hydrophobic lipid environment from polar water, there is an observed fluorescence blue-shift from ~350 nm in water to ~330 nm in the lipid bilayer with a typical increase in fluorescence quantum yield [27]. The background-corrected fluorescence spectra during the folding reaction of OmpA into NDs and SUVs are shown in Figure 5. The earliest time point taken at 1 minute after initiation of the folding reaction into NDs and SUVs exhibits λ_{max} values of 351 and 352 nm, respectively. These emission maxima are higher in energy than OmpA unfolded in urea, where λ_{max} is 356 nm. This fast initial blue-shift of λ_{max} relative to OmpA in urea is indicative of OmpA interaction with the lipid bilayer prior to the insertion and folding process [7]. The fluorescence data presented here agree with previous characterization of an OmpA membrane-bound intermediate adsorbed to a DOPC lipid bilayer surface within 1 or 2 minutes after initiation of the folding reaction [47].

After ~1 hour in the presence of NDs or SUVs, the values for λ_{max} are the most blue-shifted at 337 nm. This 19 nm emission blue-shift relative to OmpA in urea is consistent with literature values reported for OmpA folded in the bilayer [7, 18, 22, 27]. The initial binding of OmpA to a membrane surface (within minutes) and the sequential slow step of folding (within hours) agree with published results [8, 35, 47, 48]. Based on the intensity-weighted decomposition method [27] of the tryptophan fluorescence, nearly identical folding yields of 97 ± 2% (NDs) and 99 ± 1% (SUVs) were observed. The folding rate into NDs was slower, with an exponential rise time of 21 ± 5 mins, compared to SUVs, which had an exponential rise time of 9 ± 4 mins.

The results from fluorescence, which reveal changes in local environment for tryptophan residues, can be compared to results from SDS-PAGE differential mobility studies, which measures global structure. The observation of native (in SUVs) and unfolded (in urea) OmpA as two distinct bands on a gel has been previously documented [5, 6, 25]. The calculated folding yield of OmpA based on gel band densities are 88 ± 12% (NDs) and 97 ± 2% (SUVs). The average yield for folding into NDs as assessed by gel band density is 9% lower than the average yield based on fluorescence (97 ± 2%), but within one standard deviation given the large spread of yields in NDs. The folding rates are also noticeably slower for NDs compared to SUVs.

The kinetics probed by fluorescence reveals changes in local environment of tryptophan, while the kinetics obtained by gel mobility experiments reflect changes in the formation of global structure. The faster folding rate in NDs reported by fluorescence reflects the expectation that adsorption and partial insertion of OmpA into the bilayer precedes the formation of OmpA global structure [49]. The observation that the folding yields are greater than 88% for the two independent methods of gels and fluorescence gives confidence that OmpA folds successfully into NDs.

4.6.4 Native OmpA in NDs

Three independent experiments indicate that OmpA is folded with the same structure in NDs as in SUVs. UVRR reveals the vibrational structure of biomolecules, and excitation with 228 nm selectively enhances Raman signal from aromatic residues, in particular tryptophan, with minimal contribution from protein backbone and buffer. UVRR complements fluorescence spectroscopy (local environment) and gel mobility studies (global structure) by revealing site-specific information and non-covalent molecular interactions.

The single-tryptophan mutant, W129, was studied by UVRR because this non-native tryptophan residue exhibits a unique peak present at 785 cm^{-1}, near the shoulder of the W18 mode, which we have interpreted as an enhanced hydrogen-out-of-plane (HOOP) mode. This HOOP mode is only present for tryptophan residues at positions 129 and 15, and only when OmpA is folded in OG detergent micelles and DMPC SUVs (Figure 6) [18, 36, 50]. When OmpA is unfolded in urea or adsorbed onto DPPC SUVs, the vibrational peak at 785 cm^{-1} is absent. Thus, this HOOP mode can be utilized as a marker to indicate whether OmpA refolded into NDs. The W129 HOOP mode appears only under folding conditions in the presence of micelles, SUVs, and NDs. We hypothesize that this HOOP mode gains intensity because of the perturbation of the indole π electrons resulting from an interaction with a nearby charge during folding [51]. This perturbation is most likely induced by intramolecular interactions rather than intermolecular interactions, such as protein-lipid interactions, because the mode is intense when OmpA is folded in OG micelles, and OG has no charged groups. The mode is also intense when OmpA is folded in DMPC SUVs, which have zwitterionic head groups. One possible explanation for the enhanced HOOP intensity is that a charged residue of the protein in the

vicinity of the non-native tryptophan placed at position 129 interacts with the indole side chain and perturbs the vibrations.

Structural insights were also gained through digestion studies and CD measurements. In the presence of Arg-C, a membrane-protected fragment remained in both NDs and SUVs. This observation indicates that OmpA has the same general inserted structure in both environments. The β-barrel secondary structure is preserved in NDs, as shown in CD spectra (Fig. S1). The CD spectra also highlight an important benefit of NDs; the highly scattering nature of SUVs is a known challenge to CD spectra [52, 53], and this challenge is overcome by using optically clear ND samples. The poor S/N of the CD spectra in SUVs at 205-210 nm can be contrasted with the smooth curve for NDs in the same wavelength range.

The finding that OmpA retains similar structure in NDs as in SUVs complements the general conclusions from NMR studies that have confirmed similar OmpA structure in NDs and detergent micelles and bicelles. Sequence-specific NMR assignments provided evidence of near-identical polypeptide backbone conformations for OmpA and OmpX in NDs and detergent micelles [54]. A second NMR structural study confirmed that the two independently folded N- and C- terminal domains of OmpA were connected via a flexible linker, with the C-terminus periplasmic domain correctly located outside the membrane, in both micelles and NDs [55].

4.6.5 Folding of the OmpA adsorbed intermediate

The adsorbed intermediate refers to OmpA that interacts with the surface of the bilayer, but is not inserted into the hydrocarbon core; this species is generated when the bilayer is in the gel phase, below the phase transition temperature to the fluid phase. The adsorbed intermediate has been shown to consist of β-sheet secondary structure and is completely degradable by trypsin [40] and Arg-C protease in solution (as shown in Figure 3). The OmpA adsorbed intermediate in

the presence of DPPC SUVs exhibits a fluorescence emission that is blue-shifted by up to 13 nm relative to unfolded OmpA in urea, and exhibits similar secondary structure to the folded protein [5, 7]. Similarly, the fluorescence emission of OmpA adsorbed onto DMPC LUVs after 12 hours of incubation in the presence of 100 and 200 nm diameter LUVs is 342 and 341 nm, respectively (blue-shift of ~14 nm relative to unfolded OmpA in urea, Fig. S4). The fluorescence maxima of the OmpA adsorbed intermediate on gel phase DMPC SUVs and DMPC NDs are blue-shifted 11 and 13 nm, respectively, relative to unfolded OmpA in urea. These values are consistent with previously reported values of an OmpA adsorbed intermediate [25]. The adsorbed intermediate that is trapped at low temperature on gel-phase DMPC SUVs can be initiated to fold via an increase in temperature to the fluid phase [35]. We have performed analogous experiments for NDs, and the data indicate that the folding behavior is similar to SUVs; the adsorbed intermediate on NDs can also be isolated at low temperatures ($< T_C$) and converted into native OmpA by raising the temperature above T_C (Fig. S5). These data indicate that the OmpA adsorbed intermediate may be valuable as an initial state for folding experiments.

4.6.6 Comparison of NDs and SUVs

The data presented here indicate that the folding reaction of OmpA into NDs exhibits no noticeable differences compared to SUVs in terms of (1) folding yield as measured by fluorescence; (2) folding yield as assed by gels; (3) secondary and tertiary structures as assessed by CD, gels, and UVRR; and (4) the adsorbed intermediate as assessed by low-temperature fluorescence experiments and gels. The only difference was the folding rates assessed by gels and fluorescence, where folding in NDs was about 2 to 3-fold slower (28 ± 4 min for gels and 21 ± 5 mins for fluorescence) compared to in SUVs (10 ± 5 min for gels and 9 ± 4 min for fluorescence). The conclusion that OmpA successfully folds into DMPC NDs is somewhat

surprising given that OmpA does not fold into DMPC LUVs [9, 10]; both LUV and ND bilayers are considered flat, with decreased exposure of hydrophobic chains relative to high-curvature SUVs [9], and with equivalent hydration levels [44]. However, one important difference between LUVs and NDs is that lipids in NDs are more dynamic compared to LUVs as revealed by the 20-fold greater lipid exchange rate in NDs [44]. While the belt peptide results in more packed and ordered lipids [46], the discontinuities at the edge of the ND may give rise to the defects near the edges that not only enhance lipid exchange, but also facilitate the folding of OmpA. The observation of the 2 to 3-fold decrease in folding rate in NDs compared to SUVs indicates there may be a larger barrier to fold into NDs. However, the high yield of folding into NDs and SUVs combined with the spectroscopically undifferentiable structures in both types of bilayers suggests that the thermodynamically favored conformation of OmpA is equivalent in NDs and SUVs.

The ability to perform folding experiments in NDs offers experimental advantages. With less than one OmpA per ND, there is no crowding or other protein-protein effects on the folding reaction, thus simplifying the interpretation of data. Additionally, the size of the ND can be varied by adjusting the ratio of the lipid:scaffold protein/peptide, or by altering the length of the scaffold protein/peptide to incorporate different sizes of membrane proteins [20, 38, 39]. The inherently homogenous and stable NDs enable reproducible and extended experiments that are sometimes challenging to accomplish with thermodynamically unstable SUVs. The optical clarity of NDs is another important benefit because optical experiments, such as absorption, CD, and vibrational spectroscopy can be pursued with minimal artifacts. These and other improvements in experimental conditions for membrane protein folding will help unveil new insights into this fundamental process in biology.

4.7 Summary

The findings presented here indicate that OmpA spontaneously inserts and folds into NDs with comparable yield and a 2- to 3-fold slower rate relative to SUVs. The results from SDS-PAGE mobility, digestion, steady-state fluorescence, UVRR, and CD studies suggest the OmpA secondary and tertiary structures are preserved upon folding in NDs. These data indicate that NDs may be an improved alternative to commonly-used SUVs for studies of membrane protein folding because of the inherent stability and homogeneity of NDs.

4.8 Acknowledgements

We thank Prof. Michael Tauber for providing the use of the Jasco J-815 spectrometer for CD studies. We thank Dr. Sang Ho Park (Opella group) for gifting us with preliminary 14A belt peptide samples. We also thank Dr. Ignacio López-Peña, Joel Rivera, Jen Daluz, and Justine Liang for assistance with the UVRR setup. D.K.A was supported by the Molecular Biophysics Training Grant, NIH Grant T32 GM008326.

Chapter 4, in full, is a reprint of the material with permission from D. K. Asamoto, G. Kang, and J. E. Kim, Folding of the β-barrel membrane protein OmpA into nanodiscs, Biophysical Journal, 2019, 118, 1-12. The dissertation author was the primary investigator and author of this paper. Copyright 2019, Cell Press.

4.9 References

[1] Y. Arinaminpathy, E. Khurana, D.M. Engelman, M.B. Gerstein, Computational analysis of membrane proteins: the largest class of drug targets, *Drug Discovery Today* 14 (2009) 1130-5.

[2] J.T. Marinko, H. Huang, W.D. Penn, J.A. Capra, J.P. Schlebach, C.R. Sanders, Folding and misfolding of human membrane proteins in health and disease: from single molecules to cellular proteostasis, *Chem. Rev.* 119 (2019) 5537-606.

[3] J.P. Schlebach, D. Peng, B.M. Kroncke, K.F. Mittendorf, M. Narayan, B.D. Carter, C.R. Sanders, Reversible folding of human peripheral myelin protein 22, a tetraspan membrane protein, *Biochemistry* 52 (2013) 3229-41.

[4] R. Koebnik, K.P. Locher, P. Van Gelder, Structure and function of bacterial outer membrane proteins: barrels in a nutshell, *Mol. Microbiol.* 37 (2000) 239-53.

[5] T. Surrey, F. Jahnig, Refolding and oriented insertion of a membrane-protein into a lipid bilayer, *Proc. Natl. Acad. Sci. U.S.A.* 89 (1992) 7457-61.

[6] T. Surrey, F. Jahnig, Kinetics of folding and membrane insertion of a beta-barrel membrane-protein, *J. Biol. Chem.* 270 (1995) 28199-203.

[7] K.M. Sanchez, G.P. Kang, B.J. Wu, J.E. Kim, Tryptophan-lipid interactions in membrane protein folding probed by ultraviolet resonance Raman and fluorescence spectroscopy, *Biophys. J.* 100 (2011) 2121-30.

[8] A.H. Dewald, J.C. Hodges, L. Columbus, Physical determinants of beta-barrel membrane protein folding in lipid vesicles, *Biophys. J.* 100 (2011) 2131-40.

[9] J.H. Kleinschmidt, L.K. Tamm, Secondary and tertiary structure formation of the beta-barrel membrane protein OmpA is synchronized and depends on membrane thickness, *J. Mol. Biol.* 324 (2002) 319-30.

[10] C.L. Pocanschi, G.J. Patel, D. Marsh, J.H. Kleinschmidt, Curvature elasticity and refolding of OmpA in large unilamellar vesicles, *Biophys. J.* 91 (2006) L75-L7.

[11] B.R. Lentz, T.J. Carpenter, D.R. Alford, Spontaneous fusion of phosphatidylcholine small unilamellar vesicles in the fluid phase, *Biochemistry* 26 (1987) 5389-97.

[12] B.F. de Arcuri, G.F. Vechetti, R.N. Chehin, F.M., Goni, R.D., Morero, Protein-induced fusion of phospholipid vesicles of heterogeneous sizes, *Biochem. Biophys. Res. Commun.* 262 (1999) 586-90.

[13] D. Marsh, Lateral pressure profile, spontaneous curvature frustration, and the incorporation and conformation of proteins in membranes, *Biophys. J.* 93 (2007) 3884-99.

[14] T.H. Bayburt, Y.V. Grinkova, S.G. Sligar, Self-assembly of discoidal phospholipid bilayer nanoparticles with membrane scaffold proteins, *Nano. Lett.* 2 (2002) 853-6.

[15] L.N. Ojemyr, C. von Ballmoos, R.B. Gennis, S.G. Sligar, P. Brzezinski, Reconstitution of respiratory oxidases in membrane nanodiscs for investigation of proton-coupled electron transfer, *FEBS Lett.* 586 (2012) 640-5.

[16] T.H. Bayburt, S.G. Sligar, Membrane protein assembly into nanodiscs, *FEBS Lett.* 584 (2010) 1721-7.

[17] A. Baumann, S. Kerruth, J. Fitter, G. Buldt, J. Heberle, R. Schlesinger, K. Ataka, In-Situ observation of membrane protein folding during cell-free expression, *Plos One* 11 (2016).

[18] K.M. Sanchez, J.E. Gable, D.E. Schlamadinger, J.E. Kim, Effects of tryptophan microenvironment, soluble domain, and vesicle size on the thermodynamics of membrane protein folding: lessons from the transmembrane protein OmpA, *Biochemistry* 47 (2008) 12844-52.

[19] R.C. MacDonald, R.I. MacDonald, B.P. Menco, K. Takeshita, N.K. Subbarao, L.R. Hu, Small-volume extrusion apparatus for preparation of large, unilamellar vesicles, *Biochim. Biophys. Acta* 1061 (1991) 297-303.

[20] S.H. Park, S. Berkamp, G.A. Cook, M.K. Chan, H. Viadiu, S.J. Opella, Nanodiscs versus macrodiscs for NMR of membrane proteins, *Biochemistry* 50 (2011) 8983-5.

[21] A. Shaw, McLean, M., and Sligar, S., Phospholipid phase transitions in homogenous nanometer scale bilayer discs, *FEBS Lett.* 556 (2003) 260-4.

[22] J.E. Kim, G. Arjara, J.H. Richards, H.B. Gray, J.R. Winkler, Probing folded and unfolded states of outer membrane protein A with steady-state and time-resolved tryptophan fluorescence, *J. Phys. Chem. B* 110 (2006) 17656-62.

[23] B. Keil, Specificity of Proteolysis, Springer Science & Business Media, 2012, 1992.

[24] R.J. Krueger, T.R. Hobbs, K.A. Mihal, J. Tehrani, M.G. Zeece, Analysis of endoproteinase Arg C action on adrenocorticotrophic hormone by capillary electrophoresis and reversed-phase high-performance liquid chromatography, *J. Chromatogr.* 543 (1991) 451-61.

[25] N.A. Rodionova, S.A. Tatulian, T. Surrey, F. Jahnig, L.K. Tamm, Characterization of two membrane-bound forms of OmpA, *Biochemistry* 34 (1995) 1921-9.

[26] S. Ohnishi, K. Kameyama, Escherichia coli OmpA retains a folded structure in the presence of sodium dodecyl sulfate due to a high kinetic barrier to unfolding, *Biochim. Biophys. Acta* 1515 (2001) 159-66.

[27] G. Kang, Lopez-Pena, I., Bhakta, S., and Kim, J. . Probing membrane protein structure and dynamics by fluorescence spectroscopy. Encyclopedia of Analytical Chemistry: John Wiley & Sons, Ltd; 2013.

[28] H.S. Shafaat, K.M. Sanchez, T.J. Neary, J.E. Kim, Ultraviolet resonance Raman spectroscopy of a beta-sheet peptide: a model for membrane protein folding, *J. Raman Spectrosc.* 40 (2009) 1060-4.

[29] N.D.R.a.G. Salvesen, Handbook of Proteolytics Enzymes (Third Edition), Elsevier 2013.
[30] J.H. Kleinschmidt, Folding kinetics of the outer membrane proteins OmpA and FomA into phospholipid bilayers, *Chem. Phys. Lipids* 141 (2006) 30-47.

[31] J.H. Kleinschmidt, M.C. Wiener, L.K. Tamm, Outer membrane protein A of E-coli folds into detergent micelles, but not in the presence of monomeric detergent, *Protein Sci.* 8 (1999) 2065-71.

[32] H.D. Hong, L.K. Tamm, Elastic coupling of integral membrane protein stability to lipid bilayer forces, *Proc. Natl. Acad. Sci. U.S.A.* 101 (2004) 4065-70.

[33] G.P. Kang, I. Lopez-Pena, V. Oklejas, C.S. Gary, W.H. Cao, J.E. Kim, Forster resonance energy transfer as a probe of membrane protein folding, *Biochim. Biophys. Acta* 1818 (2012) 154-61.

[34] E.J. Danoff, K.G. Fleming, Membrane defects accelerate outer membrane beta-barrel protein folding, *Biochemistry* 54 (2015) 97-9.

[35] J.H. Kleinschmidt, L.K. Tamm, Folding intermediates of a beta-barrel membrane protein. Kinetic evidence for a multi-step membrane insertion mechanism, *Biochemistry* 35 (1996) 12993-3000.

[36] D.E. Schlamadinger, M.M. Daschbach, G.W. Gokel, J.E. Kim, UV resonance Raman study of cation-pi interactions in an indole crown ether, *J. Raman Spectrosc.* 42 (2011) 633-8.

[37] I.G. Denisov, S.G. Sligar, Nanodiscs in membrane biochemistry and biophysics, *Chem. Rev.* 117 (2017) 4669-713.

[38] J.E. Rouck, J.E. Krapf, J. Roy, H.C. Huff, A. Das, Recent advances in nanodisc technology for membrane protein studies (2012-2017), *FEBS Lett.* 591 (2017) 2057-88.

[39] M.A. McLean, M.C. Gregory, S.G. Sligar, Nanodiscs: a controlled bilayer surface for the study of membrane proteins, *Annu. Rev. Biophys.* (2018).

[40] J.H. Kleinschmidt, Folding of beta-barrel membrane proteins in lipid bilayers - Unassisted and assisted folding and insertion, *Biochim. Biophys. Acta* 1848 (2015) 1927-43.

[41] M. Herrmann, B. Danielczak, M. Textor, J. Klement, S. Keller, Modulating bilayer mechanical properties to promote the coupled folding and insertion of an integral membrane protein, *Eur. Biophys. J.* 44 (2015) 503-12.

[42] G.M. Anantharamaiah, J.L. Jones, C.G. Brouillette, C.F. Schmidt, B.H. Chung, T.A. Hughes, A.S. Bhown, J.P. Segrest, Studies of synthetic peptide analogs of the amphipathic helix. Structure of complexes with dimyristoyl phosphatidylcholine, *J. Biol. Chem.* 260 (1985) 10248-55.

[43] R.M. Epand, A. Gawish, M. Iqbal, K.B. Gupta, C.H. Chen, J.P. Segrest, G.M. Anantharamaiah, Studies of synthetic peptide analogs of the amphipathic helix. Effect of charge distribution, hydrophobicity, and secondary structure on lipid association and lecithin:cholesterol acyltransferase activation, *J. Biol. Chem.* 262 (1987) 9389-96.

[44] M. Miyazaki, Y. Tajima, T. Handa, M. Nakano, Static and dynamic characterization of nanodiscs with apolipoprotein A-I and its model peptide, *J. Phys. Chem. B* 114 (2010) 12376-82.

[45] E.S. Salnikov, G.M. Anantharamaiah, B. Bechinger, Supramolecular organization of apolipoprotein-A-I-derived peptides within disc-like arrangements, *Biophys. J.* 115 (2018) 467-77.

[46] D. Martinez, M. Decossas, J. Kowal, L. Frey, H. Stahlberg, E.J. Dufourc, R. Riek, B. Habenstein, S. Bibow, A. Loquet, Lipid internal dynamics probed in nanodiscs, *Chemphyschem* (2017).

[47] J.H. Kleinschmidt, L.K. Tamm, Time-resolved distance determination by tryptophan fluorescence quenching: probing intermediates in membrane protein folding, *Biochemistry* 38 (1999) 4996-5005.

[48] J. Kleinschmidt, den Blaauwen, T., Driessen A., and Tamm, L., Outer membrane protein A of Escherichia coli inserts and folds into lipid bilayers by a concerted mechanism, *Biochemistry* 38 (1999) 5006-16.

[49] J.H. Kleinschmidt, Membrane protein folding on the example of outer membrane protein A of Escherichia coli, *Cell. Mol. Life Sci.* 60 (2003) 1547-58.

[50] E.A. Milan-Garces, S. Mondal, J.B. Udgaonkar, M. Puranik, Intricate packing in the hydrophobic core of barstar through a CH-pi interaction, *J. Raman Spectrosc.* 45 (2014) 814-21.

[51] D.E. Schlamadinger, J.E. Gable, J.E. Kim, Hydrogen bonding and solvent polarity markers in the UV resonance Raman spectrum of tryptophan: application to membrane proteins, *J. Phys. Chem. B* 113 (2009) 14769-78.

[52] H. Chakraborty, B.R. Lentz, A simple method for correction of circular dichroism spectra obtained from membrane-containing samples, *Biochemistry* 51 (2012) 1005-8.

[53] B.A. Wallace, D. Mao, Circular dichroism analyses of membrane proteins: an examination of differential light scattering and absorption flattening effects in large membrane vesicles and membrane sheets, *Anal Biochem* 142 (1984) 317-28.

[54] L. Susac, R. Horst, K. Wuthrich, Solution-NMR characterization of outer-membrane protein A from E. coli in lipid bilayer nanodiscs and detergent micelles, *Chembiochem* 15 (2014) 995-1000.

[55] H. Ishida, A. Garcia-Herrero, H.J. Vogel, The periplasmic domain of Escherichia coli outer membrane protein A can undergo a localized temperature dependent structural transition, *Biochim. Biophys. Acta* 1838 (2014) 3014-24.

Chapter 5
Evolution of local solvation of tryptophan during folding of OmpA into nanodiscs

Chapter 5 is being prepared for submission

5.1 Abstract

Outer membrane protein A (OmpA) is a model system for the study of membrane protein folding and the insertion of OmpA into small unilamellar vesicles (SUVs) has been characterized extensively. Recently, OmpA was shown to spontaneously fold into an improved bilayer mimic, nanodiscs (NDs), which serves as valuable mimics of the more planar cell membrane. Stern-Volmer quenching experiments on OmpA mutants that contain single-tryptophan residues at native positions 7, 15, 57, 102, or 143 were performed to elucidate the change in local solvation during folding into NDs. A sphere-of-action quenching model that combines both static and dynamic components gave rise to Stern-Volmer quenching constants, K_D, for OmpA denatured in 8.0 M urea, aggregated in buffer, and fully folded in NDs. The average K_D values were $K_D^{denatured}$ (5.9 M^{-1}) > $K_D^{aggregated}$ (5.3 M^{-1}) > K_D^{folded} (1.0 M^{-1}). Bimolecular quenching constants, k_q, derived from published lifetimes and the Stern-Volmer graphs revealed the evolution of k_q during the 5-hour folding reaction into NDs. Desolvation timescales based on the Stern-Volmer graphs were 65 minutes (W102), 36-41 minutes (W7, W15, W57), and 28 minutes (W143). The evolution of λ_{max} during folding into NDs revealed fast and slow components for change in environment, τ_{enviro}^{fast} and τ_{enviro}^{slow}, of 4-9 minutes and 14-64 minutes, respectively. These results are similar to those for the folding reaction in SUVs and suggest that in both bilayer mimics, there is an initial fast step associated with a large change in polarity to a hydrophobic environment, followed by a slower dehydration process and equilibration within the hydrophobic environment. Intensity-weighted decomposition analysis revealed an average

folding time of ~23 minutes across all mutants, indicating that the desolvation timescale is slower than the formation of the tertiary structure.

5.2 Introduction

Cellular proteins are distinguished as either membrane associated or water-soluble. Despite the prevalence and importance of membrane proteins, comprising nearly 30% of the human genome, and accounting for approximately 60% of current drug targets, relatively little information is known about membrane proteins compared to the vast amount of knowledge on soluble proteins [1]. The study of membrane proteins is an ongoing challenge due to their insolubility in aqueous solutions, their tendency to denature or aggregate outside of their native hydrophobic lipid environment, and the added complexity of the bilayer. Furthermore, the majority of membrane proteins require detergents for solubility, which may interfere with or distort their native structures and/or dynamics.

The study of membrane proteins within bilayers is a challenging area of research that has grown over the past few decades. The majority of membrane protein studies focus on native structure determination and function within lipid bilayers, while few studies provide details about their folding mechanisms. Much of the knowledge of membrane protein folding has emerged from a small set of model membrane proteins, such as Outer membrane protein A (OmpA). OmpA consists of 325 amino acid residues and forms an 8-stranded antiparallel β-barrel transmembrane domain and a soluble C-terminal periplasmic domain [2]. β-barrel membrane proteins are typically less hydrophobic than α-helical systems, and thus, proteins such as OmpA are able to fold spontaneously from a fully denatured state in the presence of bilayer mimics. A primary tool in the study of protein folding, including OmpA folding, is fluorescence spectroscopy. Wild-type OmpA contains five native tryptophan residues, four of which are

located near the extracellular membrane-aqueous interface, and one that is located on the periplasmic side of the membrane (Figure 1). The fluorescence from these and non-native tryptophan has been used extensively for spectroscopic studies of membrane protein folding [3, 4]. OmpA is able to fold into different types of bilayers of small unilamellar vesicles (SUVs). Recently, we showed that OmpA can spontaneously insert and fold into a phospholipid nanodisc (ND, Figure 1), which is an improved bilayer mimic with *in vitro* experimental benefits, compared to traditional SUVs [5].

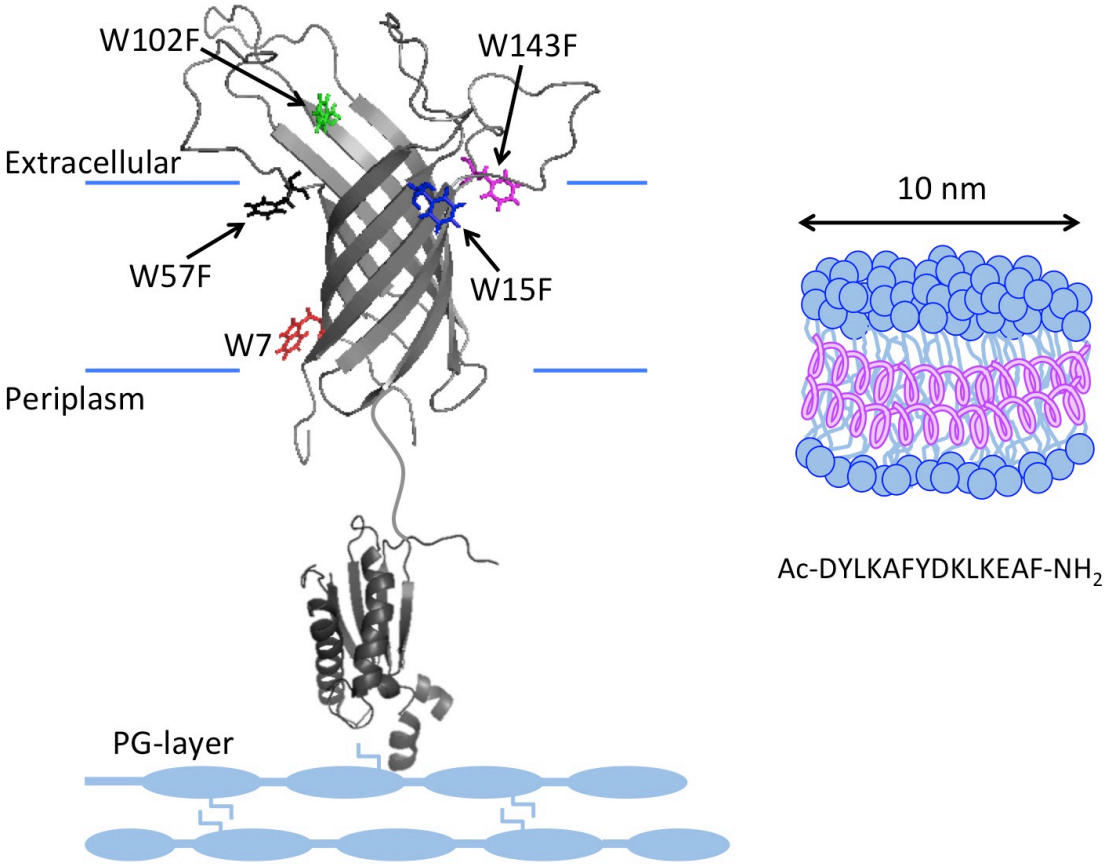

Figure 5.1 Solution NMR structure of the transmembrane domain of OmpA mutant with single tryptophan at position 7 (PDB ID 2GE4, 1 conformer) and solution NMR structure of the periplasmic domain (PDB ID 2MQE). The native tryptophan at position 7 (W7) is shown in red. The remaining four native tryptophan residues at positions 15, 57, 102, and 143 have been mutated to phenylalanine and are shown in blue (W15F), black (W57F), green (W102F), and pink (W143F), respectively. The membrane bilayer is shown as blue horizontal lines. The peptidoglycan-layer (PG-layer) is shown as blue ovals. The proposed two-domain structure with the periplasmic domain associated with the PG-layer is adapted from reference [6]. The location and orientation of the periplasmic domain relative to the lipid bilayer is not known and thus, is arbitrary in this figure. A cartoon representation of a nanodisc bilayer is shown on the right with the 14A belt peptide (pink α-helices) sequence labeled.

One challenging, but very important, topic in the study of membrane protein folding is the evolution of the solvation environment during folding. In particular, the change in protein environment from bulk water to bulk lipid is likely to involve the expulsion of water during insertion and folding into a lipid bilayer. This expulsion of water has been proposed to be one of the rate-limiting steps to folding [7]. Computational studies on the dynamics of membrane protein folding have assessed the role of water, however simulations describing kinetics of membrane protein folding are often complex and time consuming, resulting in the omission of important properties that might affect the native folding mechanism [8-10].

A simple, indirect measure of solvation is extrinsic fluorescence quenching. Bimolecular fluorescence quenching experiments have been used to measure the accessibility of fluorophores by use of an external quencher [11-13]. Dynamic (collisional) quenching involves close interaction between fluorophore and quencher (< 5 Å) within the lifetime of the excited state of the fluorophore, leading to the de-excitation of the fluorophore to the ground state without the emission of a photon [11]. As proteins fold and insert into the bilayer, the fluorophore becomes buried and inaccessible to the quencher in solution. As a result, fluorescence quenching becomes inefficient and an increase in fluorescence intensity is observed [11].

In addition to dynamic quenching, a static mechanism that involves a ground-state, dark complex may also contribute to the loss of fluorescence. One type of static quenching relevant for tryptophan is “sphere-of-action” quenching. This quenching mechanism occurs when tryptophan and the quencher are in close proximity at the moment of excitation, and there exists a volume element, V, within which fluorescence emission is immediately quenched with a probability of unity [11, 12]. It has been shown that typically, the sphere-of-action static volume component, V, increases with solvent exposure to quencher and decreases to low values as the

fluorophore becomes buried in the lipid membrane or becomes protected by the protein itself [12, 14]. Because both dynamic and static quenching mechanisms require close interaction between fluorophore and quencher within the lifetime of the excited state, quenching experiments can provide information about the changes in dynamics and solvent exposure of membrane proteins as well as other biochemical systems.

In the present study, we utilize bimolecular fluorescence quenching with acrylamide and time-resolved Stern-Volmer analysis, as a straightforward method to investigate the kinetics of desolvation of OmpA during folding into NDs. These studies can be compared to the kinetics associated with formation of secondary and tertiary structures as well as with folding into SUVs [15] to elucidate differences between these two bilayer mimics. As with the prior study in SUVs, the present experiments were performed on single-tryptophan mutants, which allowed for site-specific studies throughout the transmembrane domain. In addition to the folding studies, quenching experiments were also performed on steady-state conformations, including denatured and aggregated OmpA as well as adsorbed onto the ND bilayer. The analysis combines both dynamic and static quenching mechanism components and the results may be used to complement previous OmpA folding studies which discuss formation of secondary and tertiary structure during folding.

5.3 Materials and Methods

5.3.1 Expression, isolation, and purification of single tryptophan OmpA mutants

The single-tryptophan full-length OmpA mutants used in this study were expressed and purified according to a previously established procedure [16]. Wild-type OmpA contains five native tryptophan residues at positions 7, 15, 57, 102, and 143. Five OmpA mutants were generated in which a single tryptophan residue was retained and the remaining four out of the

five native tryptophan residues were replaced with phenylalanine to allow for site-specific investigations. These mutants are referred to as W7, W15, W57, W102, and W143, respectively. In addition, a full-length mutant, W0, in which all five native tryptophan residues were mutated to phenylalanine (W7F/W15F/W57F/W102F/W143F) was generated as a control protein to account for fluorescence signal from the 17 native tyrosine residues. Concentrated stock protein solutions which contained 150-615 μM protein and 8.0 M urea in 20 mM potassium phosphate buffer (KP_i, pH 7.3) were diluted to appropriate concentrations for the present experiments. All reagents were purchased from Thermo Fisher Scientific (Waltham, MA), Genesee Scientific Corporation (El Cajon, CA), MP Biomedicals (Santa Ana, CA), and GoldBio (St. Louis, MO) unless otherwise stated and used as received.

5.3.2 Preparation of nanodiscs (NDs)

Preparation of 1,2-dimryistoyl-*sn*-glycero-3-phosphocholine (DMPC) NDs was followed according to a published procedure [17]. Briefly, 25 mg of DMPC (MW 677.95 g/mol) dissolved in chloroform was dried under nitrogen gas for at least 5 hours. A 6.4 mg/mL lipid concentration was achieved by re-suspending the dried lipid film in 3.9 mL of 20 mM KP_i buffer at pH 8.0. Separately, a 10 mg/mL solution of 14A belt peptide (MW 1792.06 g/mol) with sequence Ac-DYLKAFYDKLKEAF-NH_2 (truncated analog of 18A peptide, purchased from NeoScientific at >98% purity, Cambridge, MA) was made by dissolving an appropriate mass of peptide in 0.6-1.1 mL of 20 mM KP_i buffer at pH 8.0. The self-assembly of approximately 10 nm diameter NDs were generated by adding 0.5 mL of the 6.4 mg/mL aqueous lipid solution to 0.5 mL of the 10 mg/mL belt peptide solution resulting in a final lipid-to-peptide ratio of 1.67 in a final volume of 1.0 mL. This lipid-to-peptide ratio of 1.67 has been previously reported to generate 10 nm

diameter NDs [17]. The ND solution was incubated overnight at room temperature prior to use. Each experiment in this study used fresh NDs that were generated the previous night.

5.3.3 Sample preparation for fluorescence quenching experiments

Other compounds and reagents used in the experiments include N-acetyl-tryptophanamide, abbreviated NATA (Sigma Aldrich), urea (MP Biomedicals), acrylamide (Thermo Fisher Scientific), dipotassium phosphate (Thermo Fisher Scientific), and potassium dihydrogen phosphate (Thermo Fisher Scientific). These samples were used as received.

Concentrated denatured protein primary stock solutions contained 150-615 μM protein, 8.0 M urea, and 20 mM KP_i buffer at pH 7.3. Appropriate volumes of protein primary stock solutions were used to create secondary stock protein solutions of 140 μM OmpA, 4.5 M urea, and 20 mM KP_i buffer at pH 8.0. A slightly basic pH of 8.0 results in efficient folding of OmpA into NDs [5]. All OmpA mutants are denatured in 4.5 M urea [16].

For folding experiments, five individual 200 μL samples were prepared which contained 10 μM protein (14 μL of 140 μM secondary stock solution), 0.3 M urea, and acrylamide concentrations of 0, 0.1, 0.2, 0.3, or 0.4 M, diluted from a primary 1.0 M acrylamide stock solution. To each of the five samples, an appropriate amount of solution of NDs was added to achieve a final lipid-to-protein ratio of ~300-to-1; this ratio resulted in folding yields of 76-96% for all mutants. Appropriate volumes of KP_i buffer at pH 8.0 were added to achieve a final total volume of 200 μL.

Sample preparation for adsorbed protein experiments was identical to the preparation for folding experiments. However, experiments on the adsorbed state were performed below the phase transition temperature of the ND to allow adsorption, but not insertion and folding.

Experiments on aggregated and denatured OmpA were performed on 200 μL samples, each containing 10 μM protein, acrylamide (0.0, 0.1, 0.2, 0.3, or 0.4 M), and different concentrations of urea. Samples for aggregated OmpA contained a final urea concentration of 0.3 M. Samples for denatured OmpA contained 8.0 M urea.

5.3.4 Fluorescence quenching spectroscopic measurements

All fluorescence measurements were collected using a Jobin-Yvon SPEX Fluorolog FL3-11 spectrofluorometer. For folding experiments, the folding reaction was initiated by dilution of urea from 4.5 M to the final urea concentration of 0.3 M. All ND-acrylamide-urea-buffer solutions (without protein) were allowed to incubate at 37 °C for at least 15 minutes prior to the addition of protein to ensure that the NDs were equilibrated above their phase transition temperature and in the fluid phase. Fluorescence spectra for each acrylamide concentration were acquired every 5 minutes for the first 2 hours (including a time = 0 minute, which is immediately after addition of protein), and then every 20 minutes for the remaining 3 hours, for a total folding time of 5 hours. Samples were maintained at 37 °C throughout the experiment in a 10 mm x 2 mm quartz cuvette sealed with a Teflon cap. The samples were excited along the 2 mm path length with 295 nm light. Fluorescence was collected along the 10 mm path length at right angle geometry. The excitation and emission bandpass were 3 nm. Spectra of each sample without protein were collected prior to the folding experiment; these blank spectra were used to subtract background signal from the NDs, urea, and buffer and thus, enabled the isolation of fluorescence signal from the protein. The temperature dependence of NATA emission was investigated because fluorescence spectra were acquired at different temperatures. The wavelength of maximum emission remained 360 nm and the fluorescence intensities decreased ~23% with an increase in temperature from 21 °C (room temperature) and 37 °C (data not shown).

Additional experiments were performed for steady-state conformations: adsorbed, aggregated, and denatured. To probe the adsorbed state, denatured protein from the secondary stock solution was added to the equilibrated solution of NDs. Fluorescence spectra were obtained below the ND phase transition at 16 °C (T_m = ~29 °C, [18]). Spectra of samples without protein served as blanks and were used to isolate signal from protein only. The temperature dependence of fluorescence emission of a mixture of model compounds N-acetyl-tryptophanamide (NATA) and N-acetyl-tyrosinamide at low temperature and high temperature showed that the intensity at 360 nm decreased ~23% with an increase in temperature from ~17 °C to ~33 °C. This change in intensity is attributed to tryptophan, and not tyrosine, because a separate study of only NATA showed that the fluorescence intensity decreased ~23% with an increase in temperature from 21 °C (room temperature) and 37 °C. The temperature dependence of the intensity is not expected to significantly affect the Stern-Volmer analysis because the fluorescence spectra in the absence and presence of quencher are measured at the same temperature. However, it is known that there is a very modest temperature dependence of the Stern-Volmer constants because of the known effects of temperature on the dynamic and static components of quenching. The wavelength of maximum emission remained constant at 360 nm (data not shown) over these temperatures.

To probe the aggregated and denatured states, appropriate amounts of primary protein stock solutions containing denatured protein were added to two sets of five separate samples, which gave a final protein concentration of 10 μM and final urea concentrations of 0.3 M for aggregated studies and 8.0 M for denatured studies. Each of the two sets of samples contained acrylamide concentrations of 0, 0.1, 0.2, 0.3, and 0.4 M. The protein-urea-acrylamide solutions were allowed to incubate at room temperature for at least 5 minutes prior to the collection of fluorescence spectra. Spectra of the acrylamide-urea-buffer solutions without protein served as

blanks and were subtracted from raw protein spectra to isolate signal from protein only. SDS-PAGE mobility experiments were performed on representative folded, adsorbed, aggregated, and denatured protein samples to confirm the correct conformation of OmpA via apparent molecular weights [19-21].

5.3.5 Fluorescence measurements to confirm the stability of NDs in the presence of acrylamide

An experimental benefit of the use of NDs over other types of lipid bilayer systems is its long-term stability [22]. It has been reported that the long-term stability of assembled discs can remain stable for 1-2 weeks or for at least 50 days, depending on their size [23]. In addition, NDs have been reported to be stable when stored at 4 °C for up to 2 months [23]. To test the stability of the NDs in the presence of acrylamide at 37 °C, fluorescence measurements of NDs were obtained at 37 °C in the presence of 0.0, 0.1, 0.2, 0.3, 0.4, and a high concentration of 1.0 M acrylamide. Fluorescence spectra were acquired with 295 nm excitation and emission was collected from 310 to 504 nm. Spectra of NDs in the presence of acrylamide at each acrylamide concentration were collected every 10 minutes for a total of 2 hours. Fluorescence spectra of the 14A belt peptide in the presence of 0.0, 0.1, 0.2, 0.3, 0.4, and 1.0 M acrylamide at 37 °C were also collected every 10 minutes for a total of 1 hour. No changes in the fluorescence intensities, emission wavelength, or shape of the fluorescence curve were observed for any of the acrylamide concentrations, indicating that both NDs and belt peptide remained stable under these experimental conditions (Figure 5.2).

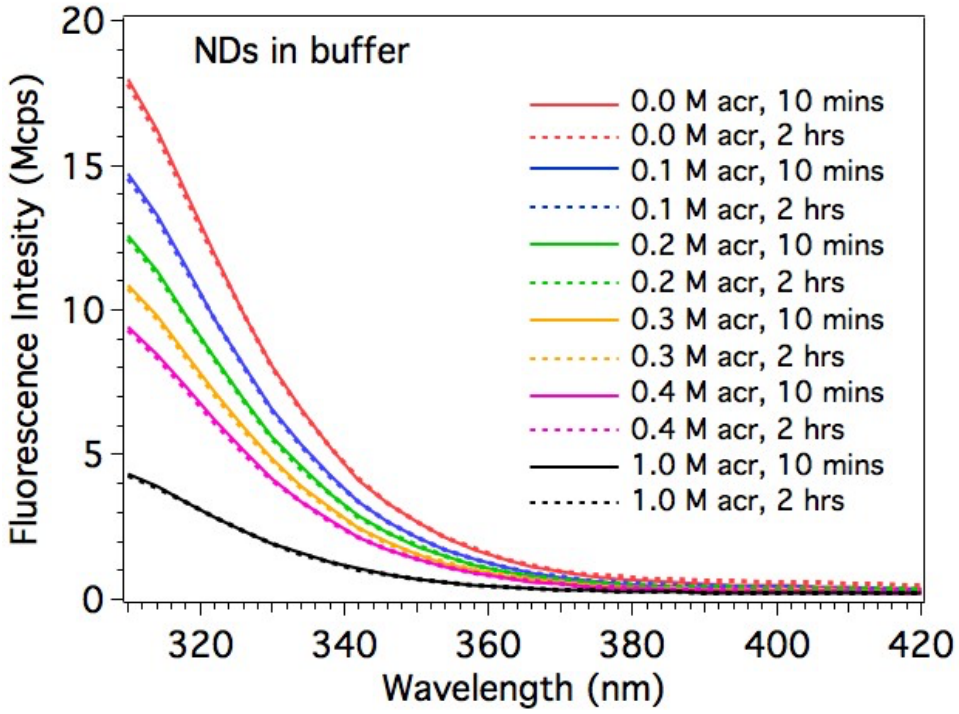

Figure 5.2 Fluorescence spectra of NDs in the presence of 0.0 (red), 0.1 (blue), 0.2 (green), 0.3 (orange), 0.4 (pink), and 1.0 M (black) acrylamide at 37 °C. The excitation wavelength was 295 nm. The Raman signal from water was removed via subtraction of a water-only spectrum. Solid lines are spectra collected after 10 minutes of incubation at 37 °C. Dashed lines are spectra collected after 2 hours of incubation at 37 °C.

5.3.6 Circular dichroism (CD) spectroscopy

The kinetics of formation of OmpA's secondary structure during folding into NDs was probed by circular dichroism (CD) spectroscopy using a Jasco J-815 spectrometer. Concentrated wild-type OmpA (340 μM) denatured in 8.0 M urea was diluted into an equilibrated ND solution (pH 8.0) at 33 °C, to achieve a final protein concentration of 3 μM. Prior to the addition of protein, the ND-buffer solution (without protein) was allowed to equilibrate at 33 °C for at least 20 minutes. The initiation of the folding reaction resulted from dilution of 8.0 M urea to a final urea concentration of 0.3 M. The final lipid-to-protein ratio was ~100-to-1 based on the absorption difference spectrum. CD spectra were acquired at time points: 0, 8, 16, 30, 46, 60, 120, 180, and 240 minutes after the initiation of the folding reaction. The sample chamber was continuously purged with nitrogen gas and held at a constant temperature of 33 °C during the 4 hour folding period. CD spectra were acquired in a sealed 1 mm path length quartz cuvette from 204-260 nm with 4 second data integration time, 1 nm data pitch, and 10 nm/min scanning speed. One accumulation was acquired at each time point for samples with and without protein. The background signal was subtracted from the raw spectra of protein to remove contribution of signal from the ND-urea-buffer background using Igor Pro analysis software.

5.4 Results

Site-specific insights into the desolvation process during the folding and insertion of OmpA into NDs were obtained by bimolecular fluorescence quenching experiments. Time-resolved fluorescence emission spectra of single-tryptophan OmpA mutants in the presence of NDs and acrylamide concentrations of 0.0 to 0.4 M were collected during a folding reaction and the resulting Stern-Volmer quenching constants and desolvation kinetics were determined. SDS-PAGE differential mobility analysis was performed to confirm that the presence of acrylamide did not significantly hinder the folding yield; the yield changed less than 10% across all concentrations of acrylamide relative to in the absence of acrylamide. The total duration of the folding experiments was 5 hours. This timescale is appropriate because it was previously shown that the spontaneous, unassisted, *in vitro* folding and insertion of OmpA to its native form, reaches completion within the first 2-3 hours in the presence of DMPC NDs and DMPC SUVs [5, 24].

5.4.1 Stern-Volmer analysis to investigate the evolution of the bimolecular quenching constants during folding into NDs

To isolate emission from OmpA, fluorescence spectra from samples without protein, and thus attributed to the ND-acrylamide-urea-buffer background, were acquired at the beginning of the experiment and subtracted from the appropriate raw OmpA fluorescence spectrum. Subtraction scalars, denoted c, in Equation 1 were varied between 0.85 and 1.1.

$$F_{obs} = \text{raw spectrum-c} \times \text{background spectrum} \quad \text{Eqn. 1}$$

In Eqn. 1, the background corrected protein emission spectra, F_{obs}, were further corrected for an inner-filter effect, according to Eqn. 2 due to significant absorption in the UV region from acrylamide and NDs.

$$F_{corr} = F_{obs} \times 10^{\left(\frac{A_{ex}+A_{em}}{2}\right)} \quad \text{Eqn. 2}$$

In Eqn. 2, F_{obs} and F_{corr} are the background and inner-filter effect corrected OmpA fluorescence spectra, respectively. The term A_{ex} and A_{em} denote the absorption values of the excitation and emission wavelengths, respectively. In our studies, A_{ex} and A_{em} were determined at 295 nm and 350 nm, respectively. Both A_{ex} and A_{em} values were for a 2 mm excitation path length. The assumption of 0.2 mm for A_{em} is an estimate, because the actual emission path length is approximately 5 mm (half of 10 mm path length). However, the absorption values for A_{em} at 350 nm was very small, approximate absorbance of 0.004, so the absorption of emitted light along the emission path is negligible. The final spectra, F_{corr}, were analyzed for each mutant and each acrylamide concentration. Figure 5.3 shows representative fluorescence spectra for W102 folding into NDs in the absence of acrylamide (0 M acrylamide) and in the presence of the highest concentration of acrylamide (0.4 M acrylamide). Similar plots were constructed with 0.1, 0.2, and 0.3 acrylamide. The fluorescence maximum, λ_{max}, blue-shifted from ~354 nm to ~337 nm upon folding; the magnitude of the blue-shift depended on the OmpA mutant. The observed ~17 nm blue-shift upon folding into bilayers has been previously characterized as a transition from tryptophan being exposed to a polar environment to a more hydrophobic environment [3, 19, 25]. The λ_{max} intensities, obtained from Gaussian fits to the data, during folding at each acrylamide concentration were plotted as a function of reaction time (Figure 5.3 inset). The λ_{max} intensities were determined independent of emission wavelength, which varied systematically from ~354 nm to ~337 nm depending on the OmpA mutant. Stern-Volmer plots were generated for all mutants at each time point during folding using Eqn. 3, where F_0 and F refer to F_{corr} intensities in the absence and presence of acrylamide, respectively.

Dynamic model: $$\frac{F_0}{F} = K_{SV} \times [Q] + y_{int} = k_q \tau_0 [Q] + y_{int}$$ Eqn. 3

Sphere-of-action model: $\frac{F_0}{F} = (K_D[Q] + y_{int})e^{V[Q]} = (k_q\tau_0[Q] + y_{int})e^{V[Q]}$ Eqn. 4

In Eqn. 3, K_{SV} is the Stern-Volmer dynamic (collisional) quenching constant and [Q] is the quencher, or acrylamide, concentration. Under ideal experimental conditions, the value of the y-intercept, y_{int}, should be 1. In our present analyses, y_{int} was allowed to vary between 0.95 and 1.05 to take into account slight offsets from the instrument. In addition to the purely dynamic quenching model, each Stern-Volmer plot was also fit to a combined static-dynamic quenching model or "sphere-of-action" model, Eqn. 4, yielding a dynamic quenching component, K_D, and a static volume component, V, within which the probability of quenching is 1. In our analyses, values of V were determined for the different conformations of denatured, adsorbed, aggregated, and folded OmpA. For the folding studies, the values of V at the t = 0 minute and t = 5 hour time points were determined. Additionally, an average value of V based on the t = 0 minute and t = 5 hour time points was determined for each mutant. According to Eqns. 3 and 4, the dynamic Stern-Volmer quenching constants, K_{SV} and K_D, are the product of the bimolecular quenching constant, k_q, and lifetime of the fluorophore in the absence of quencher, τ_0. The bimolecular quenching constants, k_q, were calculated by using the published values for τ_0 [25] and the experimentally determined values of K_{SV} and K_D. Representative Stern-Volmer plots for the folding of W102 into NDs and the evolution of K_D during folding are shown in Figure 5.4.

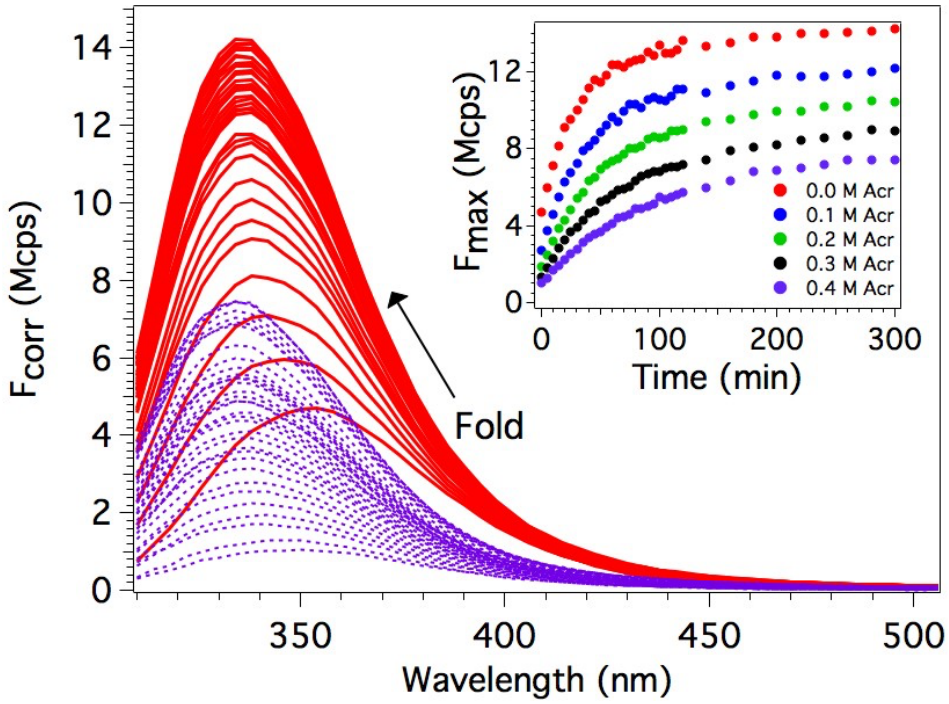

Figure 5.3 Representative fluorescence spectra during the folding reaction in the absence and presence of acrylamide. Fluorescence spectra are shown for OmpA W102 in the absence (solid red) and presence of acrylamide (0.4 M, dashed purple) during the folding into NDs (t = 0 to t = 5 hours). The spectra are corrected for background signal and the inner-filter effect (see Eqn. 1). The inset shows the maximum fluorescence intensity for each acrylamide concentration (0.0, 0.1, 0.2, 0.3, and 0.4 M) during the folding reaction.

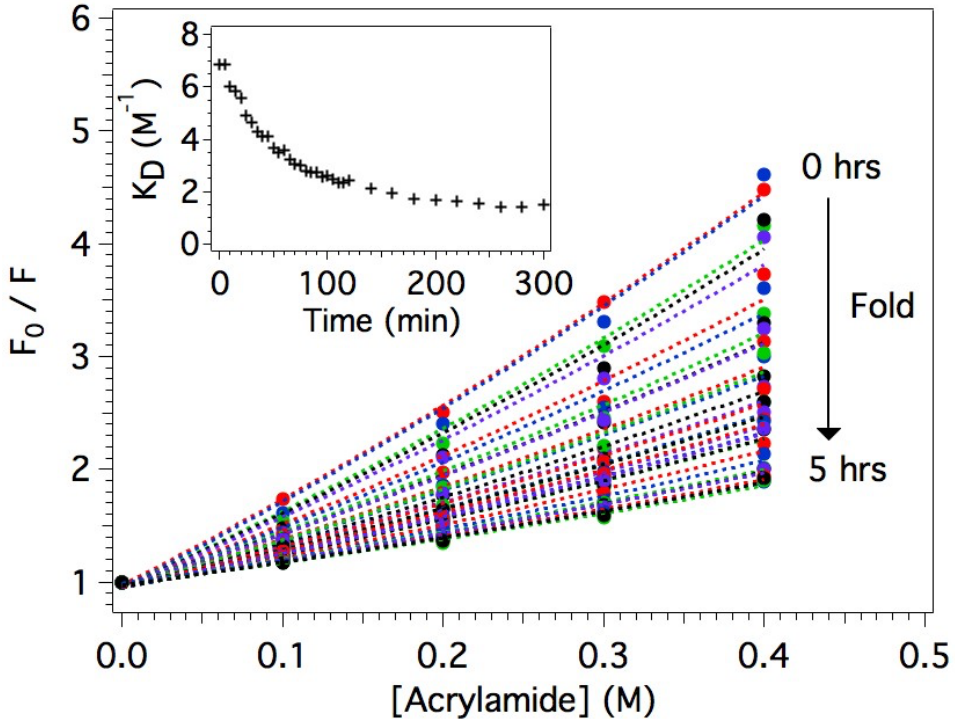

Figure 5.4 Representative Stern-Volmer plots and the evolution of K_D during folding. Stern-Volmer plots are for OmpA W102 during the folding reaction into NDs (t = 0 to t = 5 hours). The dashed curves are fits to the data using the sphere-of-action model (Eqn. 4) with V held constant at 0.46 M^{-1}. The inset shows the evolution of K_D during the folding reaction.

5.4.2 Contribution of native tyrosine residues

The fluorescence spectra of OmpA with 295 nm excitation contain signal from the single tryptophan residue as well as some signal from the 17 native tyrosine residues. A separate control experiment utilizing W0 mutant, in which signal from the 17 native tyrosine residues (Figure 5.5, panel B) were subtracted from the spectra of OmpA folding into NDs (Figure 5.5, panel C), showed that the effect of tyrosine on the K_D kinetics is less than 12% (Figure 5.5, panel F). Stern-Volmer plots with and without subtraction of tyrosine signal are shown in panels (D) and (E), respectively. An analogous analysis during folding into SUVs showed that subtraction of the signal from the 17 native tyrosine residues exhibited a difference of 7% in the K_D kinetics [15]. Therefore, tyrosine signal from the protein was included in the data analysis for all fluorescence quenching experiments.

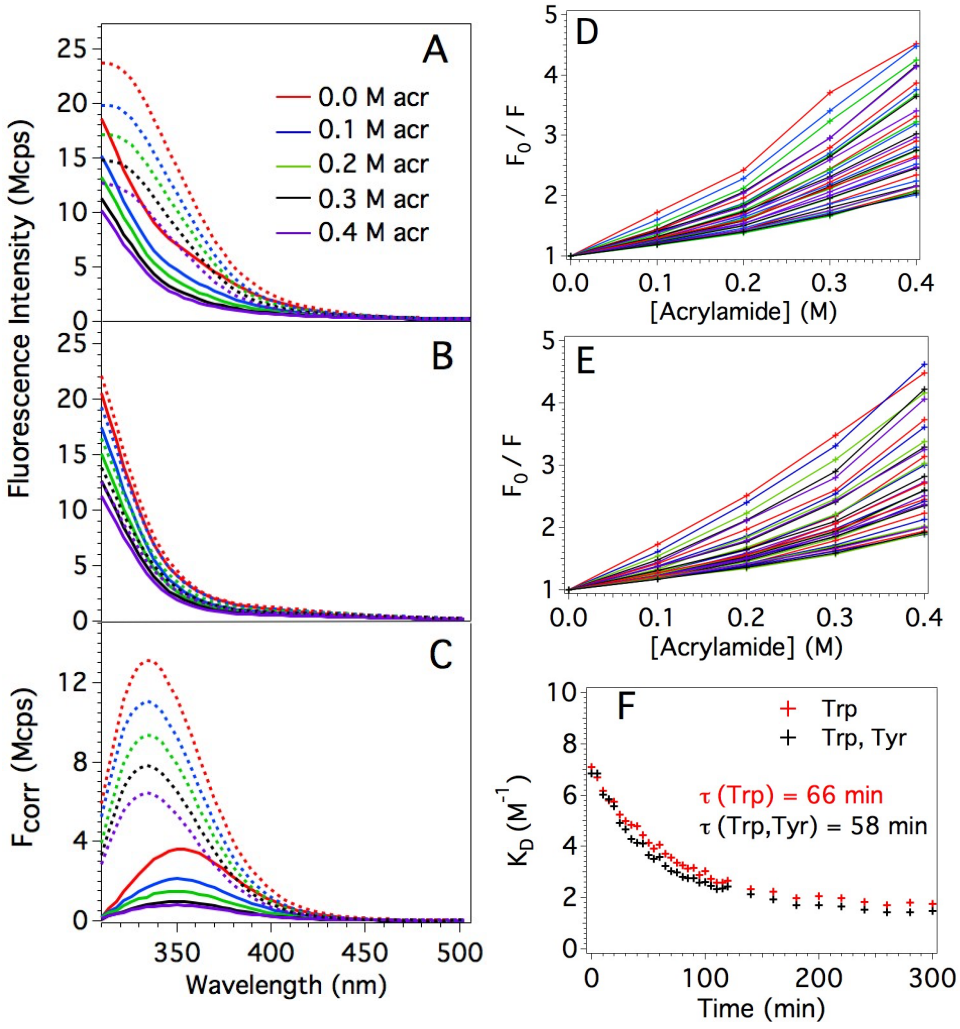

Figure 5.5 The effect of tyrosine on K_D kinetics. Raw fluorescence spectra of W102 are shown in panel (A). Fluorescence spectra of W0 are in panel (B). A W0 spectrum was subtracted from the corresponding W102 fluorescence spectrum and the isolated tryptophan fluorescence spectra, without contributions from tyrosine, are shown in panel (C). Panels (A), (B), and (C) show spectra for t = 0 hour (solid) and t = 5 hour (dashed) for five acrylamide concentrations of 0.0, 0.1, 0.2, 0.3, and 0.4 M. The Stern-Volmer plots for all time points during folding from 0 hour (highest slope) to 5 hours (smallest slope) are shown in panel (D) (solid lines that connect the data points are included to guide the eye). Analogous Stern-Volmer plots when signal from tyrosine is not subtracted from the raw spectra are shown in panel (E). Panel (F) shows the resulting kinetics of K_D with (red) and without (black) subtraction of tyrosine using the sphere-of-action model (main text Eqn. 3) and fixed V value of 0.46 M^{-1}. The data show that the effects of tyrosine on the K_D kinetics are less than 12%.

5.4.3 Determination of the volume component, V, and kinetics of K_D during folding

An upward curving Stern-Volmer plot has been shown to be indicative of the static quenching, or sphere-of-action (Eqn. 4) quenching model [11]. In this model, there is a static volume parameter, V, a volume in which the fluorophore and quencher are in such close proximity at the time of excitation, that the emitted fluorescence is immediately quenched upon excitation [11, 12]. It has been reported that V varies with the degree of static quenching and the exposure of the fluorophore [12, 14, 26], and this variation of V leads to complexities in the Stern-Volmer analysis of a folding reaction. In our first model, we used constant values of V = 1.6, 0.9, 0.6, 0.3, and 0.0 M^{-1} to analyze all folding time points for all mutants. This range of V values encompass typical values reported for proteins with single tryptophan residues [12] and also encompass the maximum and minimum range for all mutants in the present studies. The calculated values of K_D using each of these constant V values were then plotted as a function of folding time (see Table 5.1). A single exponential decay function was fit to the data, resulting in a reciprocal decay time constant, $\tau = \frac{1}{k}$, for each value of V. For example, for W7 folding into NDs ($n = 3$), τ values for V = 1.6, 0.9, 0.6, 0.3 and 0.0 M^{-1} were 33, 42, 41, 41, and 40 minutes, respectively. The average τ value for W7 folding into NDs was 39.4 minutes, resulting in a deviation of 4% for V = 0.9, 0.6, 0.3, and 0.0 M^{-1} and a deviation of 16% using V = 1.6 M^{-1}. For all mutants folding into NDs, V = 0.9, 0.6, 0.3, and 0.0 M^{-1} gave τ values that were within 5% of one another, and V = 1.6 M^{-1} resulted in the largest deviation from the others of 22% for W7. The average value of τ (across all five V values) for W7, W15, W57, W102, and W143 was 39.4, 39.6, 34.8, 66.0, and 27.4 min, respectively. All averages consisted of a total of 3 trials.

In the second model, a global fitting routine was utilized to simultaneously fit the results for t = 0 hr and t = 5 hours for all trials of all mutants in NDs. In total, there were 15 trials each

for the t = 0 hour and t = 5 hour time points for folding into NDs (5 mutants x 3 trials each). The t = 0 hour time point yielded a global fit V value of 0.62 M^{-1} ($n = 15$) and the t = 5 hour time point gave a global V value of 1.29 M^{-1} ($n = 15$). The average of these two values of V was 0.96 M^{-1} ($n = 30$). A summary of the results of the global fit for each mutant and condition are shown in Table 5.2.

It is known that there is variation in V as well as a correlation between V and solvent accessibility and/or rigidity of the local environment of tryptophan residues in proteins [12, 14]. It is expected that tryptophan residues with low solvent exposure or protected in rigid environments exhibit low or zero values of V, while tryptophan in solvent exposed or dynamic environments exhibit high values of V [12, 14, 15, 27]. Values of V have been reported in the range between 0.0 and 1.0 M^{-1} [12]; in our previous study of OmpA folding in SUVs, an average value of V of 0.46 M^{-1} [15] based on the global fits to the data was used. This previous value of 0.46 M^{-1} in SUVs differs from the present average value of 0.96 M^{-1} in NDs. The origin of this difference is not clear. It is possible that there is a high local concentration of acrylamide in NDs compared to in SUVs, leading to a high value of V in NDs. Additionally, the value of 1.29 M^{-1} (t = 5 hours) for folded OmpA compared to the t = 0 hour average value of 0.62 M^{-1} is contrary to what would be expected for folded protein. Unfortunately, given the small number of data points on account of limited sample, it is difficult to confirm the unusual high curvature in the Stern-Volmer graphs that leads to the large value of V for folded OmpA in NDs. More extensive experiments will be needed to probe this unexpected result. For the present analysis, we have opted to utilize the average V value of 0.46 M^{-1} that was previously used in our SUV studies. The resulting absolute values of K_D obviously differ for V = 0.46 M^{-1} and 0.96 M^{-1}; however, the kinetics associated with the Stern-Volmer constants were nearly identical for these two values of

V (see below). The use of 0.46 M^{-1} for NDs is reasonable due to similar native OmpA secondary and tertiary structures observed in both SUVs and NDs [5]. Additionally, the polarity of local environment for folded OmpA is similar in SUVs and NDs based on blue-shifted λ_{max} emission values of ~337 nm [5]. A final rationale to utilize V = 0.46 M^{-1} for the analysis of NDs allows for a direct comparison of site-specific kinetics during folding into both types of bilayers.

Table 5.1 Summary of V (M^{-1}), K_D (M^{-1}), τ_0 (ns), and decay time τ (min) of K_D for OmpA mutants folding into NDs. The value of V was fixed at 1.6, 0.9, 0.6, 0.3, or 0.0 M^{-1} and the resulting, best-fit value for K_D is reported using Equation 4 in the main text. The values for the fixed fluorescence lifetime (τ_0) for W7, W15, W57, W102, and W143 are for the protein in 8.0 M urea and in DMPC (J.E. Kim, G. Arjara, J.H. Richards, H.B. Gray, J.R. Winkler, *J. Phys. Chem.* B 110 (2006) 17656-62). The last column reports the inverse decay constant τ (min) for the evolution of K_D and using the indicated value of V during the folding reaction.

Sample	fixed V (M^{-1})	best-fit K_D (M^{-1})	fixed lifetime τ_0 (ns)	resulting τ (min) for evolution of K_D during folding into NDs
W7				
t = 0 hr (n=3)	1.6	2.73	3.1	
	0.9	4.30	3.1	
	0.6	5.14	3.1	
	0.3	6.02	3.1	
	0.0	6.96	3.1	
t = 5 hr (n=3)	1.6	-0.03	4.1	32.61 ± 1.21
	0.9	0.39	4.1	42.07 ± 1.69
	0.6	0.77	4.1	41.30 ± 1.67
	0.3	1.20	4.1	40.67 ± 1.65
	0.0	1.67	4.1	39.93 ± 1.61
W15				
t = 0 hr (n=3)	1.6	3.36	2.9	
	0.9	5.12	2.9	
	0.6	6.03	2.9	
	0.3	7.03	2.9	
	0.0	8.09	2.9	
t = 5 hr (n=3)	1.6	-0.03	3.7	33.61 ± 1.35
	0.9	0.32	3.7	42.15 ± 1.75
	0.6	0.67	3.7	41.45 ± 1.70
	0.3	1.08	3.7	40.57 ± 1.64
	0.0	1.52	3.7	39.96 ± 1.62
W57				
t = 0 hr (n=3)	1.6	3.14	3.5	
	0.9	4.86	3.5	
	0.6	5.73	3.5	
	0.3	6.67	3.5	
	0.0	7.67	3.5	
t = 5 hr (n=3)	1.6	-0.06	4.5	30.29 ± 1.04
	0.9	0.38	4.5	36.46 ± 0.95
	0.6	0.75	4.5	35.92 ± 0.77
	0.3	1.18	4.5	35.58 ± 0.74
	0.0	1.65	4.5	30.29 ± 1.04
W102				
t = 0 hr (n=3)	1.6	3.38	3.9	
	0.9	5.19	3.9	
	0.6	6.11	3.9	
	0.3	7.10	3.9	
	0.0	8.16	3.9	
t = 5 hr (n=3)	1.6	0.06	4.8	70.26 ± 6.19
	0.9	0.85	4.8	67.73 ± 5.57
	0.6	1.29	4.8	65.67 ± 5.19
	0.3	1.77	4.8	63.73 ± 4.86
	0.0	2.29	4.8	62.43 ± 4.65
W143				
t = 0 hr (n=3)	1.6	2.92	2.9	
	0.9	4.57	2.9	
	0.6	5.42	2.9	
	0.3	6.31	2.9	
	0.0	7.26	2.9	
t = 5 hr (n=3)	1.6	-0.04	3.7	23.27 ± 0.72
	0.9	0.30	3.7	29.03 ± 0.63
	0.6	0.65	3.7	28.59 ± 0.57
	0.3	1.04	3.7	28.32 ± 0.54
	0.0	1.46	3.7	28.13 ± 0.52

Table 5.2 Summary of V (M^{-1}) and K_D (M^{-1}) for NATA and OmpA denatured in 8.0 M urea, aggregated in 0.3 M urea, adsorbed onto NDs, and/or folding into NDs (t = 0 and 5 hr) at pH 8.0. Both V and K_D in Equation 4 were allowed to vary and the resulting best-fits are reported for each mutant. The result for a global fit with all mutants is also indicated.

Sample	best-fit K_D(M^{-1})	best-fit V (M^{-1})
NATA (urea)		
pH 8.0	11.09	1.32
OmpA (urea)		
W7 (n=2)	6.24	0.54
W15 (n=2)	6.32	0.40
W57 (n=2)	5.91	0.52
W102 (n=2)	5.12	0.78
W143 (n=2)	6.06	0.52
Global (n=10)	5.93	0.55
OmpA aggregated (0.3 M urea)		
W7 (n=1)	5.84	0.41
W15 (n=1)	5.05	0.54
W57 (n=1)	5.72	0.46
W102 (n=1)	4.77	0.72
W143 (n=1)	5.01	0.67
Global (n=5)	5.27	0.56
OmpA adsorbed (NDs)		
W7 (n=1)	4.36	0.87
W15 (n=1)	4.03	1.37
W57 (n=1)	3.57	1.59
W102 (n=1)	2.89	1.39
W143 (n=1)	4.27	1.18
Global (n=5)	3.83	1.28
OmpA folding t = 0 hr (NDs)		
W7 (n=3)	5.80	0.41
W15 (n=3)	6.23	0.50
W57 (n=3)	6.32	0.36
W102 (n=3)	5.60	0.69
W143 (n=3)	3.89	1.09
Global (n=15)	5.56	0.62
OmpA folding t = 5 hrs (NDs)		
W7 (n=3)	0.00	1.23
W15 (n=3)	0.02	1.04
W57 (n=3)	0.19	1.13
W102 (n=3)	0.01	1.59
W143 (n=3)	0.04	1.17
Global (n=15)	0.00	1.29

The bimolecular quenching constants, k_q, were calculated according to Eqn. 4 by using previously published fluorescence lifetime measurements [25] and the Stern-Volmer quenching constants, K_D, obtained from fits to the sphere-of-action model using the average V value of 0.46 M^{-1} from studies of OmpA folding into SUVs [15]. The k_q values, which are interpreted as a measurement of the exposure to the solution [26], were plotted as a function of folding time and the data were fit to a single exponential function (Figure 5.6 and Table 5.3). A reciprocal time constant, $\tau = \frac{1}{k}$, was determined for each mutant. The reciprocal time constant τ is interpreted as a desolvation time, and is identical when plotting either k_q or K_D versus folding time. The results from single exponential fits to the decay of k_q during the folding reaction into NDs ($n = 3$) gave τ_{desolv} values of 41, 41, 36, 65, and 28 min for W7, W15, W57, W102, and W143, respectively. For comparison, the values of τ_{desolv} with $V = 0.96$ M^{-1} were 42, 42, 37, 68, and 29 minutes for W7, W15, W57, W102, and W143, respectively. Therefore, use of either $V = 0.46$ M^{-1} or 0.96 M^{-1} resulted in less than 5% variation for τ_{desolv}. A summary of the K_D and k_q decay kinetics and fit parameters are shown in Table 5.3. As a final analysis, K_{SV} (t = 5 hr) and K_D values were compared and as expected, the values for K_{SV} (t = 5 hr) are higher than K_D values (Table 5.3). Despite the superior fit of the data to the sphere-of-action model, however, the temporal evolution of K_{SV} and K_D are nearly identical and vary no more than 0.3% (Figure 5.7).

5.4.4 Determination of the volume component, V, for the denatured, aggregated, and adsorbed states

OmpA in the denatured, aggregated, and adsorbed states were also investigated. Representative fluorescence spectra and Stern-Volmer plots for OmpA denatured in 8.0 M urea, aggregated in 0.3 M urea, and adsorbed onto DMPC NDs are shown in Figure 5.8. The values of

V for denatured, aggregated, and adsorbed OmpA were determined using the same methods as for the folding reaction. Namely, global fits to all mutants for each condition led to values of 0.55 M^{-1}, 0.56 M^{-1}, and 1.28 M^{-1} for denatured, aggregated, and adsorbed OmpA, respectively. A summary of these V values and corresponding K_D values are provided in Table 5.2. The high value of 1.28 M^{-1} for OmpA adsorbed onto NDs contrasts with the published value of 0.39 M^{-1} determined for OmpA adsorbed onto SUVs [15]. The structure of OmpA adsorbed onto NDs is not known, and preliminary experiments indicate different levels of solvent exposure for the adsorbed state on SUVs and NDs; therefore it does not seem reasonable to adapt the adsorbed V value of 0.39 M^{-1}. While it is possible that the local acrylamide concentration is enhanced in the NDs, leading to the high value of 1.28 M^{-1}, additional experiments will be needed to confirm this unexpectedly high value. We note that the high value of V for the adsorbed state on NDs is consistent with the high value of V for the folded protein in NDs (described above), suggesting that the local concentration of acrylamide and/or exposure to solvent is different in NDs than SUVs. Future experiments will further investigate this possibility. For the present report, we avoid further discussion about the quenching constants for OmpA mutants adsorbed onto NDs.

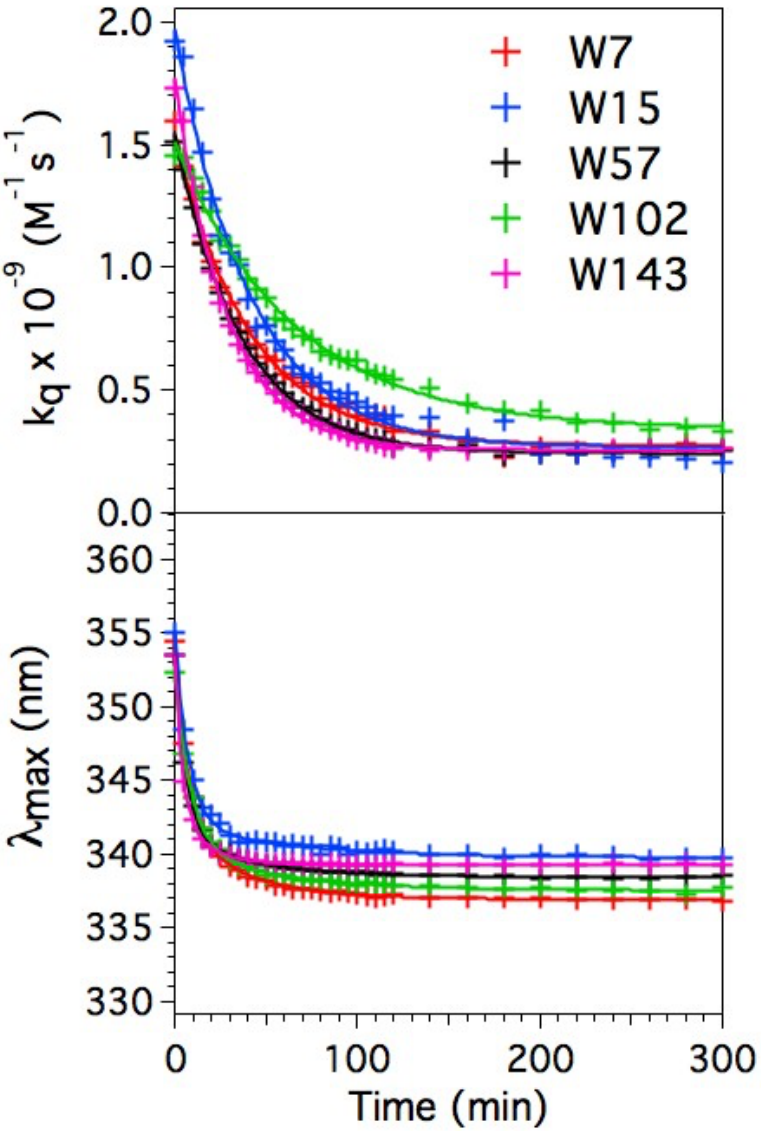

Figure 5.6 The decay of the bimolecular quenching constant, k_q, and λ_{max} during folding into NDs. The k_q values during folding were calculated from K_D values with a fixed V value of 0.46 M^{-1}. Each curve represents an average of 3 trials. The k_q kinetics (top panel) were fit to a single exponential function and the λ_{max} kinetics, obtained from the 0.0 M acrylamide samples (bottom panel) were fit to a double exponential function. The fits are shows as the solid curves.

Table 5.3 Summary of results from Stern-Volmer analysis for folding into NDs. The conditions are denatured in 8.0 M urea, aggregated in 0.3 M urea, and during folding into DMPC NDs at pH 8.0 ($t = 0$ hr and $t = 5$ hr). The change in K_D during folding, K_D ($t = 0$ hr) - K_D ($t = 5$ hr) is indicated as ΔK_D folding. The average K_D and k_q values for each mutant are indicated in the last column. The evolution of K_D and k_q during folding were fit to an exponential function $K_D(t) = Ae^{-t/\tau_{desolv}} + y_0$ or $k_q(t) = Ae^{-t/\tau_{desolv}} + y_0$ using a global analysis of multiple trials. The K_{SV} values at $t = 5$ hr were determined for each mutant using a global fit to multiple trials. Slight discrepancies in the table reflect rounding outcomes.

OmpA mutant	**W7**	**W15**	**W57**	**W102**	**W143**	
K_D (M^{-1}) (pH 8.0)						**Avg**
denatured[a]	6.2	5.8	5.8	5.9	6.0	5.9
aggregated[a]	5.3	5.0	5.4	5.3	5.4	5.3
t = 0 hr[b]	5.6	6.5	6.1	6.6	5.8	6.1
t = 5 hr[b]	1.0	0.9	0.9	1.6	0.8	1.0
ΔK_D folding	4.6	5.6	5.2	5.0	5.0	5.1
K_D decay parameters[b]						
τ_{desolv} (min)	41 ± 2	41 ± 2	36 ± 1	65 ± 5	28 ± 1	---
A (M^{-1})	4.6 ± 0.1	5.6 ± 0.1	5.2 ± 0.1	5.1 ± 0.2	5.0 ± 0.1	---
y_0 (M^{-1})	1.0 ± 0.1	0.9 ± 0.1	0.9 ± 0.1	1.5 ± 0.1	0.8 ± 0.1	---
K_{SV} (M^{-1})[c]						**Avg**
t = 5 hr	1.6	1.3	1.7	2.2	1.5	1.7
k_q (10^{-9} $M^{-1}s^{-1}$)[d]						**Avg**
denatured	2.0	2.0	1.7	1.5	2.1	1.9
aggregated	1.7	1.7	1.5	1.4	1.9	1.6
t = 0 hr	1.6	2.0	1.5	1.5	1.8	1.7
t = 5 hr	0.3	0.3	0.2	0.3	0.3	0.3
k_q decay parameters[e]						
τ_{desolv} (min)	41 ± 2	41 ± 2	36 ± 1	65 ± 5	28 ± 1	---
A (10^{-9} $M^{-1}s^{-1}$)	1.3 ± 0.1	1.7 ± 0.1	1.3 ± 0.1	1.2 ± 0.1	1.5 ± 0.1	---
y_0 (10^{-9} $M^{-1}s^{-1}$)	0.3 ± 0.1	0.3 ± 0.1	0.2 ± 0.1	0.3 ± 0.1	0.3 ± 0.1	---

[a]Values for *V* were 0.55 M^{-1} and 0.56 M^{-1} for denatured and aggregated OmpA, respectively. The error for K_D values is 7% and were derived from the sphere-of-action fits ($n = 2$ for denatured; $n = 1$ for aggregated). [b]Values for K_D at t = 0 and 5 hr were determined from the resulting parameters of the fit with *V* fixed at 0.46 M^{-1}. The errors for K_D decay parameters are derived from global fits to multiple trials for the folding reaction ($n = 3$ for all mutants). [c]The errors for K_{SV} are 5% (W7), 7% (W15), 10% (W57), 5% (W102), 9% (W143) and were derived from global fits to the same trials to determine K_D. [d]The average of the tryptophan lifetime, τ_0^{avg}, in urea and DMPC, for each OmpA mutant was used to calculate corresponding k_q values for t = 0 hr and t = 5 hr; the values for τ_0^{avg} were 3.6 ns (W7), 3.3 ns (W15), 4.0 ns (W57), 4.35 ns (W102), and 3.3 ns (W143). The known values of τ_0 in urea were used to calculate k_q for the denatured and aggregated states. The lifetimes were obtained from reference 27. [e]The errors for k_q decay parameters were derived from global fits to the same trials to determine K_D.

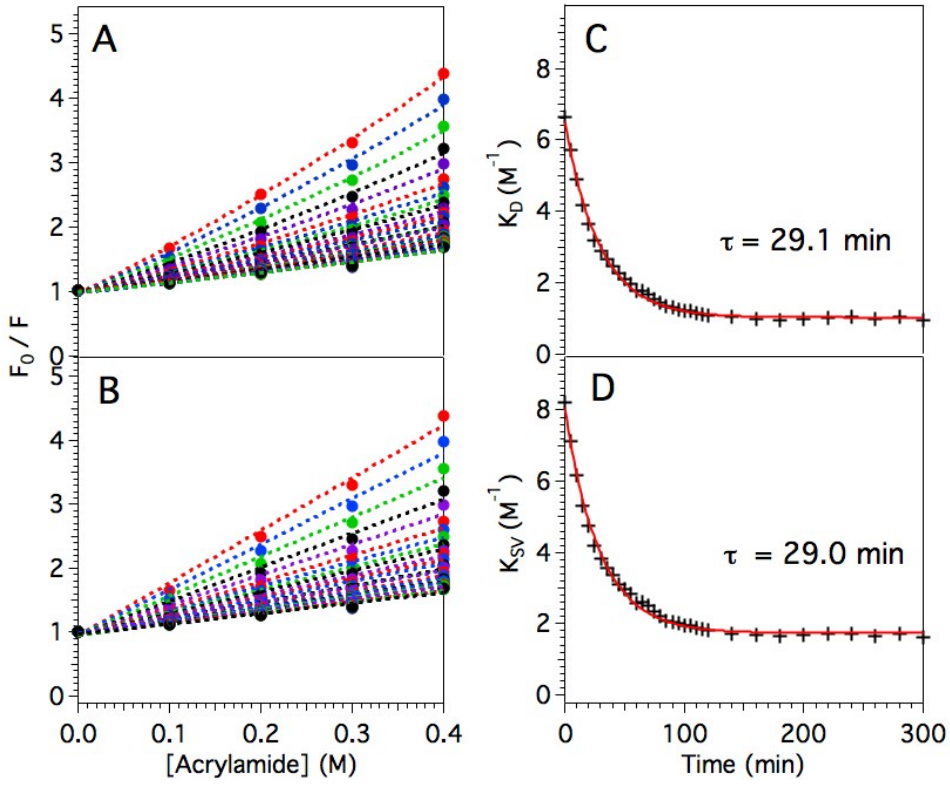

Figure 5.7 Representative Stern-Volmer plots for W7 folding into NDs. The Stern-Volmer plots in panel (A) were fit to the static + dynamic sphere-of-action model (Eqn. 4) with V fixed at 0.46 M^{-1}. The Stern-Volmer plots in panel (B) were fit to the purely dynamic model (Eqn. 3). Fits to the data in panels (A) and (B) are shown as dashed lines. The resulting K_D(from panel (A)) or K_{SV} (from panel (B)) kinetics are shown in panels (C) and (D), respectively. Exponential fits to the K_D and K_{SV} kinetics are shown as solid red curves. The resulting τ values are indicated on the plots.

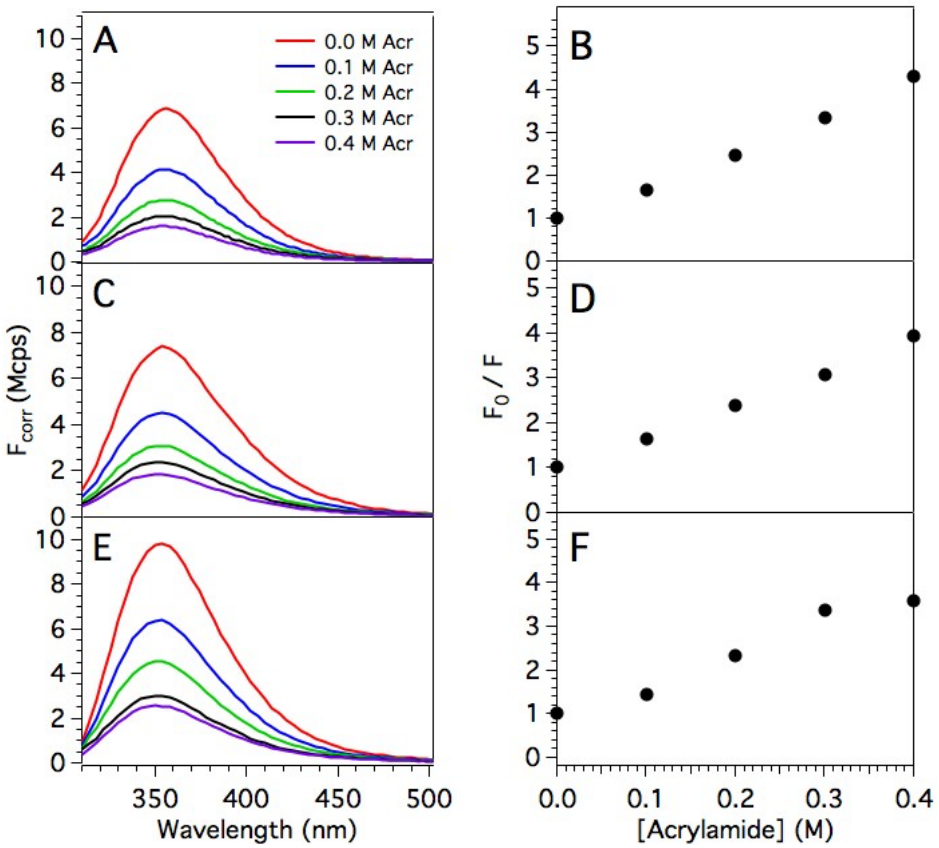

Figure 5.8 Representative fluorescence spectra (left) and Stern-Volmer graphs (right) of denatured OmpA mutant W7 in 8.0 M urea (graphs A and B), aggregated in 0.3 M urea (graphs C and D), and adsorbed onto NDs (graphs E and F). The concentration of W7 in panels (A), (C), and (E) have not been normalized to one another.

5.4.5 Kinetics of λ_{max} and folded population during folding

The kinetics of the tryptophan fluorescence λ_{max} during folding into NDs were determined by fitting Gaussian functions to the fluorescence spectra of OmpA in the absence of acrylamide (0.0 M acrylamide) and plotting λ_{max} against the corresponding folding time (Figure 5.6, bottom panel). Gaussians were fit to the fluorescence spectra in the range of 301 to 370 nm because this range encompasses the emission maximum for all data sets and across all mutants. Each kinetic trace in Figure 5.6 represents an average of 3 trials. Upon folding into NDs, the change in maximum emission wavelength from t = 0 hour to the t = 5 hour time point, referred to as $\Delta\lambda_{max}$, for W7, W15, W57, W102, and W143 were 17, 15, 15, 14, and 14 nm, respectively. These observed $\Delta\lambda_{max}$ values reported for single-tryptophan mutants during folding are consistent with previous results [15, 25]. In addition to the $\Delta\lambda_{max}$ values reported for single-tryptophan mutants, wild-type OmpA folding into NDs or SUVs has shown a $\Delta\lambda_{max}$ value of 19 nm, also in agreement with the present results [5]. The samples containing acrylamide resulted in ~2 nm blue-shift of the absolute fluorescence wavelengths, which was not observed in the fluorescence of NATA in the presence of acrylamide (data not shown). The kinetics of λ_{max} during folding were best fit to double exponential functions, which resulted in fast and slow τ values of 4-9 minutes and 14-64 minutes, respectively. A summary of λ_{max} kinetics during folding and emission wavelengths for the denatured and aggregated conformations are provided in Table 5.4.

Tryptophan fluorescence also provides insights into the fraction of folded OmpA based on decomposition of the fluorescence spectrum. This method assumes a 2-state folding model in which the folded and unfolded populations have different basis spectra [3]. Fluorescence spectra

of OmpA during folding into NDs were decomposed into these basis spectra and folding kinetics were extracted. These folding rates are included in Table 5.4.

5.4.6 Correlation between k_q and λ_{max} for different conformations of OmpA

The correlation between the bimolecular quenching constant, k_q, vs λ_{max} and K_D vs λ_{max} are shown in Figure 5.9. Generally, it is expected that the larger k_q values (and therefore K_D) should correlate with the larger λ_{max} values, due to increased accessibility of the fluorophore to the quencher. Our results follow this trend. For example, the denatured conformation exhibits the most red-shifted average λ_{max} valus of 356 nm and is correlated with the highest average k_q values of 1.9×10^{-9} M^{-1} s^{-1}. The aggregated conformation exhibits λ_{max} values of 353-356 nm and is correlated with an average k_q value of 1.6×10^{-9} M^{-1} s^{-1}. The average λ_{max} value for folded OmpA is the most blue-shifted at 338 nm and is correlated with the lowest k_q average value of 0.3×10^{-9} M^{-1} s^{-1}. Similar trends were published for the correlation between k_q and λ_{max} for OmpA in SUVs [15].

Table 5.4 Summary of results from wavelength and intensity analysis for folding into NDs. The conditions are denatured in 8.0 M urea, aggregated in 0.3 M urea, and during folding at pH 8.0 (extrapolated at t = 0 hr and t = 5 hr). The change in λ_{max} during folding, λ_{max} (t = 0 hr) - λ_{max} (t = 5 hr), is denoted as $\Delta\lambda_{max}$ folding. The evolution of λ_{max} during folding were fit to a double exponential function $\lambda_{max}(t) = A_{fast}e^{-t/\tau_{enviro}^{fast}} + A_{slow}e^{-t/\tau_{enviro}^{slow}} + y_0$ using a global analysis to multiple trials. Stated errors for the kinetic fits are upper and lower limits for multiple trials. Slight discrepancies in the table reflect rounding outcomes. Spectral decomposition into folded and unfolded basis spectra revealed the fraction of folded protein (F_{folded}), and these kinetics were fit to a single exponential function: $F_{folded} = y_0\text{-}Ae^{-t/\tau_{fold}}$.

OmpA mutant	**W7**	**W15**	**W57**	**W102**	**W143**	
λ_{max} (nm)[a]						**Avg**
denatured	356	356	356	357	357	356
aggregated	356	354	353	354	354	354
t = 0 hr[b]	354	355	353	352	353	353
t = 5 hr[b]	337	340	338	338	339	338
$\Delta\lambda_{max}$ folding	17	15	15	14	14	15
λ_{max} decay parameters[b]						
τ_{enviro}^{fast} (min) τ_{enviro}^{slow} (min)	7 ± 1 37 ± 7	8 ± 1 64 ± 23	6 ± 1 43 ± 8	9 ± 1 52 ± 8	4 ± 1 14 ± 2	---
A_{fast} (nm) A_{slow} (nm)	13 ± 1 5 ± 1	13 ± 1 2 ± 1	12 ± 1 3 ± 1	12 ± 1 3 ± 1	10 ± 1 5 ± 1	---
y_0 (nm)	337 ± 1	340 ± 1	338 ± 1	338 ± 1	339 ± 1	---
Folding kinetics[c]						
τ_{fold} (min)	21	25	19	26	23	23

[a] The error for λ_{max} values for denatured and aggregated is 0.1% based on the error of the Gaussian fit to the fluorescence curves of the 0 M acrylamide samples (*n* = 2 for denatured and *n* = 1 for aggregated). [b]Values for λ_{max} at t = 0 and 5 hr were determined from the resulting parameters of the fit. The error for λ_{max} decay parameters were derived from global fits to multiple trials for the folding reaction (n = 3 for each mutant). [c]The error for folding kinetics is 7% based on the error of the exponential fit to F_{folded} (*n* = 5).

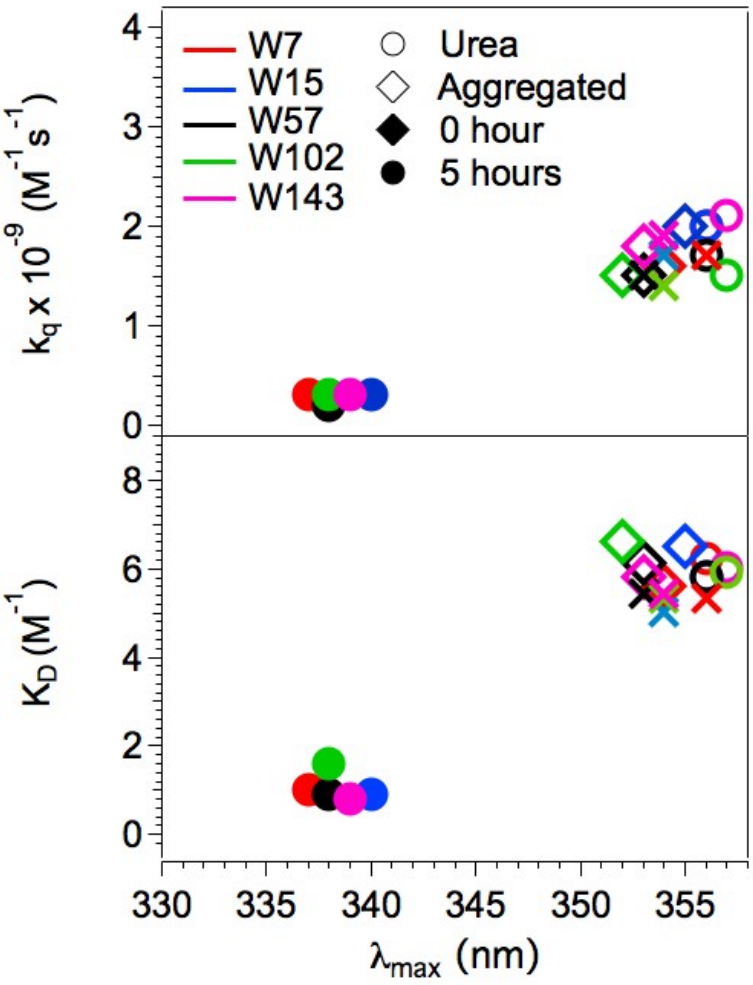

Figure 5.9 Correlation of average values of k_q, K_D, and λ_{max}. Top panel shows k_q vs. λ_{max} and bottom panel shows K_D vs. λ_{max}. In both panels, OmpA: denatured in 8.0 M urea, aggregated in buffer, $t = 0$ hr during folding into NDs, and folded in NDs at $t = 5$ hr. Markers for each conformation are shown in the legend. These values are summarized in Tables 5.3 and 5.4.

5.4.7 Kinetics of β-sheet structure formation during folding

The far UV CD spectra of proteins report on secondary structure. The native structure of OmpA consists of 8 anti-parallel β-sheet strands that form a transmembrane β-barrel domain and a soluble periplasmic domain that has been reported to be a mixture of β-sheet and α-helical structure [28]. Following the initiation of the folding reaction into NDs, nine CD spectra for wild-type OmpA were acquired at time points: 0, 8, 16, 30, 46, 60, 120, 180, and 240 minutes for two trials and 0, 8, 16, 30, 46, 60, 129, and 180 minutes for a third trial. The CD results from a single trial, after subtraction of background signal, are shown in Figure 5.10. At the earliest time point, t = 0 min, immediately after addition of protein to the ND solution, the CD spectrum displays a negative feature in the far UV region, indicative of disordered secondary structure [29]. As the folding reaction proceeds, the negative feature in the far UV region evolves and by approximately 60 minutes, a local minimum around 212 nm becomes prominent, indicating the formation of β-sheet structure [29, 30].

The molar ellipticity at 219 nm was plotted against folding time (Figure 5.10, panel C) and the data were fit to a single exponential. An inverse rate constant for formation of second structure based on CD, τ_{CD}, determined from a global fit to 3 trials resulted in a value of 28 ± 7 minutes. The molar ellipticity of NDs at 219 nm did not evolve and remained constant during the 4-hour folding period (Figure 5.10, panel B).

A comparison between the kinetics based on CD and fluorescence experiments requires a brief discussion about the conditions for these two types of experiments: the temperatures are slightly different (33 °C for CD and 37 °C for fluorescence quenching) and the lipid:protein ratios are also different (100:1 for CD and 300:1 for fluorescence quenching). Both of these differences would lead to slower folding times and thus, the τ_{CD} value of 28 minutes for the

formation of secondary structure is likely to be faster if CD experiments were performed at the same conditions as the fluorescence experiments. In terms of temperature, the folding kinetics of OmpA into lipid bilayers has been shown to be slower with lower temperature [21, 31]. More importantly, the folding kinetics are strongly dependent on the lipid:protein ratio [21, 24] and the lower lipid:protein ratio of CD experiments would also decrease the folding time. In the present experiments, the reduction of the lipid:protein ratio was necessary to minimize CD signal from the α-helical belt peptide itself; the reduction in belt peptide concentration led to an overall reduction in overall ND concentration because the ratio of lipid to belt peptide (1.67) was kept constant. Despite the reduction in ND concentration, relatively high concentration of OmpA was maintained to ensure adequate S/N of the CD signal. We previously published the dependence of OmpA folding kinetics on the lipid:protein ratio for NDs. The results showed that as the lipid:protein ratio decreased below ~200, the folding kinetics decreased by approximately 1.5× compared to a higher lipid:protein ratio of 300 [5]. One reason for this decrease in rate is because the ratio of ND:protein also decreased and there was more than one protein per ND. A summary of lipid:protein ratios and the resulting ND:protein ratios are shown in Table 5.5. The dependence of folding kinetics on lipid:protein ratios and the resulting slower folding times from decreased lipid:protein ratios has been confirmed in other OmpA folding studies [21, 24]. Therefore, the measured τ_{CD} value of 28 minutes is expected to be an upper limit and the actual kinetics of formation of secondary structure is likely faster than 28 minutes by about 1.5× when taking into account the different experimental conditions. Thus, the formation of secondary structure likely takes place around 19 minutes.

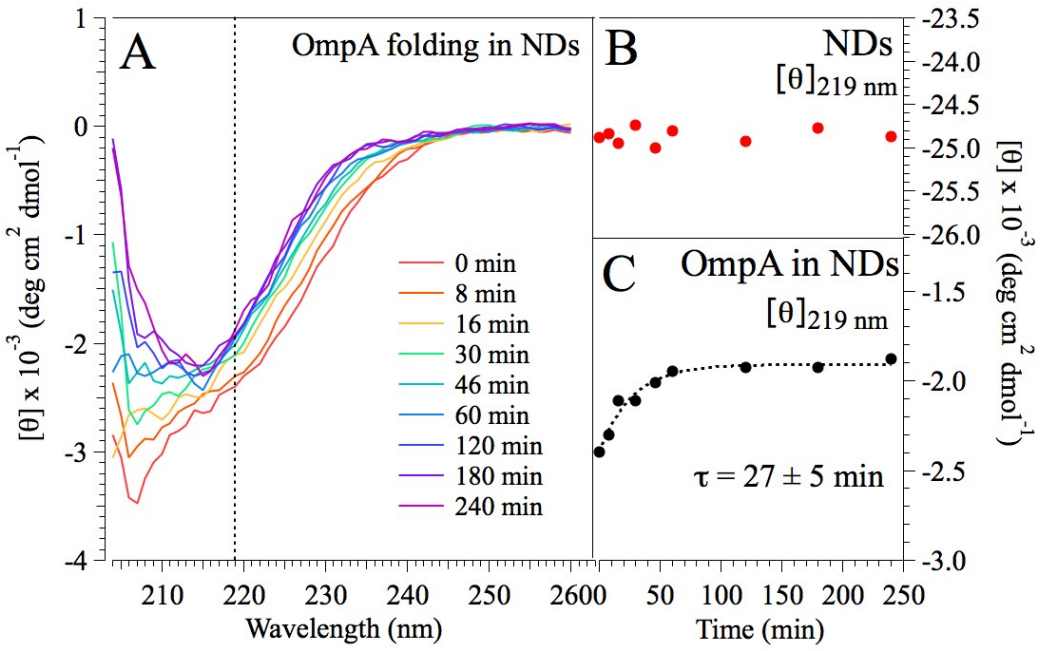

Figure 5.10 Representative trial of the evolution of CD spectra during folding of wild-type OmpA into NDs. Panel (A) shows time dependent CD spectra obtained during the folding reaction of wild-type OmpA into NDs at 33 °C. The molar ellipticity values during folding at 219 nm are indicated by the vertical black dashed line in panel (A). Panels (B) and (C) show the molar ellipticity values obtained at 219 nm for NDs in the absence of OmpA (B) and OmpA folding into NDs (C). The inverse rate constant from a single exponential fit is shown for this representative single trial. The average inverse rate constant from three trials is 28 ± 7 minutes**.**

Table 5.5 Calculated SUV:protein and ND:protein ratios

Lipid:Protein	100:1	300:1
ND:Protein*	0.67	2:1
SUV:Protein	0.02	0.05
Protein:ND*	1.5:1	0.5:1
Protein:SUV	58:1	19:1

*****The number of lipids per ND was 147, which is an average value of lipids per ND calculated from 3 references [17, 32, 33].

5.5 Discussion

The five native tryptophan residues of OmpA, which span its β-barrel transmembrane domain, are excellent spectroscopic probes for *in vitro* membrane protein folding studies. The present study utilizes single-tryptophan OmpA mutants to probe site-specific desolvation kinetics using bimolecular fluorescence quenching with acrylamide quencher. The results from these experiments provide mechanistic insight into relative timescales for insertion, folding, and desolvation during the folding of OmpA into NDs.

5.5.1 Tryptophan fluorescence quenching with acrylamide

The use of acrylamide to measure solvent accessibility of tryptophan and changes in protein conformation has been described extensively [12, 14, 26, 34]. Acrylamide is a neutral and efficient quencher of tryptophan fluorescence and it has been shown that acrylamide does not interact significantly with proteins [12]. Under ideal conditions, and in order to accurately report on the microenvironment of tryptophan residues in proteins, there should be no static interaction between the quencher and protein. Any unwanted interactions, for example between a charged quencher and the protein, could result in either an increased or decreased local concentration of the quencher and as a result, report an artificially high or low quenching constant, respectively [27]. This type of interaction could lead to a non-linear Stern-Volmer graph and add complexity to the analysis.

The upward curvature of the Stern-Volmer plots generated during folding into bilayers is indicative of contributions from both static and dynamic components (Eqn. 4) and this upward curvature is also evident in the Stern-Volmer plot of model compound N-acetyl-tryptophanamide (NATA) (Figure 5.11) with acrylamide quencher. In Eqn. 4, the static volume component, V, can be interpreted as a volume within which the fluorescence is immediately quenched upon

excitation of the fluorophore [11]. The V value remains unchanged at 1.4 M^{-1} when NATA is quenched by acrylamide in buffer or urea, however the K_D value for NATA is decreased ~25% in urea compared to in buffer. This decrease in K_D from 14.2 M^{-1} ($k_q = 4.7 \times 10^{-9}$ $M^{-1}s^{-1}$, τ_0 = 3.0 ns [35]) in buffer to 10.7 M^{-1} ($k_q = 2.4 \times 10^{-9}$ $M^{-1}s^{-1}$, τ_0 = 4.5 ns [25]) in urea reflects a change in local environment from aqueous buffer to the more viscous urea solution. The temperature dependent studies showed that an increase in temperature from room temperature to 37 °C resulted in an increase in k_q values of ~12% for a fixed V.

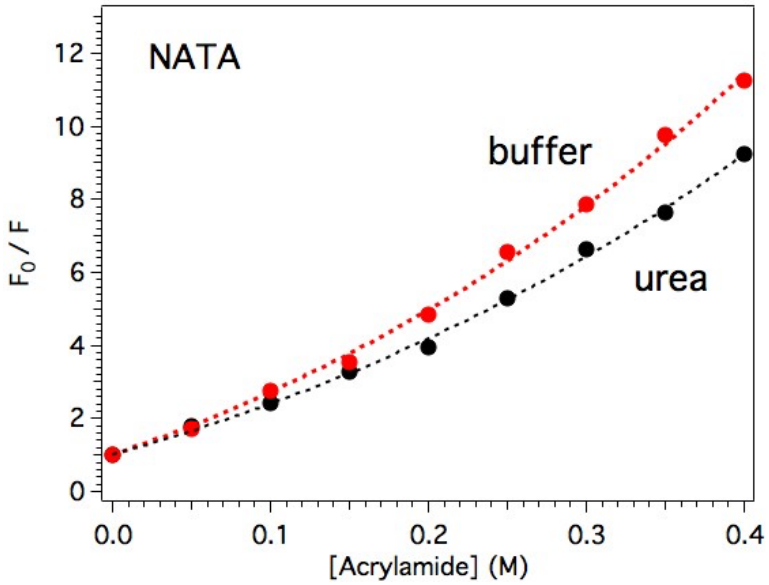

	V (M^{-1})	K_D (M^{-1})	b
buffer	1.4	14.2	0.95
urea	1.4	10.7	1.04

Figure 5.11 Stern-Volmer plots of model compound NATA in phosphate buffer (red) and urea (black) at room temperature. The data were fit to Eqn. 4 and the obtained fit parameters of V, K_D, and b are summarized in the table. This figure is reproduced from [15].

5.5.2 Evolution of bimolecular quenching constant, k_q, during folding

The evolution of the Stern-Volmer plots for the folding reaction of OmpA into NDs led to different methods to analyze and obtain desolvation kinetics, as described in our previous fluorescence quenching study for the folding of OmpA into vesicles [15]. The magnitude of k_q has been interpreted as a kinetic measurement of solvent exposure [26] and generally, low or zero values of k_q, and therefore K_D, indicate protected or buried residues in rigid protein environments with minimal or no solvent accessibility. In contrast, high values of k_q reflect more solvent accessible or highly dynamic residue(s).

The trend for the average value of k_q based the sphere-of-action model was $k_q^{denatured}(1.9 \times 10^{-9}\ M^{-1}s^{-1}) > k_q^{aggregated}\left(1.6 \times 10^{-9}\ M^{-1}s^{-1}\right) > k_q^{folded}(0.3 \times 10^{-9}\ M^{-1}s^{-1})$. As expected, the denatured and aggregated OmpA conformations exhibit the highest k_q values, reflecting exposed tryptophan to solvent in these states. The β-barrel structure of OmpA is not as hydrophobic as α-helical structures [36, 37] and may not easily aggregate in a collapsed form, which may explain the similar levels of solvent accessibility in aggregated and denatured states. The folded conformation exhibits a near zero k_q value of $0.3 \times 10^{-9}\ M^{-1}s^{-1}$, which is consistent with buried or inaccessible tryptophan to acrylamide quencher and agrees with the k_q value of folded OmpA in SUVs ($0.2 \times 10^{-9}\ M^{-1}s^{-1}$) [15]. While we have not calculated the k_q values of adsorbed OmpA, qualitatively we know that it is an intermediate state that interacts with, but does not insert into, the membrane bilayer. We have shown in a previous study that the structure of the OmpA adsorbed intermediate onto NDs is exposed to arg-C protease in solution, and thus expect that the adsorbed k_q value will more closely resemble that of the solvent exposed denatured and aggregated states.

The evolution of k_q during folding were modeled with a single exponential function (Figure 5.6, top panel) and an inverse rate constant, τ_{desolv} ($\frac{1}{k}$), gave rise to site-specific desolvation lifetimes at each of the 5 native tryptophan locations within OmpA's transmembrane domain (summarized in Table 5.3). The values for τ_{desolv} during folding into NDs were 65 minutes (W102), 36-41 minutes (W7, W15, W57) and 28 minutes (W143). The tryptophan at position 102 is unique from the others in that it is the only tryptophan that is oriented away from the bilayer and positioned towards the inner pore in the published structures [38, 39]. Given that OmpA is a non-specific pore, the long desolvation time for W102 is consistent with the presence of water in the pore after folding. The slowest desolvation kinetics of 68 minutes for position 102 in NDs differs from SUVs where W102 exhibited the same kinetics as W7, W15, and W57, all of which are lipid-facing positions. This difference between NDs and SUVs may reflect slight differences in orientation or dynamics of tryptophan 102 within the interior pore region in these two folding environments. W143 exhibits the fastest decrease in solvent accessibility (28 minutes) and this fast desolvation process at position 143 relative to the others has also been shown during folding into SUVs [15]. We have previously proposed that the relatively fast desolvation process at this location may be attributed to a more rapid entry into the bilayer or may be a result of the relative proximity in sequence to the soluble tail (transmembrane domain ends at residue 171), which may facilitate faster desolvation [15]. The differences in τ_{desolv} reflect site-specific desolvation kinetics during folding. Desolvation times for other mutants (W7, W15, W57) are comparable for NDs and SUVs.

5.5.3 Evolution of tryptophan emission probes changes in local environment during folding

The tryptophan emission blue-shift observed during folding, is attributed to a transition from unfolded OmpA in aqueous environment to the native conformation embedded within a

hydrophobic bilayer and has been discussed extensively [3, 5, 19, 25]. The evolution of λ_{max} during the folding of OmpA in the absence of acrylamide (Figure 5.6, bottom panel) showed mutant-dependent blue shifts, $\Delta\lambda_{max}$ values, of 14-17 nm, consistent with previous studies of OmpA folding in SUVs [3, 5, 19, 25]. The λ_{max} kinetics were best fit to a double exponential and the fit parameters were used to extrapolate λ_{max} at the earliest time point, t = 0 hr. Fast and slow inverse rate constants, τ_{enviro}^{fast} and τ_{enviro}^{slow}, of 4-9 minutes and 14-64 minutes, respectively were obtained from the fits, with τ_{enviro}^{fast} accounting for the majority, or 67-87% of the blue-shift. The use of double exponential functions to satisfactorily model the kinetics has been reported in previous OmpA folding studies [15, 21, 40].

Previous studies have attributed the fast component as an initial interaction, or adsorption, to the membrane bilayer [31, 40]. Kleinschmidt and Tamm showed by fluorescence that the OmpA adsorbed intermediate binds to DOPC lipid bilayers in about 6 minutes (k_1^{-1}) [31]. Our fluorescence data agree with and support an initial fast interaction with the lipid bilayer, resulting in mutant dependent τ_{enviro}^{fast} times of 4-9 minutes. The fast initial change in environment polarity can be attributed to a transition from an unfolded and solvent exposed conformation to a less polar environment, characteristic of an adsorbed intermediate that precedes the insertion and folding. We describe in detail a similar observation of an initial fast change in local environment that precedes the desolvation process for folding into SUVs [15]. The minor component, τ_{enviro}^{slow}, reflects continuous insertion and equilibration within the bilayer (14-64 minutes).

Overall, the results from the present λ_{max} kinetics in NDs are similar to those for SUVs. The fast components range from 4-9 minutes in NDs and 7-13 minutes in SUVs and the slow components range from 14-64 minutes in NDs and 25-84 minutes in SUVs. It is possible that the

kinetics for λ_{max} may be slightly faster in NDs compared to SUVs, but the errors here are relatively large and additional experiments with smaller errors will be needed to confirm any possible differences.

5.5.4 Formation of secondary structure probed by circular dichroism spectroscopy

The kinetics of formation of the secondary structure of wild-type OmpA was measured by CD spectroscopy. Figure 5.10 shows time-dependent CD spectra during the folding reaction into NDs. At the earliest time point (t = 0 min), the CD spectrum displays a large negative feature in the far UV region, indicating random structure [29]. As the folding proceeds, the CD signal in the far UV region (~205 nm) evolves to more positive molar ellipticity [θ] values. The minimum at around 212 nm, which indicates β-sheet structure [29, 30], begins to resolve at about 30 minutes after initiation of the folding reaction. A global single exponential fit to 3 trials resulted in a $[\theta]_{219nm}$ inverse rate constant, τ_{CD}, of 28 ± 7 min. As described above, the formation of secondary structure likely occurs faster than 28 minutes under the same experimental conditions as the fluorescence studies [5, 21, 24, 31, 41]. We estimate the formation of secondary structure is at least 1.5× faster, with a folding time of approximately 19 minutes, based on previous comparison of folding rates in NDs with different lipid:protein ratios [5]. Overall, the kinetics of secondary structure formation is comparable to or faster than the kinetics of desolvation for all mutants (τ_{desolv} = 28-65 minutes). These data suggest that the desolvation process does not occur faster than folding and that the hypothesis that desolvation is one of the final steps in folding may be valid.

5.5.5 Site-specific implications for desolvation and change in local environment during folding into NDs

The mutant dependent variation in k_q and λ_{max} kinetics indicate site-specific changes in the desolvation process and local environment associated with the folding of OmpA into NDs,

similar to folding into SUVs [15]. All mutants displayed a fast interaction with the lipid bilayer, within 4-9 minutes, reflected by $\tau_{\mathrm{enviro}}^{\mathrm{fast}}$. We interpret this relatively fast change in the polarity of local environment at the early stages of folding as a transition from an unfolded and solvent exposed OmpA conformation to a less polar environment resulting from an interaction with the hydrophobic lipid bilayer. W7 displayed the largest $\Delta\lambda_{\mathrm{max}}$ of 17 nm and the most blue-shifted emission of 337 nm in the folded state. This result implies that the tryptophan residue at position 7 residues in the most buried or hydrophobic environment, consistent with previous studies [25, 42].

The general trend for the desolvation kinetics, τ_{desolv}, is as follows: W143 (28 minutes) < W7, W15, W57 (36-41 minutes) < W102 (65 minutes). W143 exhibits the fastest desolvation kinetics, and this fast decrease in desolvation at position 143 was also observed during folding into SUVs [15]. We have previously suggested that the fast desolvation process at this location may be attributed to a more rapid entry into the bilayer, which is reflected in the fast λ_{max} kinetics at this position relative to the others, or a more facile desolvation due to relative proximity and interactions with the periplasmic domain [15]. W102 exhibited a low level of solvent exposure and quenching, and the slowest desolvation kinetics. The low level of quenching at this position is an interesting result given that the tryptophan at position 102 is the only tryptophan residue that is not oriented towards the lipid bilayer, and instead faces the interior of the β-barrel pore in the published structures [38, 39]. The λ_{max} of 338 nm at this position indicates a hydrophobic environment, contrary to what may be expected of a residue that is positioned towards the interior of a pore. This result may reflect a difference in dynamics or orientation of tryptophan 102 between detergent-solubilized crystal and NMR structures compared to bilayer-solubilized SUV and ND structures. Additionally, there may be a slight

difference in structure and/or dynamics in the interior pore region between folded OmpA in bilayer-solubilized SUV or ND structures given that the bimolecular quenching constant of folded W102 in NDs is the largest and the desolvation time is the slowest of all mutants studied here. We previously suggested a restriction of protein dynamics in this interior region, which may lead to decreased solvent accessibility at this position in SUVs [15]; this restriction may be eliminated in NDs.

Additional mechanistic insights are provided through folding rate constants obtained through an intensity-weighted fluorescence decomposition analysis [3, 5]. The fluorescence spectra obtained during the folding reaction for each mutant in the absence of acrylamide was decomposed into basis spectra that corresponded to fully folded and unfolded populations. Using this method, inverse rate constants, τ_{fold}, ranged from ~19-26 minutes across all mutants yielding an average folding rate constant of 23 ± 3 minutes (n = 5). The folding kinetics determined by the decomposition analysis agree with previously published decomposition folding rates for wild-type OmpA during folding into NDs [5]. Collectively, these data provide a mechanistic view of relative timescales for the insertion, folding, and desolvation process of OmpA during folding into NDs. For most mutants, the general trend is as follows: $\tau_{\mathrm{enviro}}^{\mathrm{fast}} < \tau_{\mathrm{fold}} < \tau_{\mathrm{enviro}}^{\mathrm{slow}} \leq \tau_{\mathrm{desolv}}$. The last two steps ($\tau_{\mathrm{enviro}}^{\mathrm{slow}}$ and τ_{desolv}) are comparable within the error. This result can be restated as a fast interaction, or adsorption to the lipid bilayer ($\tau_{\mathrm{enviro}}^{\mathrm{fast}}$= 4-9 minutes) followed by the folding ($\tau_{\mathrm{fold}} = 23$ minutes) and continuous insertion or equilibration, ($\tau_{\mathrm{enviro}}^{\mathrm{slow}} =$ 14-64 minutes) and lastly desolvation within the bilayer ($\tau_{\mathrm{desolv}} =$ 29-68 minutes). A summary of the kinetics is given in Table 5.6.

Table 5.6 Summary of timescales for different events during the folding of OmpA.

OmpA mutant	W7	W15	W57	W102	W143
Formation of native (fluorescence) and secondary (CD) structures					
Fluorescence τ_{fold} (min)	21	25	19	26	23
CD τ_{fold} (min)*	19				
Desolvation based on Stern-Volmer kinetics					
τ_{desolv} (min)	41 ± 2	41 ± 2	36 ± 1	65 ± 5	28 ± 1
Adsorption and insertion based on λ_{max}					
τ_{enviro}^{fast} (min)	7 ± 1	8 ± 1	6 ± 1	9 ± 1	4 ± 1
τ_{enviro}^{slow} (min)	37 ± 7	64 ± 23	43 ± 8	52 ± 8	14 ± 2

*The CD experiment is for wild-type OmpA. The experimental value of τ_{fold} of 28 minutes was corrected by a factor of 1.5× to a value of 19 minutes in order to compare the CD results to fluorescence results. See main text for details.

5.6 Conclusion

Site-specific mechanistic insight, including relevant timescales, into changes in local environment and desolvation during the folding of OmpA into NDs was investigated through bimolecular fluorescence quenching studies with acrylamide and single-tryptophan OmpA mutants. The present study utilized the sphere-of-action quenching model, which accounts for the upward curvature of the evolving time-resolved Stern-Volmer plots during OmpA folding and appropriately reflects a combination of static and dynamic components. The results for the desolvation decay constants, τ_{desolv}, for folding into NDs agree with published desolvation decay constants during folding of OmpA into SUVs. A comparison of folding rates, τ_{fold}, to the kinetics of τ_{desolv} and λ_{max}, indicate that the desolvation process occurs in the final steps of the folding mechanism.

Chapter 5 is currently in preparation for submission. Asamoto, DeeAnn K. and Kim, Judy E. The dissertation author was the primary investigator and author of this paper.

5.7 References

[1] H. Yin, A.D. Flynn, Drugging membrane protein interactions, *Annu. Rev. Biomed. Eng.* 18 (2016) 51-76.

[2] J.H. Kleinschmidt, Membrane protein folding on the example of outer membrane protein A of *Escherichia coli*, *Cell Mol. Life Sci.* 60 (2003) 1547-58.

[3] G. Kang, I. Lopez-Pena, S. Bhakta, J.E. Kim, Probing Membrane Protein Structure and Dynamics by Fluorescence Spectroscopy, John Wiley & Sons, Ltd., 2013.

[4] J.E. Horne, S.E. Radford, A growing toolbox of techniques for studying β-barrel outer membrane protein folding and biogenesis, *Biochem. Soc. Trans.* 44 (2016) 802-9.

[5] D.K. Asamoto, G. Kang, J.E. Kim, Folding of the β-Barrel membrane protein OmpA into nanodiscs, *Biophys. J.* 118 (2020) 403-14.

[6] H. Ishida, A. Garcia-Herrero, H.J. Vogel, The periplasmic domain of *Escherichia coli* outer membrane protein A can undergo a localized temperature dependent structural transition, *Biochim. Biophys. Acta* 1838 (2014) 3014-24.

[7] M.S. Cheung, A.E. García, J.N. Onuchic, Protein folding mediated by solvation: water expulsion and formation of the hydrophobic core occur after the structural collapse, *Proc. Natl. Acad. Sci. U.S.A.* 99 (2002) 685-90.

[8] Y.M. Rhee, E.J. Sorin, G. Jayachandran, E. Lindahl, V.S. Pande, Simulations of the role of water in the protein-folding mechanism, *Proc. Natl. Acad. Sci. U.S.A* 101 (2004) 6456-61.

[9] A.M. Fernández-Escamilla, M.S. Cheung, M.C. Vega, M. Wilmanns, J.N. Onuchic, L. Serrano, Solvation in protein folding analysis: combination of theoretical and experimental approaches, *Proc. Natl. Acad. Sci. U.S.A.* 101 (2004) 2834-9.

[10] U. Chawla, S. Perera, S.D.E. Fried, A.R. Eitel, B. Mertz, N. Weerasinghe, M.C. Pitman, A.V. Struts, M.F. Brown, Activation of the G-protein-coupled receptor rhodopsin by water, *Angew. Chem., Int .Ed. Engl.* 60 (2021) 2288-95.

[11] J.R. Lakowicz, Principles of Fluorescence Spectroscopy, 3rd Edition, Springer US, 2006.

[12] M.R. Eftink, C.A. Ghiron, Exposure of tryptophanyl residues in proteins. Quantitative determination by fluorescence quenching studies, *Biochemistry* 15 (1976) 672-80.

[13] J.H. Kleinschmidt, L.K. Tamm, Time-resolved distance determination by tryptophan fluorescence quenching: probing intermediates in membrane protein folding, *Biochemistry* 38 (1999) 4996-5005.

[14] M.R. Eftink, C.A. Ghiron, Exposure of tryptophanyl residues and protein dynamics, *Biochemistry* 16 (1977) 5546-51.

[15] D.K. Asamoto, I.A. Kozachenko, I. Lopez-Pena, J.E. Kim, Bimolecular quenching of tryptophan fluorescence in a membrane protein: Evolution of local solvation and environment during folding into a bilayer, *Spectrochim. Acta, Part A* (2021).

[16] K.M. Sanchez, J.E. Gable, D.E. Schlamadinger, J.E. Kim, Effects of tryptophan microenvironment, soluble domain, and vesicle size on the thermodynamics of membrane protein folding: lessons from the transmembrane protein OmpA, *Biochemistry* 47 (2008) 12844-52.

[17] S.H. Park, S. Berkamp, G.A. Cook, M.K. Chan, H. Viadiu, S.J. Opella, Nanodiscs versus macrodiscs for NMR of membrane proteins, *Biochemistry* 50 (2011) 8983-5.

[18] A.W. Shaw, M.A. McLean, S.G. Sligar, Phospholipid phase transitions in homogeneous nanometer scale bilayer discs, *FEBS Lett.* 556 (2004) 260-4.
[19] T. Surrey, F. Jähnig, Refolding and oriented insertion of a membrane protein into a lipid bilayer, *Proc. Natl. Acad. Sci. U.S.A.* 89 (1992) 7457-61.

[20] N.A. Rodionova, S.A. Tatulian, T. Surrey, F. Jähnig, L.K. Tamm, Characterization of two membrane-bound forms of OmpA, *Biochemistry* 34 (1995) 1921-9.

[21] J.H. Kleinschmidt, Folding kinetics of the outer membrane proteins OmpA and FomA into phospholipid bilayers, *Chem. Phys. Lipids* 141 (2006) 30-47.

[22] I.G. Denisov, S.G. Sligar, Nanodiscs in membrane biochemistry and biophysics, *Chem. Rev.* 117 (2017) 4669-713.

[23] F. Hagn, M.L. Nasr, G. Wagner, Assembly of phospholipid nanodiscs of controlled size for structural studies of membrane proteins by NMR, *Nat. Protoc.* 13 (2018) 79-98.

[24] J.H. Kleinschmidt, L.K. Tamm, Secondary and tertiary structure formation of the beta-barrel membrane protein OmpA is synchronized and depends on membrane thickness, *J. Mol. Biol.* 324 (2002) 319-30.

[25] J.E. Kim, G. Arjara, J.H. Richards, H.B. Gray, J.R. Winkler, Probing folded and unfolded states of outer membrane protein a with steady-state and time-resolved tryptophan fluorescence, *J. Phys. Chem. B* 110 (2006) 17656-62.

[26] M.R. Eftink, C.A. Ghiron, Fluorescence quenching of indole and model micelle systems, *J. Phys. Chem.* 80 (1976) 486-93.

[27] M.R. Eftink, C.A. Ghiron, Fluorescence quenching studies with proteins, *Anal. Biochem.* 114 (1981) 199-227.

[28] E.J. Danoff, K.G. Fleming, The soluble, periplasmic domain of OmpA folds as an independent unit and displays chaperone activity by reducing the self-association propensity of the unfolded OmpA transmembrane β-barrel, *Biophys. Chem.* 159 (2011) 194-204.

[29] N.J. Greenfield, Using circular dichroism spectra to estimate protein secondary structure, *Nat. Protoc.* 1 (2006) 2876-90.

[30] A. Micsonai, F. Wien, L. Kernya, Y.H. Lee, Y. Goto, M. Réfrégiers, J. Kardos, Accurate secondary structure prediction and fold recognition for circular dichroism spectroscopy, *Proc. Natl. Acad. Sci. U.S.A.* 112 (2015) E3095-103.

[31] J.H. Kleinschmidt, L.K. Tamm, Folding intermediates of a beta-barrel membrane protein. Kinetic evidence for a multi-step membrane insertion mechanism, *Biochemistry* 35 (1996) 12993-3000.

[32] T.D. Bradrick, A. Philippetis, S. Georghiou, Stopped-flow fluorometric study of the interaction of melittin with phospholipid bilayers: importance of the physical state of the bilayer and the acyl chain length, *Biophys. J.* 69 (1995) 1999-2010.

[33] D. Martinez, M. Decossas, J. Kowal, L. Frey, H. Stahlberg, E.J. Dufourc, R. Riek, B. Habenstein, S. Bibow, A. Loquet, Lipid Internal Dynamics Probed in Nanodiscs, *Chemphyschem.* 18 (2017) 2651-7.

[34] S.M. Akbar, K. Sreeramulu, H.C. Sharma, Tryptophan fluorescence quenching as a binding assay to monitor protein conformation changes in the membrane of intact mitochondria, *J. Bioenerg. Biomembr.* 48 (2016) 241-7.

[35] A.G. Szabo, D.M. Rayner, Fluorescence decay of tryptophan conformers in aqueous solution, *J. Am. Chem. Soc.* 102 (1980) 554-63.

[36] L.K. Tamm, H. Hong, B. Liang, Folding and assembly of beta-barrel membrane proteins, *Biochim. Biophys. Acta.* 1666 (2004) 250-63.

[37] J.D. Bryngelson, J.N. Onuchic, N.D. Socci, P.G. Wolynes, Funnels, pathways, and the energy landscape of protein folding: a synthesis, *Proteins* 21 (1995) 167-95.

[38] A. Pautsch, G.E. Schulz, High-resolution structure of the OmpA membrane domain, *J. Mol. Biol.* 298 (2000) 273-82.

[39] A. Arora, F. Abildgaard, J.H. Bushweller, L.K. Tamm, Structure of outer membrane protein A transmembrane domain by NMR spectroscopy, *Nat. Struct. Biol.* 8 (2001) 334-8.

[40] J.H. Kleinschmidt, T. den Blaauwen, A.J. Driessen, L.K. Tamm, Outer membrane protein A of *Escherichia coli* inserts and folds into lipid bilayers by a concerted mechanism, *Biochemistry* 38 (1999) 5006-16.

[41] T. Surrey, F. Jähnig, Kinetics of folding and membrane insertion of a beta-barrel membrane protein, *J. Biol. Chem.* 270 (1995) 28199-203.

[42] K.M. Sanchez, G. Kang, B. Wu, J.E. Kim, Tryptophan-lipid interactions in membrane protein folding probed by ultraviolet resonance Raman and fluorescence spectroscopy, *Biophys. J.* 100 (2011) 2121-30.

Chapter 6
Conclusions

6.1 Summary

Membrane proteins perform diverse roles that are vital to cellular function. Despite advancement in the field of membrane protein folding over the past decade, the study of integral membrane protein structures, dynamics, and folding mechanisms in lipid bilayers remain a challenge. The inherent complications of studying membrane proteins in their native-like complex lipid environments limit the use of biophysical techniques as well as the number of membrane proteins suitable for successful *in vitro* characterization and folding studies. Improvements to experimental techniques may enable more extensive studies of critical biomolecules, including membrane proteins, and provide insight into fundamental details, which can lead to continuation of advancement in this field.

In this work, both optical and non-optical techniques are employed to study the *in vitro* folding of Outer membrane protein A (OmpA), a model β-barrel integral membrane protein into lipid bilayers. We show that OmpA spontaneously inserts and folds into DMPC nanodiscs (NDs), which are an improved bilayer mimic to traditional small unilamellar vesicles (SUVs) and offer experimental benefits of optical clarity, sample homogeneity, better control of ND-to-protein ratios, and greater stability. Detailed insights into the site-specific dehydration process during folding into NDs or SUVs are provided by Stern-Volmer analysis utilizing bimolecular fluorescence quenching. The results obtained for the kinetics of desolvation and blue-shift of emission maxima during folding complement previous mechanisms of an *in vitro* concerted mechanism and indicate that the dehydration timescale is slower than the formation of tertiary structure.

6.2 Future work

The techniques used in this work, which includes fluorescence spectroscopy, UV-visible absorption spectroscopy, UV resonance Raman spectroscopy (UVRR), circular dichroism (CD) spectroscopy, and SDS-PAGE mobility studies are examples of methods to study protein folding. These tools have contributed to the on-going progress in the understanding of the dynamics, structures, and folding mechanisms of proteins. These methods may be applied to other important biomolecules to provide insights into their folding mechanisms and dynamics, including lipid-protein interactions, and inter- and intra- protein interactions during folding.

6.2.1 Molecular dynamics of OmpA bound with Skp chaperone and LPS

The seventeen kilodalton protein (Skp) is a molecular chaperone present in *Escherichia coli* that specifically interacts with outer membrane proteins (OMPs) and facilitates the transfer of OMPs across the periplasm and to the outer membrane [1]. Skp has been shown to efficiently facilitate the transfer of OmpA from its urea-denatured form to its folded form into negatively charged lipid bilayers containing dioleoylphosphatidylglycerol (DOPG) and above its isoelectric point of 5.5 [2]. Another study found that folding yields of up to 90% into 50% 1,2-dioleoyl-sn-glycero-3-phosphocholine (DOPC), 30% 1,2-dioleoyl-sn-glycero-3-phosphoethanolamine (DOPE), and 20% 1,2-dioleoyl-sn-glycero-3-phosphoglycerol (DOPG) required the presence of both Skp and lipopolysaccharide (LPS), a major component of the outer leaflet of the outer membrane [3]. Additionally, the folding kinetics into lipid bilayers were faster when unfolded OmpA was in complex with both Skp and LPS, compared to urea-unfolded OmpA [3]. These studies indicate that Skp together with LPS influence the folding of OmpA into lipid bilayers and detailed investigations regarding their interactions may provide additional insight into OmpA's folding pathways.

The binding of Skp and LPS to form a complex with OmpA is thought to induce a conformational change of OmpA (Figure 6.1) [4]. Site-directed fluorescence spectroscopy with single-tryptophan OmpA mutants revealed specific binding sites within the OmpA-Skp-LPS complex and the results indicated that interactions of Skp and LPS change the conformation of OmpA in the complex which facilitates the insertion and folding into lipid bilayers [4].

UVRR spectroscopy is a powerful vibrational technique that reports on molecular dynamics of aromatic residues using 228 nm excitation and can reveal hydrogen bonding, cation-π interactions, π-π interactions, environment polarity, and dihedral torsion angles [5]. The Skp sequence contains a single tryptophan residue, a single tyrosine residue, 3 phenylalanine residues, and multiple charged residues (UniProtKB-P0AEU7). Therefore, additional insights into the molecular dynamics of the OmpA-Skp-LPS complex, as well as the Skp-LPS complex in the absence of OmpA, may be investigated using this technique.

Tryptophan is a unique aromatic residue because it exhibits the largest accessible nonpolar surface area that is highly polarizable and contains an indole N-H moiety that is capable of forming hydrogen bonds [6]. Tryptophan also displays the greatest electrostatic potential for cation-π interactions [7]. UVRR spectroscopy using 228 nm excitation would be particularly useful for probing site-specific molecular interactions such as hydrogen bonding, cation-π interactions, or π-π interactions that contribute to the stabilization of these complexes. UVRR analysis of the W7 Fermi doublet region using 228 nm excitation would reveal the local environment of the tryptophan residues within the proteins or protein complex [5], and perhaps provide complementary results regarding site specific binding sites. By tuning the UVRR excitation wavelength to 215 and 210 nm, vibrational modes of phenylalanine and the amide backbone become enhanced, and additional analysis for these markers can be performed [8].

6.2.2 Spectroscopic investigations of Outer membrane protein T

Outer membrane protein T (OmpT) consists of a 10-stranded antiparallel β-barrel domain and serves as a hydrolytic enzyme present in the outer membrane of *Escherichia coli* [9]. The X-ray crystal structure of OmpT (PDB ID 1I78) is shown in Figure 6.2. OmpT has been identified to preferentially cleave short peptides at dibasic sites (-K-K-, -K-R-, -R-K-, and –R-R-) [9, 10]. The insertion and folding of OmpT into lipid vesicles and nanodiscs in the presence of reconstituted BAM-complex and SurA have been investigated and upon folding into lipid bilayers, it has been shown that OmpT retains its protease activity [11, 12].

Wild-type OmpT contains 8 native tryptophan residues that span its β-barrel domain, which would serve as excellent spectroscopic probes. An interesting topic of study would be to utilize site-directed mutagenesis to generate 8 single-tryptophan OmpT mutants and employ fluorescence spectroscopy experiments together with UVRR experiments to gain site-specific information on molecular dynamics, including hydrogen bonding or local environment of these native tryptophan residues. Stabilizing aromatic-aromatic interactions such as π-π interactions, cation-π interactions, amide backbone conformation, or protein-lipid interactions may also be investigated using UVRR spectroscopy [13-15]. FRET and bimolecular quenching studies utilizing the 8 single-tryptophan mutants to determine kinetics of formation of OmpT's tertiary structure and dehydration process during folding into NDs would may also be performed. It would be interesting to compare any similarities or differences in results between OmpA and OmpT's folding mechanisms.

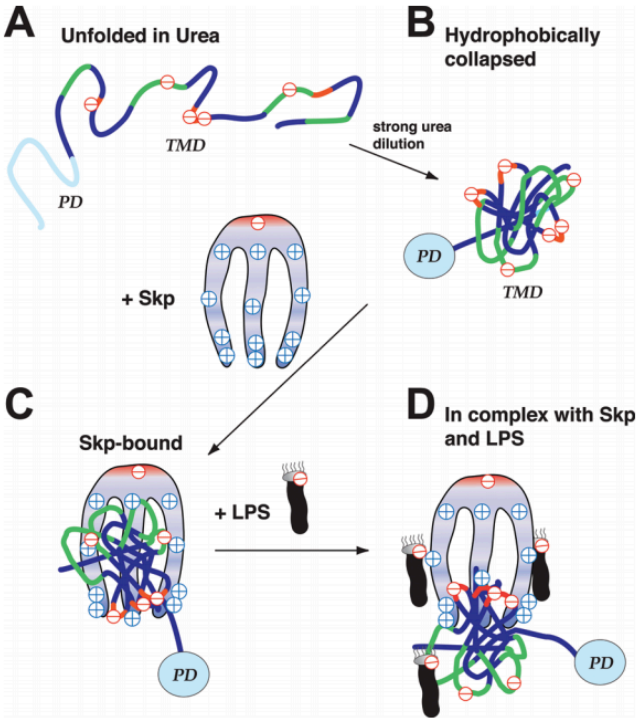

Figure 6.1 Schematic diagram of OmpA's interaction with Skp and LPS taken from reference [4]. Panel (A) shows unfolded OmpA in 8 M urea. The transmembrane regions (TMD) are colored dark blue. Polar loop and polar turn regions are colored green and red, respectively. The periplasmic domain (PD) is colored light blue. The negatively charged protein (pI ~ 5.5) is indicated by (-). Panel (B) shows the water-soluble TMD collapsed intermediate state and the independently folded PD. Panel (C) shows the positively charged Skp chaperone bound to the TMD of OmpA through electrostatic and hydrophobic interactions. Panel (D) shows the negatively charged LPS binding to the OmpA-Skp complex inducing a partial release and reorientation of OmpA.

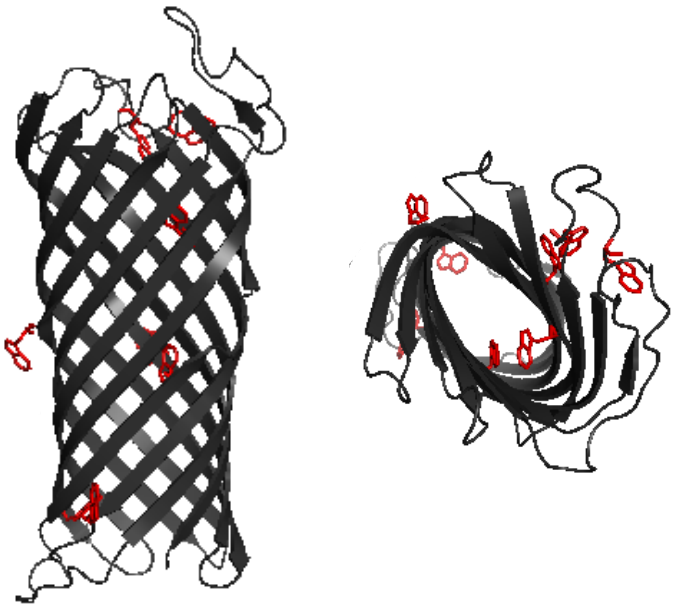

Figure 6.2 The X-ray crystal structure of outer membrane protease OmpT from *Escherichia coli* (PDB ID: 1I78). The 8 native tryptophan residues are highlighted in red. A view down the center of the β-barrel domain is shown on the right.

6.3 References

[1] R. Chen, U. Henning, A periplasmic protein (Skp) of *Escherichia coli* selectively binds a class of outer membrane proteins, *Mol. Microbio.* 19 (1996) 1287-94.

[2] G.J. Patel, S. Behrens-Kneip, O. Holst, J.H. Kleinschmidt, The periplasmic chaperone Skp facilitates targeting, insertion, and folding of OmpA into lipid membranes with a negative membrane surface potential, *Biochemistry* 48 (2009) 10235-45.

[3] P.V. Bulieris, S. Behrens, O. Holst, J.H. Kleinschmidt, Folding and insertion of the outer membrane protein OmpA is assisted by the chaperone Skp and by lipopolysaccharide, *The J. Biol. Chem.* 278 (2003) 9092-9.

[4] J. Qu, S. Behrens-Kneip, O. Holst, J.H. Kleinschmidt, Binding regions of outer membrane protein A in complexes with the periplasmic chaperone Skp. A site-directed fluorescence study, *Biochemistry* 48 (2009) 4926-36.

[5] D.K. Asamoto, J.E. Kim, UV resonance Raman spectroscopy as a tool to probe membrane protein structure and dynamics, *Methods Mol. Bio. (Clifton, N.J.)* 2003 (2019) 327-49.

[6] S. Millefiori, A. Alparone, A. Millefiori, A. Vanella, Electronic and vibrational polarizabilities of the twenty naturally occuring amino acids, *Biophys. Chem.* 132 (2008) 139-47.

[7] J.P. Gallivan, D.A. Dougherty, Cation-pi interactions in structural biology, *Proc. Natl. Acad. Sci. of the U.S.A* 96 (1999) 9459-64.

[8] I. López-Peña, B.S. Leigh, D.E. Schlamadinger, J.E. Kim, Insights into protein structure and dynamics by ultraviolet and visible resonance Raman spectroscopy, *Biochemistry* 54 (2015) 4770-83.

[9] R.A. Kramer, D. Zandwijken, M.R. Egmond, N. Dekker, In vitro folding, purification and characterization of *Escherichia coli* outer membrane protease ompT, *Eur. J. Biochem.* 267 (2000) 885-93.

[10] G. Sinsinbar, S. Gudlur, S.E. Wood, G. Ammanath, H.U. Yildiz, P. Alagappan, M. Mrksich, B. Liedberg, Outer-membrane protease (OmpT) based *E. coli* sensing with anionic polythiophene and unlabeled peptide substrate, *Angew. Chem., Int. Ed. Engl.* 59 (2020) 18068-77.

[11] J.H. Kleinschmidt, Folding of β-barrel membrane proteins in lipid bilayers - Unassisted and assisted folding and insertion, *Biochim. Biophys. Acta* 1848 (2015) 1927-43.

[12] M.G. Iadanza, B. Schiffrin, P. White, M.A. Watson, J.E. Horne, A.J. Higgins, A.N. Calabrese, D.J. Brockwell, R. Tuma, A.C. Kalli, S.E. Radford, N.A. Ranson, Distortion of the bilayer and dynamics of the BAM complex in lipid nanodiscs, *Comm. Biol.* 3 (2020) 766.

[13] K.M. Sanchez, G. Kang, B. Wu, J.E. Kim, Tryptophan-lipid interactions in membrane protein folding probed by ultraviolet resonance Raman and fluorescence spectroscopy, *Biophys. J.* 100 (2011) 2121-30.

[14] D.E. Schlamadinger, J.E. Gable, J.E. Kim, Hydrogen bonding and solvent polarity markers in the UV resonance Raman spectrum of tryptophan: application to membrane proteins, *The J. Phys. Chem. B* 113 (2009) 14769-78.

[15] D.E. Schlamadinger, B.S. Leigh, J.E. Kim, UV resonance Raman study of TrpZip2 and related peptides: π-π interactions of tryptophan, *J. Raman Spectrosc.* 43 (2012) 1459-64.